REGULATION OF BODY COMPOSITION BY THE MICROBIOTA AND

THE CIRCADIAN CLOCK

APPROVED BY SUPERVISORY COMMITTEE

_____

Lora V. Hooper, Ph.D.

_____

Carla B. Green, Ph.D.

_____

Yi Liu, Ph.D.

_____

Yihong Wan, Ph.D.

DEDICATION

Dedicated to my Dad and Mom

for

their love and support

REGULATION OF BODY COMPOSITION BY THE MICROBIOTA AND THE CIRCADIAN CLOCK

by

YUHAO WANG

DISSERTATION

Presented to the Faculty of the Graduate School of Biomedical Sciences

The University of Texas Southwestern Medical Center at Dallas

In Partial Fulfillment of the Requirements

For the Degree of

DOCTOR OF PHILOSOPHY

The University of Texas Southwestern Medical Center at Dallas

Dallas, Texas

December 2017

REGULATION OF BODY COMPOSITION BY THE MICROBIOTA AND THE CIRCADIAN CLOCK

Yuhao Wang, Ph.D.

The University of Texas Southwestern Medical Center at Dallas, 2017

Supervising Professor: Lora V. Hooper, Ph.D.

The intestinal microbiota has been identified as an environmental factor that markedly impacts energy storage and body fat accumulation, yet the underlying mechanisms remain unclear. In this dissertation, I show that the microbiota regulates body composition through the circadian transcription factor NFIL3 in intestinal epithelial cells. First, epithelial NFIL3 promotes lipid absorption and export in the intestine by regulating a circadian expression program of epithelial lipid metabolic genes. Second, *Nfil3* transcription oscillates diurnally in intestinal epithelial cells and the amplitude of the circadian oscillation is controlled by the microbiota through group 3 innate lymphoid cells (ILC3), STAT3, and the epithelial cell circadian clock. These findings provide mechanistic insight into how the intestinal microbiota regulates body composition and establish NFIL3 as an essential molecular link among the microbiota, the circadian clock, and host metabolism.

TABLE OF CONTENTS

CHAPTER TWO

PRIOR PUBLICATIONS

1. **Y. Wang**, Z. Kuang, X. Yu, K. A. Ruhn, M. Kubo and L. V. Hooper. The intestinal microbiota regulates body composition through NFIL3 and the circadian clock. *Science*. **357**, 912-916 (2017).
2. X. Yu*, **Y. Wang***, M. Deng, Y. Li, K. A. Ruhn, C. Zhang, L. V. Hooper. The basic leucine zipper transcription factor NFIL3 directs the development of a common innate lymphoid cell precursor. *Elife*. **3**, e04406 (2014). *Contributed equally.
3. S. Bel, M. Pendse, **Y. Wang**, K. A. Ruhn, B. Hassell, T. Leal, S. E. Winter, and L. V. Hooper. Paneth cells secrete lysozyme via secretory autophagy during bacterial infection of the intestine. *Science*. **357**, 1047-1052 (2017).

LIST OF FIGURES

LIST OF TABLES

LIST OF DEFINITIONS

AAAS	—	American Association for the Advancement of Science
AFP	—	Activating transcription factor
AMP	—	Adenosine mono-phosphate
ANG4	—	Angiogenin 4
ANGPTL4	—	Angiopoietin-like 4
ANOVA	—	Analysis of variance
Apo AIV	—	Apolipoprotein AIV
APC	—	Antigen presenting cell
ARNTL	—	Aryl hydrocarbon receptor nuclear translocator like
ATGL	—	Adipose triglycerides lipase
BHI	—	Brain heart infusion broth
BMAL1	—	Brain and muscle Arnt-like protein-1
BMDM	—	Bone marrow-derived macrophage
bp	—	Base pair
bZIP	—	Basic leucine zipper
CD	—	Cluster of differentiation
CD36	—	Cluster of differentiation 36, also known as platelet glycoprotein 4
cDC	—	Conventional dendritic cell
cDNA	—	Complementary deoxyribonucleic acid
CFU	—	Colony forming unit
ChIP	—	Chromatin immunoprecipitation

ChIP-seq	—	Chromatin immunoprecipitation sequencing
CK1δ	—	Casein kinases 1 delta
CK1ε	—	Casein kinases 1 epsilon
CLP	—	Common lymphoid progenitor
cm	—	Centimeter
CMP	—	Common myeloid progenitor
CMV	—	Cytomegalovirus
CoA	—	Coenzyme A
COVN	—	Conventional
CRE	—	Cre recombinase
CRY	—	Cryptochrome
Ct	—	Cycle threshold
CYP2E1	—	Cytochrome P450 family 2 subfamily E member 1
CYP7A1	—	cholesterol 7 α-hydroxylase
DC	—	Dendritic cell
DEFA5	—	Defensin, alpha 5
DEFB4	—	Defensin, beta 4
DI	—	Distilled
DBP	—	D-box binding protein
DPBS	—	Dulbecco's phosphate-buffered saline
DSS	—	Dextran sulfate sodium
DTR	—	*Diphtheria* toxin receptor
DTT	—	Dithiothreitol

E4BP4	—	E4 promoter binding protein 4
EDTA	—	Ethylenediaminetetraacetic acid
EGFP	—	Enhanced green fluorescent protein
EOMES	—	Eomesodermin
etc.	—	Et cetera
FABP4	—	Fatty acid binding protein 4
FBS	—	Fetal bovine serum
fl	—	Floxed
FPKM	—	Fragments per kilobase of transcript per million mapped reads
FUT2	—	Fucosyltransferase 2
FXR	—	Farnesoid X receptor
GAPDH	—	Glyceraldehyde 3-phosphate dehydrogenase
GATA3	—	GATA binding protein 3
GC	—	Glucocorticoid
GF	—	Germ-free
GFP	—	Green fluorescent protein
GSK-3β	—	Glycogen synthase kinase 3 beta
H&E	—	Hematoxylin and eosin
HEK-293T	—	Human embryonic kidney cells 293 with Large T antigen expression
HFD	—	High-fat diet
HPAA	—	Hypothalamus-pituitary-adrenal axis
hr	—	Hour
HSL	—	Hormone-sensitive lipase

IBD	—	Inflammatory bowel disease
ID2	—	Inhibitor of DNA binding 2
IEC	—	Intestinal epithelial cell
IFNγ	—	Interferon gamma
IgE	—	Immunoglobulin E
IgG	—	Immunoglobulin G
IL-10	—	Interleukin 10
IL-12	—	Interleukin 12
IL-13	—	Interleukin 13
IL-17	—	Interleukin 17
IL-1β	—	Interleukin 1 beta
IL-22	—	Interleukin 22
IL-22R	—	Interleukin 22 receptor
IL-23	—	Interleukin 23
IL-5	—	Interleukin 5
IL-6	—	Interleukin 6
IL2RG	—	Interleukin 2 receptor subunit gamma chain
ILC	—	Innate lymphoid cell
ILC1	—	Group 1 innate lymphoid cell
ILC2	—	Group 2 innate lymphoid cell
ILC3	—	Group 3 innate lymphoid cell
ipRGC	—	Intrinsically photoreceptive retinal ganglion cell
ITGAX	—	Integrin, alpha X

kg	—	Kilogram
LB	—	Luria-Bertani broth
LCM	—	Laser capture microdissection
LP	—	Lamina propria
LPL	—	Lipoprotein lipase
LPS	—	Lipopolysaccharide
LTi	—	Lymphoid tissue inducer
M-MLV	—	Moloney-murine leukemia virus
mg	—	Milligram
MHC	—	Major histocompatibility complex
min	—	minute
mL	—	Milliliter
MLN	—	Mesenteric lymph node
mM	—	Millimoles per liter
MRI	—	Magnetic resonance imaging
mRNA	—	Messenger ribonucleic acid
MTTP	—	Microsomal triglyceride transport protein
MyD88	—	Myeloid differentiation primary response gene 88
NAD	—	Nicotinamide adenine dinucleotide
NAMPT	—	Nicotinamide phosphoribosyltransferase
NEFA	—	Nonesterified fatted acids
NFIL3	—	Nuclear factor, IL-3 regulated
NK	—	Natural killer cell

NR1D1	—	Nuclear receptor subfamily 1, group D, member 1
OCT	—	Optimum cutting temperature compound
PAMP	—	Pathogen-associated molecular pattern
PAR	—	Proline and acidic amino acid-rich
PAS	—	Basic helix-loop-helix-PER-ARNT-SIM
PBS	—	Phosphate buffered saline solution
PCR	—	Polymerase chain reaction
pDC	—	Plasmacytoid dendritic cell
PER	—	Period
PEPCK	—	Phosphoenolpyruvate carboxykinase
PGC1α	—	Peroxisome proliferator-activated receptor gamma coactivator 1-aplpha
pH	—	Potential of hydrogen
PP5	—	Protein phosphatase 5
PPARα	—	Peroxisome proliferator activated receptor alpha
pro-DC	—	Dendritic cell progenitor
PRR	—	Pattern-recognition receptor
pSTAT3	—	Phosphorylated signal transducer and activator of transcription 3
PVDF	—	Polyvinylidene difluoride
PVN-SCG	—	Paraventricular nucleus-superior cervical ganglia
qRT-PCR	—	Quantitative real-time polymerase chain reaction
RAG	—	recombination-activating gene
REGIIIγ	—	Regenerating islet-derived 3 gamma
REV-ERBα	—	The reverse strand of c-erbA encoded protein alpha

RHT	—	Retinohypothalamic tract
RIPA	—	Radioimmunoprecipitation assay buffer
RNAseq	—	High-throughput RNA sequencing
Rorc	—	Mouse RAR-related orphan receptor gamma gene
RORα	—	Retinoic acid receptor-related orphan nuclear receptor alpha
RORγ	—	Retinoic acid receptor-related orphan nuclear receptor gamma
RPM	—	Revolutions per minute
rRNA	—	Ribosomal ribonucleic acid
SAA	—	Serum amyloid A
SCD1	—	Stearoyl-CoA-desaturase 1
SCN	—	Suprachiasmatic nucleus
SCF	—	Skp1, Cullins, F-box protein
SCFAs	—	Short chain fatty acids
SDHA	—	Succinate dehydrogenase complex flavoprotein subunit A
SDS	—	Sodium dodecyl sulfate
SDS-PAGE	—	Sodium dodecyl sulfate polyacrylamide gel electrophoresis
SEM	—	Standard error of the mean
SPF	—	Specific pathogen free
STAT3	—	Signal transducer and activator of transcription 3
T-bet	—	T-cell-specific T-box transcription factor
T2D	—	Type 2 diabetes
TBS-T	—	Tris-buffered saline, 0.1% Tween 20
TE	—	Tris-EDTA buffer

Tg	—	Transgenic
T_H1	—	Type 1 T helper cell
T_H17	—	T helper 17 cell
T_H2	—	Type 2 T helper cell
TLR-4	—	Toll-like receptor 4
TNF-α	—	Tumor necrosis factor alpha
TOX	—	Thymocyte selection-associated high mobility group box factor
UDP	—	Uridine diphosphate glucose
WHO	—	World Health Organization
WT	—	Wild-type
ZT	—	Zeitgeber times
αLP	—	α4β7 integrin-expressing common lymphoid progenitor
γδT	—	Gamma delta T cells
Δ*DC*	—	Dendritic cell specific knockout
Δ*IEC*	—	Intestinal epithelial cell specific knockout
μL	—	Microliter
℃	—	Celsius degree

CHAPTER ONE

INTRODUCTION

Although we are enjoying the so called "modern life" created by ever-advancing civilization and technology, we are also suffering some negative consequences. With consumption of high-sugar and high-fat diets, lack of exercise, frequent international travel, or staying up late for soap operas, we are carrying much more fat in our body than any time in human history. According to a survey conducted by World Health Organization (WHO) in 2014, more than 2.1 billion individuals are diagnosed as overweight or obese throughout the world, roughly 3.4 million people are dead from obesity related diseases every year, and this number is still increasing (Ng et al., 2014). Because of these shocking numbers, the worldwide obesity epidemic has become a pressing public health crisis, and has inspired intensive efforts from researchers around the world to understand the host and environmental factors that regulate human metabolism and energy homeostasis.

The trillions of commensal bacteria in our gut, or intestinal microbiota, has been identified as an essential environmental factor that markedly impacts whole body metabolism in humans. The microbiota not only facilitates energy harvest from the host diet (Murphy et al., 2010), but also has a huge influence on training the immune and metabolic systems through microbial molecules or metabolites (Cani et al., 2009). Thus, many metabolic diseases, such as malnutrition, diabetes and obesity, have been shown to be closely linked to a dysregulated intestinal microbiota (Nicholson et al., 2012). However, little is known about detailed mechanisms underlying microbiota regulation of host metabolism pathways.

The mammalian internal biological clock, or circadian clock, is another environmental factor that significantly impacts metabolic activities in humans. The circadian clock is a network

of transcription factors, present in all cells of the body, that directs diurnal oscillations in gene expression (Takahashi, 2016). Many host metabolic activities are synchronized to the 24-hour day-light cycle through the circadian clock. Disturbance of circadian clock arising from shift work or frequent international travel have been associated with an increased occurrence of metabolic diseases including obesity, diabetes and cardiovascular diseases (Bass and Takahashi, 2010). Recent studies have also suggested strong interactions between the circadian clock and the microbiota. Disruption of these interactions can profoundly impact host metabolism (Liang et al., 2015; Thaiss et al., 2014). However, little is known about the mechanisms that govern microbiota interactions with the circadian clock and how these interactions alter host metabolism.

THE MICROBIOTA AND METABOLISM

The human body is home to trillions of microorganisms. Organs or tissues that have direct contact with external environment, such as skin, lung, stomach and intestine are colonized with hundreds of different species of bacteria (Nicholson et al., 2012). Most of these bacteria are harmless to humans. In fact, we have evolved a mutualism with these tiny organisms and benefit from them. The intestinal lumen is the place that hosts the greatest number of and most diverse bacteria in human body. With pH between 5.7 to 6.7 and a temperature of 37^{o}C, it provides an optimal growth environment for housing over 100 trillion microbes, which weigh over 1.5 kg and make up to 50% of fecal contents (Evans et al., 1988; Zhao, 2013). Therefore, the word “microbiota” is usually used to refer to the commensal bacteria in the intestine.

In order to establish and maintain mutualism with gut microbiota, the host provides abundant nutrients to maintain their survival and has evolved a series of sophisticated strategies to

restrain them from invading into host tissue. For example, a single layer of epithelial cells forms a physical barrier between the lumen and host tissue. These epithelial cells secrete mucus and various antimicrobial peptides, such as defensins, lysozyme and REG3γ, to further keep bacteria away from host tissue (Mukherjee et al., 2008). In addition, the intestine is equipped with a powerful immune system which actively combats invading bacteria (Duerkop et al., 2009). In return, the commensal bacteria help the host with food digestion, provide essential fermentation products and metabolites to the host, and are closely involved in training the immune and metabolic systems of the host (Barratt et al., 2017). Due to the scope of my dissertation, I will focus on discussing the close relationship between the microbiota and host metabolism.

Food digestion and fermentation

The human diet is a mixture of carbohydrates, protein, fat, fiber and minerals. The host digestive system provides a variety of enzymes, such as protease, lipase, amylase and nuclease, to break down high molecular weight dietary components into smaller molecules that can be absorbed and used by the body (Mukherjee, 2003). However, there are some dietary components, such as certain fibers, oligosaccharides, starches and sugars, that cannot not be digested by the host alone, but require facilitation by commensal bacteria. This is because some groups of commensal bacteria are capable of fermenting those non-digestible ingredients and converting them into small water-soluble molecules, such as short-chain fatty acids (SCFAs), which are accessible to the human body (Clarke et al., 2014). The involvement of commensal bacteria in food digestion is critical for the host to efficiently acquire energy from the diet. Data have suggested that germ-free mice, which are raised in a complete sterile environment need to consume 30% more calories to maintain the same body weight as compared to conventional raised mice (Hooper and Gordon, 2001).

Other metabolites and vitamins produced by commensal bacteria are also essential for maintaining host health. Bile acid metabolites, such as cholate, hycholate and deocycholate, facilitate lipid absorption and regulate systemic glucose, cholesterol and energy homeostasis (Hylemon et al., 2009). Choline metabolites, such as methylamine, trimethylamine-N-oxide and dimethylglycine are involved in nonalcoholic fatty liver disease, obesity and cardiovascular disease (Zeisel and Blusztajn, 1994). Indole derivatives, including indoleacetate, indoxyl sulfate, melatonin and serotonin have been shown to modulate expression of anti-inflammatory genes and protect intestinal tissue from stress-induced lesions (Lee et al., 2015). Vitamin K, vitamin B12, biotin, folate, and thiamine produced by *Bifidobacterium* strengthen host immune functions and exert epigenetic effects to regulate cell proliferation (Nicholson et al., 2012).

Short-chain fatty acids (SCFAs)

SCFAs are the major end products of bacterial fermentation of carbohydrates and proteins in the intestine. The predominant SCFAs produced by commensal bacteria include butyric acid, acetic acid and propionic acid (Besten et al., 2013). Bacterial species that produce SCFAs include *Eubacterium, Roseburia, Faecalibacterium* and *Coprococcus* belonging to Clostridial clusters IV and XIVa of *Firmicutes* (Nicholson et al., 2012). SCFAs have been shown to play critical roles in many aspects of human health. For example, butyrate is the primary energy source for colonic cells. It provides about 70% of energy used for maintaining colonic cell proliferation and growth (Zeng, 2014). Butyrate also has anti-inflammatory as well as anti-carcinogenic properties (Nicholson et al., 2012; Rivera-Chávez et al., 2016). Addition of butyrate acid tumor cell lines can inhibit the growth and proliferation of those cells (Prasad, 1980). Studies have also suggested a correlation between butyrate and insulin resistance. Mice given extra butyrate are relieved from

high-fat diet induced insulin resistance and obesity, thus hinting at the involvement of butyrate in lipogenesis in adipose tissue and muscle tissue (Gao et al., 2009). Other beneficial roles provided by SCFAs include pathogen growth inhibition, stimulation of water and sodium absorption, promotion of cholesterol synthesis and tuning colonic environmental pH (Besten et al., 2013; Nicholson et al., 2012).

Germ-free mice

Gnotobiotic mice, or germ-free mice are raised in a completely sterile environment from birth. This microbe-free condition of these mice makes them an ideal model for studying the relationship between the microbiota and metabolism. As mentioned above, germ-free mice require 30% more calories to maintain the same body weight as conventionally-raised mice. This is because they are unable to fully digest and absorb nutrients from the diet without the help of commensal bacteria (Hooper and Gordon, 2001). In addition to this, germ-free mice also exhibit reduced body fat mass as compared to their conventionally-raised counterparts, even when both groups are fed *ad libitum* and have the same body weight. Notably, reduced body fat in germ-free mice can be rescued when they are transplanted with feces from conventional mice (Bäckhed et al., 2004).

More striking metabolic phenotypes can be observed when germ-free mice are fed a high-fat diet (HFD). As compared to conventional mice, germ-free mice only gain a modest amount of body weight and body fat mass, and do not show symptoms of obesity, such as insulin resistance, fatty liver or hyperglycemia, after 10 weeks of HFD feeding (Bäckhed et al., 2007; Rabot et al., 2010a). These findings suggest that germ-free mice are protected from HFD-induced obesity and indicate a crucial role for the microbiota in regulating lipid metabolism and fat accumulation in the body.

Several studies have tried to illuminate the underlying mechanisms of microbiota-regulated body fat accumulation. So far, a few proteins have been identified as being involved in this regulatory process. These proteins include Angiopoietin-like 4 (ANGPTL4), which inhibits the activity of lipoprotein lipase (LPL) (Bäckhed et al., 2007); Fatty acid binding protein 4 (FABP4), which is a fatty acid transporter expressed in epithelial cells (Su et al., 2015); and Farnesoid X receptor (FXR), which suppresses the activity of cholesterol 7 α-hydroxylase (CYP7A1), the rate-limiting enzyme in bile acid synthesis from cholesterol (Parséus et al., 2016). However, these findings can only partially and indirectly explain the causality of microbiota-regulated body fat accumulation. More detailed mechanisms need to be unraveled to fully explain the interactions between the microbiota and lipid metabolism.

The microbiota and obesity

The intestinal microbiota is a complex bacterial community that consists of hundreds of different species of bacteria. The four most dominant bacterial phyla are *Firmicutes, Bacteroidetes, Actinobacteria* and *Proteobacteria*. These four phyla combined make up >95% of total intestinal bacteria (Mahowald et al., 2009). The composition of the intestinal microbiota varies among people, and is highly dependent on factors such as the diet, the maternal microbiota and living in a community (Murphy et al., 2010; Turnbaugh et al., 2009a). Nevertheless, a sequencing-based study has revealed that the microbiota composition of an individual person can be stable over the long term (Faith et al., 2013). Though studies on germ-free mice have suggested a direct causal relationship between the microbiota and lipid metabolism as mentioned above, the composition of the microbiota has also been shown to closely relate to the occurrence of obesity and other metabolic diseases.

Large scale sequencing and metagenomics studies have repeatedly revealed alterations of microbiota composition in obese individuals as compared to lean individuals. The most dramatic alterations seen in the majority of obese individuals are a reduction in the proportion of the *Bacteroidetes* phylum and an elevation in the proportion of the *Firmicutes* phylum percentage (Greiner and Bäckhed, 2011; Turnbaugh et al., 2006). This observation makes the ratio of *Bacteroidetes* and *Firmicutes* an important hallmark for obesity. Later studies have indicated that the abundance of *Bacteroidetes* can be rapidly and reproducibly altered by diet and body weight, whereas the abundance of *Firmicutes* is more dependent on individual's genetic background (David et al., 2015; Goodrich et al., 2014). In addition, obese individuals exhibit a significant reduction of total bacterial number, as well as microbial diversity (Turnbaugh et al., 2009b). These alterations suggest that the microbiota is a potential causal factor in obesity.

A study led by Dr. Jeffery Gordon first demonstrated a causal effect of the microbiota in inducing obesity. In that study, feces from twin sister discordant for obesity were collected by the researchers. When feces from the obese twin were transplanted into germ-free mice, those mice quickly adapted to the fecal microbiota and rapidly gained body weight and body fat. They eventually exhibited obese phenotypes even when they were fed a normal low-fat chow. In contrast, germ-free mice transplanted with feces from the lean twin maintained a lean phenotype throughout the experiment (Ridaura et al., 2013). Interestingly, the increased adiposity of germ-free mice that received obese feces was prevented if they were co-housed with lean feces recipients. This suggested that the lean microbiota is more likely to transmit between individuals and is more efficient in colonizing the intestine (Ridaura et al., 2013). A follow-up study has further confirmed this conclusion (Griffin et al., 2016).

The microbiota and insulin resistance

Insulin resistance is the predominant feature of type 2 diabetes (T2D). In T2D patients, the adipose tissue usually exhibits elevated infiltration of macrophages and increased production of pro-inflammatory cytokines, such as IL-1β, IL-6 and TNF-α (Weisberg et al., 2003). This suggests the involvement of innate immunity in initiating insulin resistance and T2D. The trillions of bacteria in the intestinal lumen provide constant and diverse stimuli, such as lipopolysaccharide (LPS), flagella fragments, and peptidoglycan that activate the innate immune system and trigger pro-inflammatory cytokine secretion. Indeed, LPS infusion is sufficient to initiate insulin resistance through TLR-4 activation in mice (Cani et al., 2007). HFD feeding increases plasma endotoxin levels in mice (Cani et al., 2008). Mono-association of germ-free mice with the LPS producing bacterial species *Enterobacter cloacae,* in combination with HFD feeding, efficiently induces obesity and insulin resistance (Fei and Zhao, 2012). Therefore, LPS produced by Gram-negative bacteria in the intestine has been considered as a prerequisite for initiation of insulin resistance and T2D. However, the underlying mechanism is still unclear.

THE CIRCADIAN CLOCK AND METABOLISM

The circadian clock is the internal biological clock system that synchronizes biological activities to the everyday 24-hour day-night cycle. This internal clock system has been found to exist in all kinds of living organisms, including bacteria (Clodong et al., 2007), plants (Dodd et al., 2005), insects (Panda et al., 2002), invertebrates (Sehgal, 1995) and mammals (Takahashi et al., 2008a). A finely-tuned circadian clock system is essential to maintain systemic homeostasis. In mammals, a dysregulated or disturbed circadian clock has been linked to many immune and metabolic diseases, such as inflammatory bowel disease (IBD) (Yu et al., 2013), rheumatoid arthritis

(Arvidson et al., 1994), type 2 diabetes (Saini et al., 2016), obesity (Turek et al., 2005), cardiovascular disease (Scheer et al., 2009), and even some types of cancer (Sancar et al., 2015). The mammalian circadian clock machinery can be found in almost every cell in the body. In order to synchronize information about circadian timing and to coordinate biological activities in all cells, a two-level hierarchical system, consisting of the central clock and the peripheral clock, has been evolved (Mohawk et al., 2012).

The central clock, which is located in the hypothalamic suprachiasmatic nucleus (SCN), is the master circadian controller driving behavioral rhythms in the body. The SCN is composed of over 20,000 neurons, each of which is thought to contain cell-autonomous circadian oscillating machinery (Welsh et al., 2010). The SCN generates circadian rhythms primarily based on the dominant environmental timing cue: light. When environmental light is captured by the intrinsically photoreceptive retinal ganglion cell (ipRGC) on the retina, the photic input is directly conveyed to activate the SCN neurons through the retinohypothalamic tract (RHT) (Do and Yau, 2010). The activated SNC neurons then pass this timing signal to peripheral tissues through neural transmitters, hormones or body temperature (Mohawk et al., 2012).

Peripheral clocks are cell autonomous clock oscillators located in virtually all non-SCN cells, tissues and organs, such as liver, lung, adipose tissue, kidney and intestine etc. (Mohawk et al., 2012). Peripheral tissues cannot receive environmental light stimulation directly. Instead, they synchronize to the central clock by receiving master timing signals provided by SCN. As mentioned, SCN regulation of peripheral clocks can occur via neural transmitters, hormones or body temperature. For example, the dominant entraining signal for the submandibular salivary glands is provided through paraventricular nucleus-superior cervical ganglia (PVN-SCG) (Mohawk et al., 2012; Vujovic et al., 2008); rhythmic glucocorticoid (GC) production is controlled

by both hypothalamus-pituitary-adrenal axis (HPAA) and adrenal rhythmic steroid secretion (Son et al., 2008); peripheral clocks in liver, kidney, lung and fibroblasts are sensitive to temperature changes and can be reset by low-amplitude temperature pulses (Brown et al., 2002; Mohawk et al., 2012). In addition to these master entraining signals from the SCN, peripheral clocks can also be reset by local timing cues, such as food intake, locomotor activity, diet, or drugs. For example, the liver clock is particularly sensitive to feeding patterns. Rearranging feeding times can rapidly shift the phase of rhythmic expression of hepatic genes and proteins (Damiola et al., 2000; Stokkan et al., 2001).

Molecular regulation of the core circadian clock

The cell autonomous circadian clock machinery is an autoregulatory negative-feedback transcriptional network (FIGURE 1) (Lowrey and Takahashi, 2004; Nader et al., 2010). The main circadian regulatory negative-feedback loop comprises the basic helix-loop-helix-PER-ARNT-SIM (PAS) transcriptional activators brain and muscle Arnt-like protein-1 (BMAL1) and CLOCK, as well as Period (PER1 and PER2) and Cryptochrome (CRY1 and CRY2) (King et al., 1997; Kume et al., 1999; Takahashi et al., 2008a). BMAL1 and CLOCK form a heterodimer and activate the transcription of *Per* and *Cry* during the daytime. The PER and CRY proteins also form a heterodimer and translocate into the nucleus to repress the transcription and activity of the BMAL1:CLOCK complex during the night (Koike et al., 2012; Lee et al., 2001). The phosphorylated PER and CRY proteins are progressively ubiquitinated by specific E3 ligase and are eventually degraded by the proteasome (Koike et al., 2012; Shirogane et al., 2005). Once the abundance of PER and CRY gradually decrease in the cytoplasm, the transcription of BMAL1 and

CLOCK increase accordingly. This rhythmic expressional oscillation of BMAL1/CLOCK and PER/CRY make up the core of the circadian clock machinery.

In addition to PER and CRY, BMAL1:CLOCK complex can activate a variety of other transcription factors, which also feed back to regulate the transcription of *Bmal1,* and form auxiliary circadian regulatory feedback loops (FIGURE 1). These include, but are not limited to, the reverse strand of c-erbA-encoded protein alpha/beta (REV-ERBα/β), a transcriptional repressor; retinoic acid receptor-related orphan nuclear receptor alpha/gamma (RORα/γ), a transcriptional activator; peroxisome proliferator activated receptor alpha (PPARα), a transcriptional activator; D-box binding protein (DBP), a transcriptional activator; and peroxisome proliferator-activated receptor gamma coactivator 1-aplpha (PGC1α), a transcriptional activator (Bass and Takahashi, 2010; Nader et al., 2010).

The core circadian machinery is also fine-tuned by additional mechanisms. For example, the CRY proteins can be targeted by adenosine mono-phosphate (AMP) for degradation through the SCF/FBXL3 ubiquitin ligase (Takahashi et al., 2008b); the PER proteins can be targeted by Casein kinases (CK1δ and CK1ε) for degradation through Skp1, Cullins, F-box protein (SCF)/b-TrCP ubiquitin ligase complex (Gallego and Virshup, 2007; Takahashi et al., 2008b); the REV-ERB proteins can be phosphorylated and stabilized by glycogen synthase kinase 3 beta (GSK-3β) (Yin et al., 2006); the serine/threonine protein phosphatase 5 (PP5) interacts with CRY to regulate its phosphorylation state (Gallego and Virshup, 2007; Partch et al., 2006); Sirtuin 1 (SIRT1), an NAD^+-dependent protein deacetylase rhythmically binds to the BMAL1:CLOCK complex and promotes the deacetylation and degradation of PER2 (Asher et al., 2008). These post-translational regulatory mechanisms feed into to the main and auxiliary feedback loops to build a precisely controlled core circadian machinery.

Circadian regulation of lipid metabolism

Lipid metabolism is tightly controlled by the circadian clock in order to coordinate with sleep-wake and feeding cycles. In the liver and adipose tissue, the expression of major lipid metabolic proteins are diurnally oscillating. For example, PPARα, which promotes mitochondrial fatty acid β-oxidation is directly regulated by BMAL1:CLOCK complex(Liu et al., 2013); cholesterol 7α-hydroxylase (CYP7A1), which is a rate-limiting enzyme for cholesterol and bile acid synthesis loses expressional rhythmicity in *Rev-erbα*$^{-/-}$ mice (Duez et al., 2008); adipose TAG lipase (ATGL) and hormone-sensitive lipase (HSL), which are rate limiting enzymes for lipolysis and hydrolysis exhibit disturbed diurnal variations in both *Clock* or *Bmal1* mutant mice (Shostak et al., 2013; Haemmerle et al., 2006). The circadian regulation of key enzymes involved in lipid synthesis and metabolism in liver and adipose tissue leads to diurnal oscillations of circulating nonesterified fatted acids (NEFA) (Pan and Hussain, 2009).

In the intestine, transcriptional analysis of intestinal epithelial cells, where dietary lipids are absorbed and initially processed, reveals diurnal rhythms in the expression of many genes involved in lipid absorption and metabolism, such as apolipoprotein AIV (*Apoa4*), apolipoprotein B (*Apob*), fatty acid binding protein (*Fabp*) and microsomal triglyceride transport protein (*Mttp*) (Bailey et al., 2014; Pan and Hussain, 2009). Genetic mutation of the core circadian clock protein CLOCK in mice results in similar micronutrient uptake between the light phase and dark phase in mice (Hoogerwerf et al., 2007). Deletion of nocturnin, a circadian deadenylase that plays a crucial role in regulating chylomicron export protects mice from high-fat diet induced obesity (Douris et al., 2011). These findings establish that lipid uptake and metabolism in the intestine is regulated by the circadian clock.

Circadian regulation of glucose metabolism

Although systemic glucose levels are highly dependent on insulin secretion induced by food consumption, there is also evidence for insulin-independent regulation of circulating glucose through the circadian clock. First, blood glucose levels in both human and mice will increase in the morning before waking and feeding (Bolli and Gerich, 1984). Second, fasting rats does not halt the diurnal fluctuation of circulating blood levels (La Fleur et al., 1999). Third, surgical removal of the SCN disrupts glucose homeostasis even in mice are fed *ad libitum* (La Fleur et al., 1999). Fourth, CLOCK protein mutation or BMAL1 protein knockout in mice suppresses the diurnal variation in glucose and triglycerides (Rudic et al., 2004).

Indeed, many important enzymes involved in glycogenesis and gluconeogenesis are regulated by the hepatic circadian clock. Uridine diphosphate glucose (UDP)-glucose-glycogen glucosyltransferase, a key enzyme that catalyzes the reaction of UDP-glucose and (1,4-α-D-gluosyl)$_n$ to form UDP and (1,4-α-D-gluosyl)$_{n+1}$, exhibits its maximum level during the dark phase in mice (Pan and Hussain, 2009). In contrast, glycogen phosphorylase, a rate limiting enzyme that converts terminal α-1,4-glycosidic bonds into glucose-1-phosphate exhibits peak levels during the light phase in mice (Ishikawa and Shimazu, 1980; Pan and Hussain, 2009). Moreover, phosphoenolpyruvate carboxykinase (PEPCK), a key enzyme in gluconeogenesis that converts oxaloacetate into phosphoenolpyruvate and carbon dioxide exhibits diurnal rhythms in its expression in liver (Kida et al., 1980). Later studies suggested that the rhythmic expression of PEPCK is governed by hepatic BMAL1 (Lamia et al., 2008).

Notably, insulin secretion itself also has been shown to be regulated by the circadian clock. Mice with a pancreas-specific deletion of *Bmal1* exhibit severe glucose intolerance and defective insulin secretion (Sadacca et al., 2010). The phase of oscillation of pancreatic islet genes involved

in insulin signaling is delayed in both *Clock* and *Bmal1* mutant mice (Marcheva et al., 2010). *Clock* disruption leads to impaired glucose tolerance, reduced insulin secretion and defects in size and proliferation of pancreatic islets (Marcheva et al., 2010). Thus，circadian regulation is a critical mechanism for regulating systemic glucose and insulin homeostasis.

Reciprocal regulation between the circadian clock and metabolism

Though physiological behaviors are precisely controlled by the circadian clock to follow the day-night light cycle, some metabolic activities or metabolites can modify the output from the circadian clock. One example is learned from NAD^+ (nicotinamide adenine dinucleotide) metabolism. NAD^+ is a coenzyme involved in redox reactions. Electron transfer reactions between NAD^+ and NADH allow it to become an important substrate for enzymes involved in posttranslational modification (Belenky et al., 2007). NAD^+ is synthesized and regenerated from nicotinamide by the enzyme nicotinamide phosphoribosyltransferase (NAMPT). This process is activated by the BMAL1:CLOCK complex, and thus the NAD^+ concentration in cells exhibit diurnal oscillation across the day-night cycle (Ramsey et al., 2009). This is consistent with the fundamental role of the circadian clock in regulating metabolic activities. However, studies also indicate that rhythmic formation of BMAL1:CLOCK heterodimers is markedly influenced by NAD^+/NADH redox status (Bass and Takahashi, 2010; Kalsbeek et al., 2008). The rhythmic synthesis of NAD^+ results in circadian oscillation of the NAD-dependent protein deacetylase SIRT1 in the cytosol. This oscillation of cytosolic SIRT1 is crucial for maintaining a high-amplitude of circadian expression of key circadian genes, such as *Baml1, Cry1, Per2 and Rorγ* by directly binding to the BMAL1:CLOCK complex and promoting deacetylation and degradation of PER2 (Asher et al., 2008; Nakahata et al., 2009).

Interactions between the microbiota and the circadian clock

Recent studies have revealed close interactions between the microbiota and the circadian clock. The microbiota composition in both human and mice exhibits diurnal variations that driven by feeding rhythms. This diurnal compositional change drives global programming of the host circadian, epigenetic and metabolite oscillations (Leone et al., 2015a; Thaiss et al., 2016). Notably, ablation of host circadian clock components PER1 and PER2, or induction of jet-lag in mice disturbs normal feeding rhythmicity and leading to disrupted microbiota compositional fluctuations and metabolic dysregulations, such as glucose intolerance and obesity (Thaiss et al., 2014). Moreover, HFD feeding profoundly alters oscillatory transcriptional programs in the liver, as well as composition of intestinal microbiota (Eckel-Mahan et al., 2013; Murakami et al., 2016). The alteration of hepatic circadian transcriptional programs has been shown to require microbiota-driven expression of PPARγ, as seen in antibiotic treated mice which are protected from this alteration (Murakami et al., 2016). These evidences have clearly demonstrated the reciprocal interactions between the microbiota and the circadian clock, and have suggested profound consequences and physiological importance of these interactions.

As mentioned in previous section, mice raised in a germ-free condition do not gain as much body weight and body fat as conventionally raised mice when fed a HFD (Bäckhed et al., 2004; Rabot et al., 2010b). In addition to this, a recently study has further revealed a markedly impaired central and peripheral clock gene expression in germ-free mice (Mukherji et al., 2013). This provides additional evidence that indicates essential interactions between the microbiota and the circadian clock in regulating metabolism, and is also the starting point of my dissertation, the goal of which is to understand the molecular basis of these interactions.

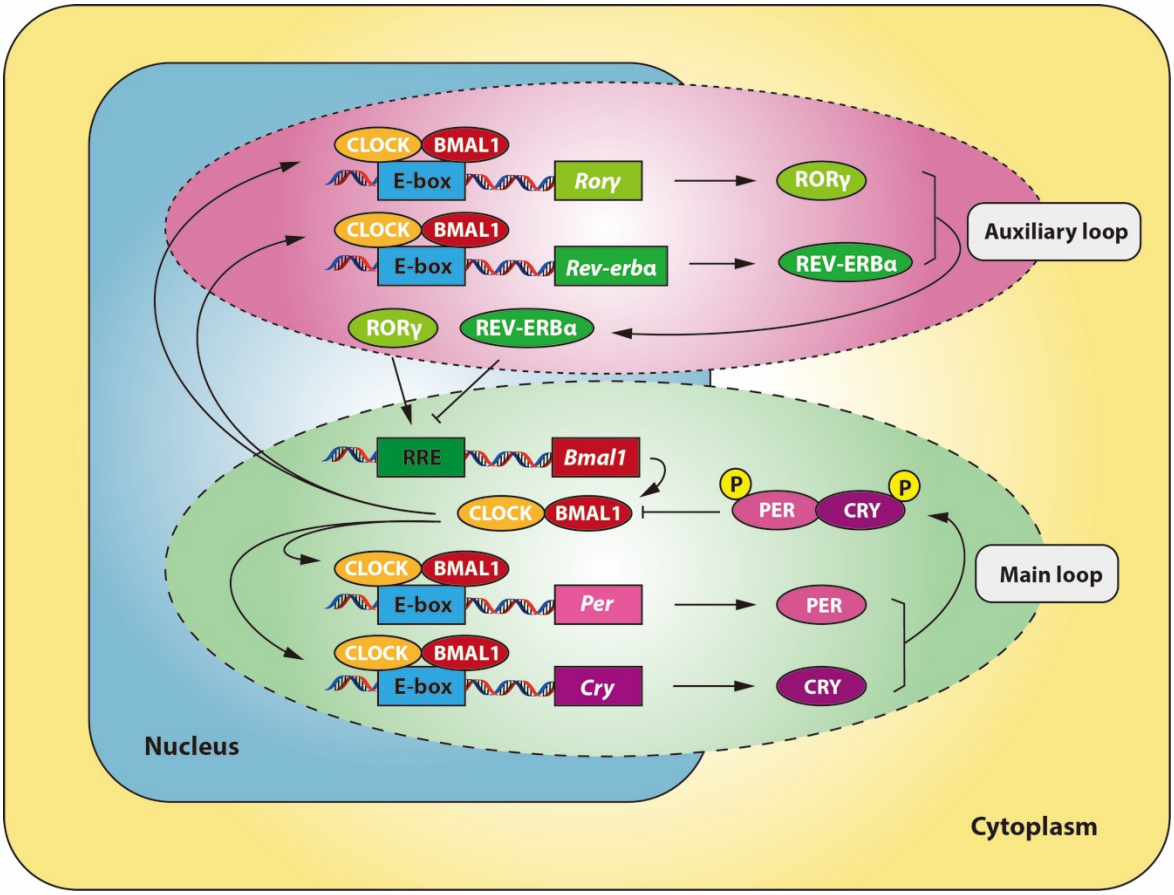

FIGURE 1: Molecular regulation of the mammalian circadian clock

Schematic illustration of the molecular basis of the circadian clock in mammalian cells (modified from [Nader et al., 2010]). In the main loop, the BMAL1:CLOCK complex activates PER and CRY, which then form a dimer to inhibit the activity of BMAL1:CLOCK. In the auxiliary loop, the BMAL1:CLOCK complex activates REV-ERBα and RORγ, which repress or activate the transcription of *Bmal1* respectively. These feedback loops work together to generate the circadian rhythms in mammalian cells.

CHAPTER TWO

MATERIALS AND METHODS

Mice

C57BL/6 wild-type mice were bred and maintained in the SPF barrier at the University of Texas Southwestern Medical Center. *Rev-erbα*$^{-/-}$ mice (B6.129S2-*Nr1d1*^{tm1Shcb}/Cnrm) were initially obtained from the European Mutant Mouse Archive. *Cd11c*-DTR (B6.FVB-Tg(*Itgax*-DTR/EGFP)57Lan/J), *Myd88*$^{-/-}$ (B6.129P2(SJL)-*Myd88*$^{tm1.1Defr}$/J), *Rag1*$^{-/-}$ (B6.129S7-Rag1^{tm1Mom}/J), *Rorc*$^{gfp/gfp}$ (B6.129P2(Cg)-*Rorc*^{tm2Litt}/J), *Id2*$^{gfp/-}$ (B6.129S(Cg)-*Id2*$^{tm2.1Blh}$/ZhuJ), *Stat3*$^{fl/fl}$ (B6.129S1-*Stat3*^{tm1Xyfu}/J), *Myd88*$^{fl/fl}$ (B6.129P2(SJL)-*Myd88*^{tm1Defr}/J), *Villin*-cre (B6.Cg-Tg(*Vil1*-cre)997Gum/J) and *Cd11c*-cre (B6.Cg-Tg(*Itgax*-cre)1-1Reiz/J) mice were purchased from Jackson Laboratory. *Nfil3*$^{fl/fl}$ mice were obtained from Dr. Masato Kubo at RIKEN Institute in Japan (Motomura et al., 2011). *Nfil3*$^{\Delta IEC}$, *Stat3*$^{\Delta IEC}$ and *Myd88* $^{\Delta IEC}$ mice were generated by crossing *Nfil3*$^{fl/fl}$, *Stat3*$^{fl/fl}$ or *Myd88*$^{fl/fl}$ mouse with a mouse expressing Cre recombinase under the control of the intestinal epithelial cell-specific *Villin* promoter (*Villin*-cre mouse) (Madison et al., 2002). *Myd88*$^{\Delta DC}$ mice were generated by crossing *Myd88*$^{fl/fl}$ mouse with a mouse expressing Cre recombinase under the control of the dendritic cell-specific *Villin* promoter (*Cd11c*-cre mouse) (Caton et al., 2007). Germ-free C57BL/6 mice were bred and maintained in the gnotobiotic mouse facility at the University of Texas Southwestern Medical Center as described (Cash et al., 2006). 6-14 week old mice were used for all experiments. Male mice wereused for all metabolic studies. All mice were housed under a 24 hour light:dark cycle, with lights on for 12 hours (Zeitgeber times [ZT] 0-12). Mice were fed *ad*

libitum. All experiments were performed using protocols approved by the Institutional Animal Care and Use Committees of the UT Southwestern Medical Center.

Diet

Regular chow diet (5KA1) containing 22% protein, 16% fat and 62% carbohydrates was purchased from LabDiet. Western style high-fat diet (AIN-76A) containing 16% protein, 40% fat and 44% carbohydrates was purchased from TestDiet. The regular chow diet was sterilized by autoclaving, high-fat diet was sterilized by irradiation.

Antibodies, cytokines and chemicals

Anti-NFIL3 antibody was produced in rabbits by Pacific Immunology (Ramona, CA). The peptide sequence used as epitope was: Cys-RSPENKFPVIKQEPVELESFAREAREER (29aa). Anti-REV-ERBα antibody (PA5-29865), anti-CD36 antibody (PA1-16813) and anti-STAT3 antibody (06-596) were purchased from ThermoFisher. Anti-STAT3 antibody (4904S) and anti-phospho-STAT3 antibody (9131S) were purchased from Cell Signaling. Anti-αTubulin antibody (ab4074) and anti-SDHA (Mito 70) antibody (ab14715) were purchased from Abcam. Recombinant mouse IL-23 (589004) and IL-22 (576206) were purchased from BioLegend. Diphtheria toxin from *Corynebacterium diphtheriae* (D0564) was purchased from Sigma. STAT3 inhibitor Stattic (sc-202818) was purchased from Santa Cruz. Flagellin from *Salmonella typhimurium* (SRP8029) and Lipopolysaccharides from *Salmonella enterica* serotype enteritidis (L2012) were purchased from Sigma-Aldrich.

Body composition analysis

Mouse body composition was analyzed by an EchoMRI™-100H analyzer (Taicher et al., 2003). I first calibrated the system by running a test scan with the system calibration tube. I then recorded mouse body weight and then put mouse into the measuring tube and started the scan after placing the tube into the analyzer.

Glucose tolerance test

Mice were fasted overnight before the glucose tolerance test. On the day of the test, the initial blood glucose level was first recorded using a OneTouch Ultra2 blood glucose meter. Then mice were intraperitoneally injected with 2 mg/gram body weight of D-(+)-glucose solution (Sigma-Aldrich G8769). Blood glucose was monitored and recorded at 15, 30, 60, 90 and 120 minutes after glucose injection.

Insulin tolerance test

Mice were fasted overnight before the insulin tolerance test. On the day of the test, the initial blood glucose level was first recorded using a OneTouch Ultra2 blood glucose meter. Then mice were intraperitoneally injected with 0.5 U/kg body weight insulin (Eli Lilly, Humulin R [U-100]). Blood glucose was monitored and recorded at 15, 30, 60, 90 and 120 minutes after insulin injection.

Real-time metabolic chamber analysis

Real-time metabolic chamber analysis was conducted using the TSE Labmaster System (Tasan et al., 2009) and was performed by Metabolic Phenotyping Core at the University of Texas

Southwestern Medical Center. In brief, 12 age- and gender-matched mice were housed separately and were acclimated in the metabolic chamber for 5 days. On day 6, metabolic activities were monitored and recorded continuously for 5 days. The following metabolic parameters were recorded: food consumption, water consumption, movement, heat production, oxygen consumption and carbon dioxide production.

Serum triglyceride quantification

Mice were fasted overnight before blood collection. The following morning, blood was collected through facial vein bleeding. Serum was separated using a Z-Gel serum separation tube (SARSTEDT 41.1378.005). The serum was used for triglyceride quantification immediately or frozen at -80^{o}C until use. Serum triglycerides were quantified using Triglycerides Liquid Stable Reagent (Thermo Scientific TR22421) according to the manufacturer's manual. Data were acquired by a SpectraMax M5e multi-mode microplate reader (Molecular Device LLC).

Microbiota depletion using antibiotics

An antibiotic cocktail was prepared by dissolving 1 gram neomycin sulfate (Research Products International 1405-10-3), 1 gram gentamicin sulfate (Research Products International 1405-41-0), 1 gram metronidazole (Research Products International 443-48-1), 1 gram streptomycin sulfate (Research Products International 3810-74-0) and 0.5 gram vancomycin hydrochloride (Research Products International 1404-93-9) in 1 liter drinking water. Mice were maintained on antibiotic water throughout the high-fat diet treatment. Antibiotic water was replenished every two weeks. To evaluate the efficiency of the microbiota depletion, fresh feces were collected and homogenized in sterile PBS. The homogenate was soun down to precipitate food debris, and 50 μL of the

supernatant was spread onto a pre-warmed BHI-5% calf blood agar plate. The plate was incubated at 37^{o}C for overnight in an anaerobic GasPak jar (BD 260626) with GasPak EZ anaerobe container system sachets (BD 260678).

Laser capture microdissection and RNA purification

The laser capture microdissection protocol was adapted and modified from one that was previous described (Stappenbeck et al., 2002). To prepare a frozen tissue sample, 5 cm of fresh distal small intestine was taken and thoroughly flushed with ice-cold PBS using a syringe to remove luminal contents. The intestinal lumen was then filled with optimum cutting temperature compound (OCT) (Fisher Scientific 23-730.571) using a gavage needle. OCT-filled intestinal tissue was embedded into a Cryomold (Tissue-Tek 4557) filled with OCT, and was snap frozen in liquid Cytocool (Thermo Scientific 8323) then stored at -80 ^{o}C.

To make frozen sections, frozen intestinal tissue embedded in OCT was taken out from -80 ^{o}C and placed at -20 ^{o}C for 20 minutes to warm up. Frozen tissue was then transferred into a Cryostat (Leica CM1950) and was cut into 7 μm sections according to the manufacturer's manual. Frozen sections were stored at -80 ^{o}C.

To perform laser capture microdissection, frozen tissue sections were removed from -80 ^{o}C and thawed at room temperature for 1 minute. Thawed tissue section was first fixed in 70% ethanol for 1 minute followed by 10 dips in distilled water. Fixed tissue sections were then stained with methyl green for 10 seconds and washed in two changes of distilled water. Methyl green stained tissue sections were then rinsed in 70% ethanol followed by 90% ethanol, and stained with eosin for 10 seconds followed by two washes in 90% ethanol. Eosin-stained sections were rinsed in 100% ethanol for 1 minute and dehydrated in two changes of xylene. The freshly stained

sections were immediately used for laser capture microdissection of intestinal epithelial cells using an Arcturus PixCell IIe system according to manufacturer's instructions, and 5,000-10,000 pulses (cells) were obtained from each section.

To extract total RNA from isolated intestinal epithelial cells, 14 μl RNA Extraction Buffer from the PicoPure RNA Isolation Kit (Life Technology 12204-01) was immediately added onto freshly isolated cells. Cells were incubated at 42 ^{o}C for 30 min for complete RNA extraction. Extracted RNA was purified using PicoPure RNA Isolation Kit following the manufacturer's protocol and stored at -80^{o}C until use. RNA quality and concentration were determined by Agilent 2100 Bioanalyzer or RiboGreen RNA Assay Kit (Thermo Fisher R11490).

Whole tissue RNA extraction

1 cm of fresh distal small intestine was taken and thoroughly flushed with ice-cold PBS using a syringe to remove luminal contents. Intestinal tissue was immediately used for RNA extraction and purification using a RNeasy Midi Kit (Qiagen 75144) according to the manufacturer's protocol, or snap frozen in liquid nitrogen and stored at -80^{o}C until use. RNA quality and concentration were determined by a NanoDrop 2000 spectrophotometer (Thermo Scientific).

cDNA synthesis and quantitative real-time PCR

Frozen RNA purified from isolated intestinal epithelial cells or whole intestinal tissue was thawed on ice. cDNA was synthesized from purified RNA using M-MLV Reverse Transcriptase (ThermoFisher 28025021) kit following the manufacturer's protocol. Quantitative real-time PCR (qRT-PCR) was performed using Platinum SYBR Green qPCR SuperMix-UDG (Thermo Fisher 11733046) on a QuantStudio 7 Flex Real-Time PCR System (Applied Biosystems) with default

setting. Relative expression values were determined using the comparative Ct (ΔΔCt) method (Schmittgen and Livak, 2008), and transcript abundances were normalized to *Gapdh* transcript abundance. Primer sequences are given in TABLE 1.

Chromatin immunoprecipitation (ChIP) assay

10 cm distal small intestine was flushed with ice-cold PBS. The intestine was cut open and sliced into ~0.5 cm pieces. Intestine pieces were washed intensively 3 times using ice-cold DPBS, and then incubated in DBPS containing 10 mM EDTA at 37 ^{o}C for 10 minutes with shaking at 250 RPM. Intestinal epithelial cells were released by vortex for 1 minute and the cell suspension was transferred into a new 50 mL conical. Cells were spun down at 300×g for 5 minutes and washed once with ice-cold PBS. Isolated intestinal epithelial cells were first fixed in 1% formaldehyde at room temperature for 10 minutes and quenched in 125 mM glycine on ice for 10 minutes. Cells were resuspended in 0.5 ml lysis buffer (20 mM Tris-HCl, pH 8, 60 mM KCl, 1 mM EDTA, 0.5% NP-40) and incubated at 4^{o}C for 15 minutes. Nuclei were pelleted at 800×g at 4^{o}C for 10 minutes and resuspended in 250 µl RIPA buffer (Thermo Scientific 89900) and sonicated using a Bioruptor Pico sonication device (Diagenode). The sonicated lysate was centrifuged at top speed for 10 minutes at 4^{o}C and the supernatant of the sonicated lysate was pre-cleared and incubated with 2.5 µg primary antibody (anti-REV-ERBα or anti-STAT3 depending on the experiment). After overnight incubation, 30 µl protein G magnetic beads were added and incubated for 1.5h at 4^{o}C. Beads were washed 6 times with LiCl wash buffer (100 mM Tris-HCl pH 7.5, 500 mM LiCl, 1% NP-40, 1% sodium deoxycholate). DNA was recovered in 150 µl of TES buffer (TE pH8.0 with 1% SDS, 150 mM NaCl, and 5 mM dithiothreitol) by resuspending the beads at 65°C for 8 hours. DNA samples were purified using ChIP DNA Clean & Concentrator (Zymo Research D5205).

Relative enrichment of promoters was calculated as the ratio of specific antibody pull-down to non-specific IgG pull-down. Primer sequences used for ChIP assay are given in Table 1.

Western blot

Intestinal epithelial cells were isolated from mouse ileum using 10 mM EDTA buffer as described above. Cells were resuspended in 0.5 ml lysis buffer (20 mM Tris-HCl, pH 8, 60 mM KCl, 1 mM EDTA, 0.5% NP-40) and incubated at 4^{o}C for 15 min. Nuclei were pelleted at 800×g at 4^{o}C for 10 minutes and resuspended in 250 µl RIPA buffer (Thermo Scientific 89900) and sonicated using a Bioruptor Pico sonication device (Diagenode). The sonicated lysate was centrifuged at top speed for 10 minutes at 4^{o}C and the supernatant of the sonicated lysate was separated in a 4-20% gradient SDS-PAGE gel (Biorad 4561093) using a Biorad Mini-PROTEAN® Tetra Vertical Electrophoresis Cell, then transferred to a PVDF membrane (Biorad 1704156) using a Biorad Trans-Blot Turbo Transfer System. Membranes were first blocked with 5% nonfat milk in TBS-T buffer (0.1% Tween-20 in Tris-buffered saline) at room temperature for 1 hour, then sequentially incubated with target-specific primary antibodies at 4^{o}C for overnight, and appropriate HRP-conjugated secondary antibodies at room temperature for 1 hour. Protein bands were visualized using a Bio-Rad ChemiDoc™ system.

Intestinal organoid culture

10 cm distal small intestine was taken and flushed with ice-cold PBS. The intestine was cut open and sliced into ~0.5 cm pieces. Intestine pieces were washed gently by pipetting using ice-cold DPBS for 15-20 times until clean, and then incubated in Gentle Cell Dissociation Reagent (StemCell 07174) at room temperature for 20 minutes with gentle shaking. Intestinal crypts were

released by vortex at medium speed and were filtered through a 70 μm cell strainer. Isolated crypts were centrifuged at 200×g for 5 minutes at 4°C and then washed 3 times using cold PBS containing 0.1% BSA. Crypts were resuspended in 10 ml DMEM/F12 medium and crypt number was counted using a hemocytometer. ~3000 crypts were centrifuged at 200×g for 5 minutes at 4°C. 150 μL complete IntestiCult Organoid Growth Medium (StemCell 06005) was added to the pellet together with an equal volume of Matrigel GFR Basement Membrane Matrix (Corning 356230). 50 μL of crypt/Matrigel suspension was carefully seeded onto the center of each well of a 24-well plate. The plate was incubated at 37°C for 10 min to set the Matrigel and then 600 μL of complete IntestiCult Organoid Growth Medium was added to each well. Crypts were grown at 37°C for organoid growth and organoid cultures were passaged every 7-10 days. Where indicated, 1 ng/mL recombinant IL-22 and/or 30 μM Stattic were added into the culture.

Mono-associations of germ-free mice and flagellin/LPS challenge

Age-matched germ-free mice were mono-colonized with 2×10^9 cfu log phage *Bacteroids thetaiotaomicron* (VPI-5482), *Enterococcus faecalis* (ATCC-29212), *E. coli* (K235, ATCC-13027) or *Escherichia coli* (O127:K63, ATCC-12740), or with 1×10^9 cfu log phase *Salmonella typhimurium* (strain 1433) through oral gavage. Mice were fed on sterile regular chow diet *ad libitum* and were giving free access to sterile drinking water. Fresh feces were collected and plated every day to monitor the colonization efficiency. Mice were sacrificed 3 days after colonization for tissue collection.

For flagellin challenge, age-matched germ-free mice were given 2 μg flagellin (Sigma-Aldrich SRP8029) every day for 3 days delivered through the retro-orbital vein and were sacrificed the following day after the last injection. For LPS challenge, age-matched germ-free mice were

given 500 μg LPS (Sigma-Aldrich L2012) every 12 hours for 3 days by oral gavage and were sacrificed 12 hours after the last treatment. Mice were fed on a regular chow diet *ad libitum* and were given free access to sterile drinking water for both challenges.

Luciferase assay

A 504 bp fragment of the *Rev-erbα* promoter was cloned into a pGL3-promoter firefly luciferase reporter vector (Promega E1761). 2×10^4 HEK-293T cells were seeded into each well of a 96-well plate one day before transfection. 50 ng of empty vector, wild-type STAT3-encoding vector (*Stat3* Flag pRc/CMV), or dominant active STAT3 (Stat3-C Flag pRc/CMV)-encoding vector were transfected together with 50 ng *Rev-erbα* promoter reporter vector and 10 ng Renilla reporter vector using FuGene HD Transfection Reagent (Promega 04709705001). 18 hours after transfection, luciferase activity was determined using the Dual-Glo Luciferase Assay System (Promega E2920) following the manufacturer's protocol. The Renilla luciferase co-reporter was used to normalize luciferase activity. *Stat3* Flag pRc/CMV (Addgene plasmid #8707) and *Stat3*-C Flag pRc/CMV (Addgene plasmid #8722) were kind gifts from Dr. James Darnell.

Oil Red O staining

2 cm of fresh distal small intestine was taken and thoroughly flushed with ice-cold PBS using a syringe to remove luminal contents. The intestinal lumen was then filled with optimum cutting temperature compound (OCT) (Fisher Scientific 23-730.571) using a gavage needle. OCT filled intestine tissue was embedded into a Cryomold (Tissue-Tek 4557) filled with OCT, and was snap frozen in liquid Cytocool (Thermo Scientific 8323) then stored at -80 ^{o}C. 7 μm frozen sections were cut and fixed in 10% buffered formalin for 1 minute at room temperature. Fixed slides were

washed with running water and rinsed with 60% isopropanol. Slides were then stained with a freshly prepared oil red O (Sigma O0625) working solution (60% of 0.5g/100mL oil red O stock solution dissolved in isopropanol, 40% distilled water) for 15 min at room temperature. Stained slides were rinsed in 60% isopropanol followed by 2 changes of water, and then stained with Methyl Green (Amsbio 4800-30-18) for 10 seconds to visualize nuclei. Images were captured using a Zeiss AxioImager M1 microscope.

Hematoxylin & Eosin (H&E) staining

Fresh small intestine or colon was taken and washed thoroughly using cold PBS. Tissues were fixed in Bouin's fixative (RICCA 1120-16) overnight at 4^{o}C, then washed with 50% ethanol multiple times until clean. Fixed tissues were paraffin embedded then cut into 7 μm sections on glass slides. Slides were sequentially stained with hematoxylin and eosin as described (Fischer et al., 2008). Images were captured using a Zeiss AxioImager M1 microscope.

Lipid quantification in intestinal epithelial cells

5 cm distal small intestine was taken, and all the fat tissue attached to the intestine was carefully removed. Intestinal epithelial cells were isolated from the ileum using 10 mM EDTA as described above. Isolated epithelial cells were weighed and 10 mg (wet weight) epithelial cells were used for lipid extraction using a Lipid Extraction Kit (Cell Biolabs STA-162). Extracted lipids were air dried and resuspended in 50 μl cyclohexane. Epithelial lipids were quantified using a Lipid Quantification Kit (Cell Biolabs STA-613) and a SpectraMax M5e multi-mode microplate reader (Molecular Device LLC).

Neutral lipid quantification in fecal pellets

Fresh feces were collected and weighed. Fecal lipids were extracted using a Lipid Extraction Kit (Cell Biolabs STA-162). Extracted lipids were air dried, resuspended in 100 µl isopropanol, and quantified using a Lipid Quantification Kit for neutral lipids (Cell Biolabs STA-617) and a SpectraMax M5e multi-mode microplate reader (Molecular Device LLC).

RNA sequencing and data analysis

Small intestine samples at 6 time points (4 hours apart, 3 samples for each time point) across a circadian cycle were collected. RNA was extracted and purified from intestinal epithelial cells isolated by laser capture microdissection as described above. Laser captured epithelial cells from 3 mice were pooled together for RNAseq at each time point. RNA quality was assessed by an Agilent 2100 Bioanalyzer. Sequencing libraries were prepared using the TruSeq RNA sample preparation kit v2 (Illumina). Sequencing was performed on an Illumina HiSeq 2500 for signal end 50 bp length reads. Sequence data were mapped against the mm10 genome using TopHat and FPKMs were generated using Cuffdiff with default parameters. Altered expression was defined as a >2-fold increase or decrease in average FPKM reads over all 6 time points compared between the two groups.

16S rRNA sequencing and data analysis

Fecal DNA was extracted and purified from freshly collected feces using the FastDNA Spin Kit (MP Biomedicals 116560-200) and a FastPrep-24 5G Homogenizer. Sequencing libraries were prepared using the HotStarTaq Plus Master Mix Kit (Qiagen) with primers flanking variable regions V3-V4. Sequencing was performed on a MiSeq following the manufacturer's guidelines.

Operational taxonomic units (OTUs) were defined by clustering at 3% divergence (97% similarity). Final OTUs were taxonomically classified using BLASTn against a curated database derived from RDPII and NCBI.

Recombinant IL-23 and IL-22 treatment

Myd88$^{-/-}$ mice were injected intraperitoneally with 1.5 μg of carrier-free recombinant mouse IL-23 (BioLegend 589006) or IL-22 (BioLegend 576206) every other day for a total of 4 treatments. Mice were sacrificed on the day following the last injection.

DSS treatment

Age- and sex- matched *Nfil3*$^{fl/fl}$ mice and *Nfil3*$^{\Delta IEC}$ mice were co-housed for at least 3 weeks. Mice were given *ad libitum* access to drinking water containing 3% dextran sulfate sodium (DSS). Body weights were monitored and recorded for 9 consecutive days. Mice were sacrificed at day 9, and colon tissues were collected and fixed in Bouin's fixative for histological inspection using H&E staining method as described above.

Statistics

All data are shown as means±SEM. Statistical analysis was performed using a two-tailed Student's t-test or a one-way ANOVA test. For all tests, P-values lower than 0.05 were considered statistically significant.

TABLE 1: List of qRT-PCR primers

Primer name		Sequence
Nfil3	Forward	5'-CTTTCAGGACTACCAGACATCCAA-3'
	Reverse	5'-GATGCAACTTCCGGCTACCA-3'
Rev-erbα	Forward	5'-ACATGTATCCCCATGGACGC-3'
	Reverse	5'-CTGGTCGTGCTGAGAAAGGT-3'
Cd36 (Wang et al., 2014)	Forward	5'-TCATATTGTGCTTGCAAATCCAA-3'
	Reverse	5'-TGTAGATCGGCTTTACCAAAGATG-3'
Scd1 (Wang et al., 2014)	Forward	5'-CTTCTTCTCTCACGTGGGTTG-3'
	Reverse	5'-CGGGCTTGTAGTACCTCCTC-3'
Il1β	Forward	5'-TGGTACATCAGCACCTCACAAGCA-3'
	Reverse	5'-AGGCATTAGAAACAGTCCAGCCCA-3'
Il6	Forward	5'-CTATGAAGTTCCTCTCTGCAAGAGAC-3'
	Reverse	5'-GGGAAGGCCGTGGTTGTC-3'
Il22	Forward	5'-CATGCAGGAGGTGGTACCTT-3'
	Reverse	5'-CAGACGCA GCATTTCTCAG-3'
Reg3g	Forward	5'-TTCCTGTCCTCCATGATCAAAA-3'
	Reverse	5'-CATCCACCTCTGTTGGGTTCA-3'
Defa5	Forward	5'-AGGCTGATCCTATCCACAAAACAG-3'
	Reverse	5'-TGAAGAGCAGACCCTTCTTGGC-3'
Nfil3 ChIP	Forward	5'-GAAAGCGGGTAGGTTTCCCA-3'
	Reverse	5'-AACCAAGCTAGACCCGGTTG-3'
Rev-erbα ChIP	Forward	5'-TAGGTGGAGTGTGCCTATTCCT-3'
	Reverse	5'-CACCCTGACTCTTCAGAAAACC-3'
Exon control for ChIP	Forward	5'-ATGGAGACAGTGACAGAGCAAA-3'
	Reverse	5'-AACCTCCAGTTTGTGTCAAGGT-3'

CHAPTER THREE

THE CIRCADIAN TRANSCRIPTION FACTOR NFIL3 REGULATES LIPID METABOLISM IN INTESTINAL EPITHELIAL CELLS

Data presented in this chapter has been published in *Science*, volume 357, pages 912-916 (2017).

INTRODUCTION TO NFIL3

NFIL3, which stands for Nuclear Factor, Interleukin 3 (IL-3) regulated, is a PAR family basic leucine zipper transcription factor (bZIP) (Cowell, 2002). NFIL3 was first discovered as a transcriptional activator of the IL3 promoter in human T cells, and was named after this finding (Zhang et al., 1995). NFIL3 is also named E4BP4 because of an independent discovery which identified it as a transcriptional repressor that bound to an activating transcription factor (ATF) DNA consensus sequence site in the adenovirus E4 promoter (Cowell et al., 1992).

NFIL3 can function as either a transcriptional activator or repressor depending on the promoter types of its target genes (Yu et al., 2014; Yu et al., 2013). Initial studies on NFIL3 were primarily focused on the immune system because of its pivotal role in regulating cell survival, cytokine production and cell differentiation of many immune cells (Male et al., 2012). The later discovery that NFIL3 expression is directly regulated by the circadian clock revealed it to be important link between the circadian clock and the immune system (Takahashi, 2016). NFIL3 expression can be either directly activated by the BMAL1:CLOCK dimer or repressed by REV-

ERBα (Cho et al., 2016; Takahashi, 2016). However, studies on *Clock*$^{-/-}$ mice have suggested that repression of *Nfil3* expression by REV-ERBα is the dominant circadian regulatory mechanism of NFIL3 (Noshiro et al., 2016).

NFIL3 regulation of immune cell development and function

NFIL3 plays key roles in regulating the development and function of many immune cells. First, NFIL3 is critical for the development of CD8α^{+} conventional dendritic cells (cDCs), which serve as important antigen presenting cells that present endocytosed antigen particles on MHC class I complexes to CD8^{+} cytotoxic T cells. Notably, studies on *Nfil3*$^{-/-}$ mice have suggested that the development of CD8α^{-} cDCs, plasmacytoid DCs (pDCs) and various DC progenitors (pro-DCs) are not affected by NFIL3 (Kashiwada et al., 2011).

Second, NFIL3 regulates cytokine production by macrophages. NFIL3 expression increases during macrophage activation through lipopolysaccharide (LPS) stimulation. Depletion of NFIL3 in bone marrow-derived macrophages (BMDMs) leads to IL-12 overproduction (Kobayashi et al., 2011). Notably, one study has suggested that this increase in NFIL3 expression is dependent on macrophage intrinsic secretion of IL-10 (Lang et al., 2002).

Third, NFIL3 protects IL-3-dependent B cells from apoptosis. Overexpression of NFIL3 in pro-B cell lines protects those cells from cell death (Yeung et al., 2004). In addition, studies on *Nfil3*$^{-/-}$ mice also reveal an essential role of NFIL3 in regulating class switching to immunoglobulin E (IgE) in B cells (Kashiwada et al., 2010).

Fourth, NFIL3 regulates type 2 cytokine production in T_H1 and T_H2 cells. NFIL3 deficiency in T_H2 cells impairs the production of type 2 cytokines, such as IL-5, IL-10 and IL-13.

Interestingly, overexpression of NFIL3 in T_H1 cells also leads to forced production of IL-10 and IL-13 in those cells (Motomura et al., 2011).

Fifth, NFIL3 directs the circadian differentiation of T_H17 cells through direct repression of the transcription of *Rorγt* in naïve T cells. *Nfil3*$^{-/-}$ mice exhibit exaggerated expansion of T_H17 cells. Disruption of regular circadian rhythms in mice also leads to abnormal expansion of T_H17 cells and predisposes mice to inflammation (Yu et al., 2013).

Sixth, NFIL3 regulates the development of a common lymphoid progenitor (αLP) for all subgroups of innate lymphoid cells (ILCs) through thymocyte selection-associated high mobility group box factor (TOX). αLP gives rise to all subgroups of ILCs including natural killer (NK) cells and lymphoid tissue inducer (LTi) cells (Geiger et al., 2014; Seillet et al., 2014; Yu et al., 2014). The involvement of NFIL3 hints at diurnal oscillations in ILC development.

NFIL3 regulation of other cell types

In addition to the immune cells mentioned above, a few studies have suggested additional roles for NFIL3 in other cell types. For example, there is evidence that NFIL3 regulates the growth and survival of motoneurons. Overexpression of NFIL3 in purified motoneurons promotes axonal growth and protects cells from death triggered by the removal of neurotrophic factors or activation of death receptors (Junghans et al., 2004). Further, overexpressed NFIL3 has been detected in various cancer cells, which suggests a role for NFIL3 in supporting tumor cell survival (Cowell, 2002; Silvestris et al., 2008). One recent study has reported that the tumor supporting role of NFIL3 is largely through repression of TNF-related apoptosis ligand (TRAIL) and antagonized hydrogen peroxide (H_2O_2)-induced cell death (Keniry et al., 2013).

RESULTS

Epithelial NFIL3 regulates body composition

NFIL3, a circadian clock regulated basic leucine zipper transcription factor, has been identified as an important link between the immune system and the circadian clock. Prior studies of NFIL3 have revealed its important physiological functions in regulating cell differentiation, cell survival, and cytokine production in a variety of immune cells (Male et al., 2012). However, very little is known about the physiological importance of NFIL3 in non-immune cell types.

The intestinal epithelial cell is another cell type that expresses NFIL3. By performing quantitative real-time polymerase chain reaction (qRT-PCR), I found that the expression of *Nfil3* in intestinal epithelial cells significantly decreased in germ-free mice, which are completely devoid of microorganisms, as compared to conventionally raised mice (FIGURE 2). This result accorded with a prior study in antibiotic-treated mice in which the authors also observed reduced *Nfil3* expression in intestinal epithelial cells (Mukherji et al., 2013). This finding suggested that epithelial NFIL3 might regulate a physiological activity which is responsive to the intestinal microbiota.

To identify the physiological functions of NFIL3 in intestinal epithelial cells, I generated an epithelial cell-specific *Nfil3* knockout mouse ($Nfil3^{\Delta IEC}$) by crossing a mouse carrying a loxP-flanked (floxed, *fl*) *Nfil3* allele ($Nfil3^{fl/fl}$) (Motomura et al., 2011) with a mouse expressing CRE recombinase under the control of the intestinal epithelial cell-specific *Villin* promoter (Madison et al., 2002). $Nfil3^{\Delta IEC}$ mice raised on a low-fat regular chow diet exhibited decreased body weights as compared to their co-housed $Nfil3^{fl/fl}$ littermates (FIGURE 3A). Body composition analysis by magnetic resonance imaging (MRI) revealed that $Nfil3^{\Delta IEC}$ mice had reduced body fat and increased body mass relative to $Nfil3^{fl/fl}$ littermates (FIGURE 3B,C). To rule out the possibility that

the body composition differences between *Nfil3*$^{\Delta IEC}$ and *Nfil3*$^{fl/fl}$ littermates were due to the off-target effects of CRE recombinase, I analyzed and compared the body compositions of Villin-Cre mice and *Nfil3*$^{fl/fl}$ mice. Villin-Cre mice showed similar body fat and lean body mass when compared to *Nfil3*$^{fl/fl}$ mice (FIGURE 4A,B), suggesting that the body composition differences between *Nfil3*$^{\Delta IEC}$ and *Nfil3*$^{fl/fl}$ mice were entirely dependent upon epithelial NFIL3.

Body composition is highly influenced by behavior (Dunn et al., 1999). To study whether mice lacking epithelial NFIL3 exhibit behavioral alterations that might influence their metabolic phenotypes, I monitored physical activity and other metabolic parameters of *Nfil3*$^{\Delta IEC}$ and *Nfil3*$^{fl/fl}$ mice using a metabolic chamber system. Both *Nfil3*$^{\Delta IEC}$ and *Nfil3*$^{fl/fl}$ mice consumed a similar amount of food during the day and night (FIGURE 5), and exhibited similar physical activity patterns (FIGURE 6) and similar energy utilization patterns (FIGURE 7A-C). These results suggested that lack of epithelial NFIL3 does not alter metabolically-relevant behaviors in mice.

Previous studies have established a strong connection between NFIL3 and intestinal immunity (Male et al., 2012; Yu et al., 2013; 2014). To investigate whether altered body composition in *Nfil3*$^{\Delta IEC}$ mice was caused by aberrant intestinal immune activities, I examined the histological morphology of small intestine and colon from those mice. In comparison with *Nfil3*$^{fl/fl}$ littermates, *Nfil3*$^{\Delta IEC}$ mice did not show morphological or pathological changes in their small intestine or colon (FIGURE 8A,B). I also challenged *Nfil3*$^{\Delta IEC}$ and *Nfil3*$^{fl/fl}$ mice with 3% dextran sodium sulfate (DSS), which is commonly used for inducing colitis (Gaudio et al., 1999) in animal models. After treatment for 9 days, both *Nfil3*$^{\Delta IEC}$ and *Nfil3*$^{fl/fl}$ mice had similar body weight loss (FIGURE 9A) and exhibited similar colitis-related morphological changes in colon (FIGURE 9B). Further, I compared the expression of key pro-inflammatory cytokines and antimicrobial peptides in the small intestines of *Nfil3*$^{\Delta IEC}$ and *Nfil3*$^{fl/fl}$ mice, finding no significant differences between the

two groups (FIGURE 10A-F). These results indicated that reduced body weight and body fat mass in *Nfil3*$^{\Delta IEC}$ mice were not due to a defective intestinal immune system.

Lack of epithelial NFIL3 protects mice from diet-induced obesity

The reduced body weight and body fat in *Nfil3*$^{\Delta IEC}$ mice encouraged me to think about a possible role for epithelial NFIL3 in regulating epithelial cell-intrinsic lipid metabolism. To further investigate the physiological importance of epithelial NFIL3 in regulating lipid metabolism and body composition, I placed *Nfil3*$^{\Delta IEC}$ and their *Nfil3*$^{fl/fl}$ littermates on a Western-style high-fat diet (HFD). After 10 weeks of feeding, both *Nfil3*$^{\Delta IEC}$ and *Nfil3*$^{fl/fl}$ mice gained significant body weight (FIGURE 11A). However, *Nfil3*$^{\Delta IEC}$ mice maintained lower body weights than their *Nfil3*$^{fl/fl}$ littermates (FIGURE 11A). Body composition analyzed by MRI revealed that *Nfil3*$^{\Delta IEC}$ mice had markedly lower body fat percentages and higher lean body mass percentages as compared to *Nfil3*$^{fl/fl}$ mice (FIGURE 11B,C). Reduced body fat in *Nfil3*$^{\Delta IEC}$ mice was confirmed by comparing the size and weight of epididymal fat pads with those of *Nfil3*$^{fl/fl}$ mice (FIGURE 12A,B).

Mice with a high percentage of body fat induced by HFD virtually always also exhibit other symptoms of obesity, such as elevated blood triglycerides, increased liver fat accumulation, and insulin resistance (Haslam and James, 2005). Because *Nfil3*$^{\Delta IEC}$ mice fed a HFD maintained a low body fat percentage, I next sought to determine whether those mice were also protected from other obesity symptoms. Indeed, *Nfil3*$^{\Delta IEC}$ mice fed a HFD had significantly lower blood triglycerides (FIGURE 13A) and much less fat accumulation in liver (FIGURE 13B) then their *Nfil3*$^{fl/fl}$ littermates. The glucose tolerance test revealed that *Nfil3*$^{\Delta IEC}$ mice fed a HFD were more glucose tolerant than *Nfil3*$^{fl/fl}$ mice (FIGURE 13C); the insulin tolerance test revealed that *Nfil3*$^{\Delta IEC}$ mice fed a HFD were more sensitive to insulin than *Nfil3*$^{fl/fl}$ mice (FIGURE 13D). These results indicated

that mice lacking epithelial NFIL3 are protected from HFD-induced obesity and its associated symptoms.

The composition of the intestinal microbiota markedly impacts systemic metabolism (Cani et al., 2008). Diet switching has been shown to rapidly reshape the microbial composition in the intestine (Turnbaugh et al., 2009a). To investigate whether the lean phenotypes of *Nfil3*$^{\Delta IEC}$ mice were due simply to alterations in the taxonomic composition of the microbiota, I performed 16S ribosomal RNA (rRNA) sequencing on fecal microbiomes from *Nfil3*$^{\Delta IEC}$ and *Nfil3*$^{fl/fl}$ mice. Principle coordinate analysis of the 16S rRNA results revealed that the microbiota compositions did not vary between *Nfil3*$^{\Delta IEC}$ and *Nfil3*$^{fl/fl}$ mice before or after diet switching (FIGURE 14). This suggested that the lean phenotypes of the *Nfil3*$^{\Delta IEC}$ mice were not due to alterations in microbiota composition of the microbiota.

Diet-induced obesity requires both epithelial NFIL3 and the microbiota

Obesity induced by high-fat diet feeding has been shown to be dependent on the intestinal microbiota. Germ-free mice raised in a completely sterile environment are protected from diet-induced obesity (Bäckhed et al., 2004; Rabot et al., 2010a). Given that expression of epithelial NFIL3 was markedly reduced in germ-free mice (FIGURE 1), I hypothesized that the NFIL3-dependent body fat accumulation also depends on the microbiota. To determine this, I used an antibiotic cocktail to deplete the microbiota in *Nfil3*$^{\Delta IEC}$ mice and their *Nfil3*$^{fl/fl}$ littermates during HFD feeding. Compared to the untreated group, the *Nfil3*$^{\Delta IEC}$ mice treated with antibiotics gained similar amount of body fat and had a lean body mass (FIGURE 15A,B). However, the *Nfil3*$^{fl/fl}$ littermates treated with antibiotics gained significantly lower amounts body fat and had a higher lean body mass (FIGURE 15A,B). This result provided solid evidence that diet-induced body fat

accumulation requires both epithelial NFIL3 and the microbiota. This indicated that NFIL3 is a causal link between the microbiota and body fat accumulation.

Epithelial NFIL3 regulates the circadian expression of key lipid metabolic genes

The fact that mice lacking epithelial NFIL3 are protected from diet-induced obesity suggested that epithelial NFIL3 might regulate lipid metabolic genes that are essential in regulating body fat accumulation. To understand the mechanism by which epithelial NFIL3 regulates fat storage and body composition, I compared the transcriptomes of epithelial cells from *Nfil3*$^{\Delta IEC}$ and *Nfil3*$^{fl/fl}$ mice. Because NFIL3 is a circadian transcription factor which exhibits diurnal oscillating transcriptional rhythms (Curtis et al., 2014), I isolated intestinal epithelial cells by laser capture microdissection (Stappenbeck et al., 2002) and performed an RNA-seq analysis on those cells at multiple times points across the 24-hour day-light cycle. There were 33 transcripts that had at least a 2-fold increase or decrease in their average diurnal expression between *Nfil3*$^{\Delta IEC}$ and *Nfil3*$^{fl/fl}$ mice (FIGURE 16A). Note that most of them were had diurnal rhythms in *Nfil3*$^{fl/fl}$ mice but lost their rhythms in *Nfil3*$^{\Delta IEC}$ mice (FIGURE 16A). Among the 33 transcripts, I identified 17 that were known to function in lipid uptake and metabolism (FIGURE 16A). For example, this list included *Cd36*, encoding a transporter that imports dietary fatty acids into intestinal epithelial cells (Coburn et al., 2000); *Scd1*, encoding a stearoyl-CoA-desaturase 1 that converts saturated fatty acids to monounsaturated fatty acids (Ntambi et al., 2002); *Cyp2e1*, encoding a fatty acid hydroxylase (Leclercq et al., 2000); and *Fabp4*, encoding a fatty acid binding protein (Furuhashi and Hotamisligil, 2008). Previous studies have shown that mice lacking each of these genes are protected from HFD-induced obesity and/or insulin-resistance (Coburn et al., 2000; Furuhashi and Hotamisligil, 2008; Ntambi et al., 2002; Zong et al., 2012). This result suggested that altered

metabolic phenotypes in *Nfil3*$^{\Delta IEC}$ mice might be the consequence of lowered expression of those genes. Notably, in contrast to the differential expression of these 33 genes, core circadian clock genes like *Bmal1* (*Arntl*), *Per2*, and *Nr1d1* (*Rev-erbα*) retained their rhythmic expression in the *Nfil3*$^{\Delta IEC}$ mice, indicating that the core clock machinery remained intact (FIGURE 16A).

To validate that RNA-seq result, I performed qRT-PCR to compare *Cd36* and *Scd1* transcript abundance in isolated epithelial cells from *Nfil3*$^{\Delta IEC}$ and *Nfil3*$^{fl/fl}$ mice. Both *Cd36* and *Scd1* showed reduced expression in *Nfil3*$^{\Delta IEC}$ mice at time point ZT4, which is when their diurnal expression peaked according to RNA-seq result (FIGURE 16B). Expression of both *Cd36* and *Scd1* was also reduced in germ-free mice, consistent with the fact that germ-free mice had decreased expression of epithelial *Nfil3* (FIGURE 16B). Reduced expression of *Cd36* in *Nfil3*$^{\Delta IEC}$ mice and germ-free mice was further confirmed at the protein level by Western blot analysis (FIGURE 16C). These results indicated that epithelial NFIL3 might regulate fat storage by actively regulating circadian expression of lipid metabolic genes in the intestinal epithelium.

Nfil3$^{\Delta IEC}$ mice show lowered uptake of dietary lipid

Intestinal epithelial cells are responsible for uptake of fatty acids from the diet. After reaching the intestine, high molecular weight dietary fat gets broken down into fatty acids by digestive enzymes and is then transported into intestinal epithelial cells through transporters that reside in the apical membrane of epithelial cells. Inside epithelial cells, fatty acids are processed to form triglycerides and further packaged into chylomicrons, which are lipoprotein particles that consist mostly of triglycerides and other phospholipids, cholesterol and proteins (Abumrad and Davidson, 2012). Packaged chylomicrons are transported to the lacteal, the capillary lymph ducts in the intestine. They then merge into the lymphatic circulation and eventually are exported to the blood circulation.

This process has been revealed by previous studies to show diurnal rhythmicity, resulting in daily variations in circulating lipids (Bremner et al., 2000). Disruption of rhythms in chylomicron export, as seen in mice lacking Nocturnin, is associated with a lean phenotype (Douris et al., 2011). Given the fact that expression of key metabolic genes involved in epithelial lipid uptake and processing were significantly reduced in *Nfil3*$^{\Delta IEC}$ mice, I hypothesized that reduced body weight and body fat mass in *Nfil3*$^{\Delta IEC}$ mice might due to defective epithelial cell uptake and processing dietary lipids, by which result in lowered export of lipids to the circulation for storage in adipose tissue.

To test this hypothesis, I performed Oil Red O staining of lipids in small intestinal tissues from *Nfil3*$^{\Delta IEC}$ and *Nfil3*$^{fl/fl}$ mice fed a HFD, in order to reveal epithelial cells that harbor lipids. As expected, *Nfil3*$^{fl/fl}$ mice harbored abundant lipids within the epithelial layer. In contrast, *Nfil3*$^{\Delta IEC}$ mice harbored significantly less lipid within the epithelial layer (FIGURE 17A), suggesting reduced lipid absorption by their epithelial cells. In addition, *Nfil3*$^{\Delta IEC}$ mice showed reduced lipid staining in subepithelial intestinal tissues as compared to *Nfil3*$^{fl/fl}$ mice (FIGURE 17B), which suggested a lowered export of epithelial lipids into the circulation in *Nfil3*$^{\Delta IEC}$ mice.

I next isolated intestinal epithelial cells from *Nfil3*$^{\Delta IEC}$ and *Nfil3*$^{fl/fl}$ mice and quantified total lipid concentrations in those cells. Consistent with the Oil Red O staining result, *Nfil3*$^{\Delta IEC}$ mice had significantly lower lipid concentrations in isolated epithelial cells than *Nfil3*$^{fl/fl}$ mice (FIGURE 18A), supporting reduced lipid absorption by the epithelial cells. As a result, feces from *Nfil3*$^{\Delta IEC}$ mice contained more lipid than those from *Nfil3*$^{fl/fl}$ mice (FIGURE 18B). Together, these results supported the idea that reduced body fat storage in *Nfil3*$^{\Delta IEC}$ mice is due to reduced lipid uptake, processing and export in intestinal epithelial cells.

CONCLUSIONS

In this chapter, I have identified epithelial NFIL3 as an important link between the intestinal microbiota and metabolism. First, using genetic mouse models, I have discovered that mice lacking epithelial NFIL3 exhibit reduced body weight and body fat mass, and are protected from HFD-induced obesity. This resembles metabolic phenotypes in germ-free mice and indicates an important role for epithelial NFIL3 in regulating lipid metabolism. Second, RNA-seq analysis of intestinal epithelial cells has revealed that epithelial NFIL3 is responsible for the circadian transcriptional rhythms of key metabolic genes, such as *Cd36, Scd1, Cyp2e1* and *Fabp4*. This accords with the molecular basis of NFIL3 as a circadian transcription factor, and indicats the possible mechanism underlying epithelial NFIL3-regulated body fat accumulation. Third, the expression of epithelial NFIL3 is highly induced by intestinal microbiota. Germ-free or antibiotic treated mice exhibit a marked reduction of NFIL3 expression in epithelial cells. Together, my studies in this chapter have unraveled NFIL3 as an essential regulator in microbiota-mediated body fat accumulation, and have further demonstrated the essential role of the microbiota in regulating body metabolism. The involvement of circadian clock, as NFIL3 is a circadian transcription factor, could also help to explain why circadian clock disruptions in humans are associated with an increased occurrence of metabolic diseases.

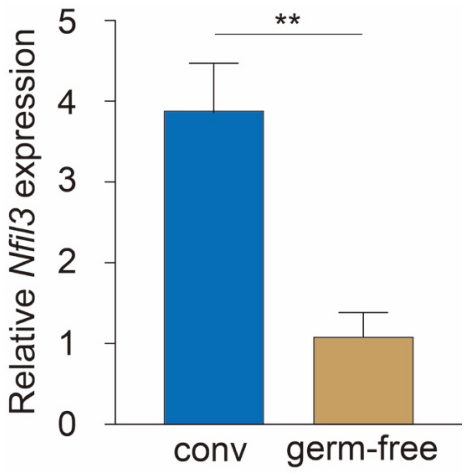

FIGURE 2: Reduced expression of epithelial *Nfil3* in germ-free mice

qRT-PCR analysis of *Nfil3* transcript abundance in small intestinal epithelial cells recovered by laser capture microdissection from conventional (conv) and germ-free mice. N=4-8 mice per group. Means±SEM are plotted; statistics were performed with Student's t-test. **p<0.01.

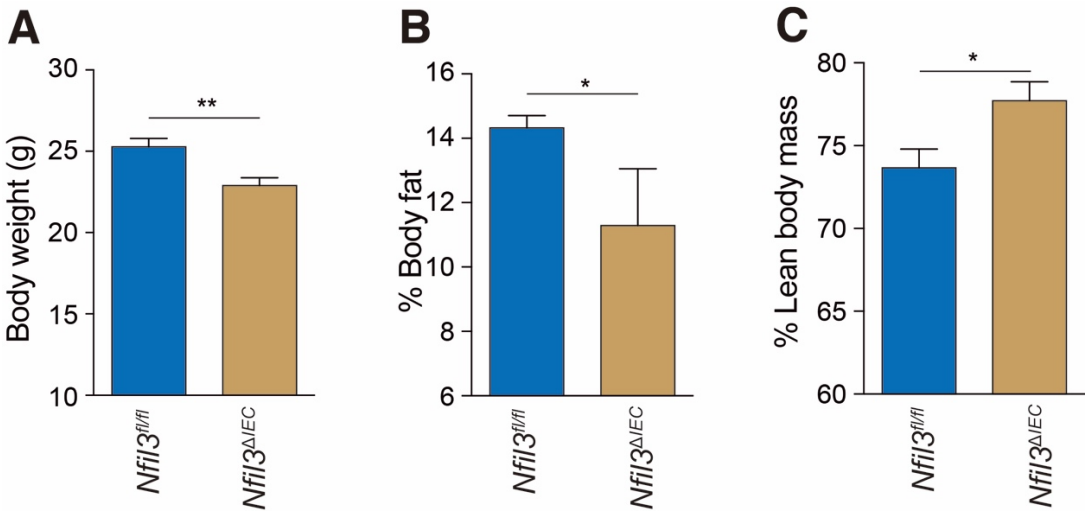

FIGURE 3: Reduced body weight and body fat but increased lean body mass in *Nfil3*$^{\Delta IEC}$ mice fed a chow diet

(A) Body weight of 8 weeks old *Nfil3*$^{fl/fl}$ and *Nfil3*$^{\Delta IEC}$ mice maintained on a chow diet. N=12 mice per group. **(B)** Body fat percentage of 8 weeks old *Nfil3*$^{fl/fl}$ and *Nfil3*$^{\Delta IEC}$ mice maintained on a chow diet. N=8 mice per group. **(C)** Lean body mass percentage of 8 weeks old *Nfil3*$^{fl/fl}$ and *Nfil3*$^{\Delta IEC}$ mice maintained on a chow diet. N=8 mice per group. Error bars represent SEM; statistics were performed with Student's t-test. *$p<0.05$, **$p<0.01$.

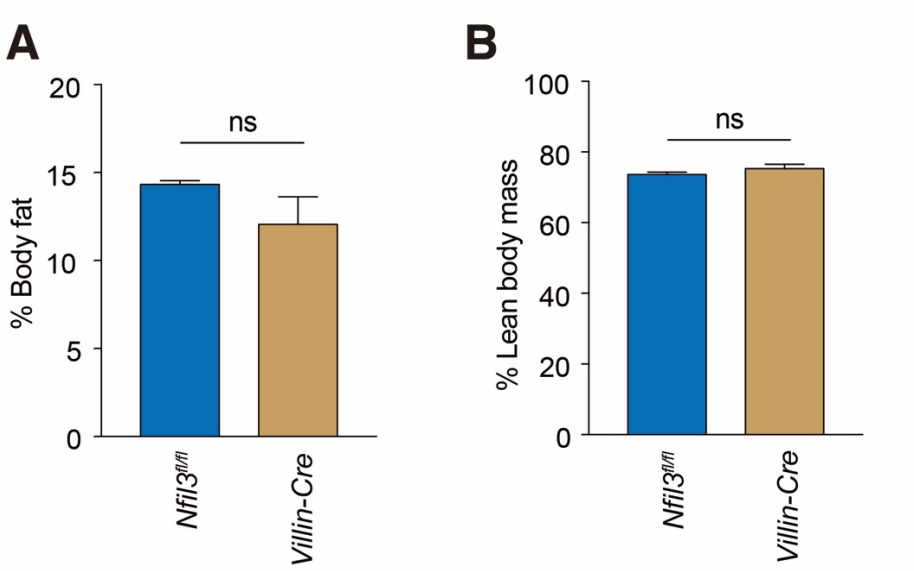

FIGURE 4: Normal body weight and body fat in *Villin*-Cre mice fed a chow diet

(A) Body fat percentage of *Nfil3*$^{fl/fl}$ and *Villin*-Cre mice maintained on a chow diet. **(B)** Lean body mass percentage of *Nfil3*$^{fl/fl}$ and *Villin*-Cre mice maintained on a chow diet. N=3 mice per group. Error bars represent SEM; statistics were performed with Student's t-test. ns, not significant.

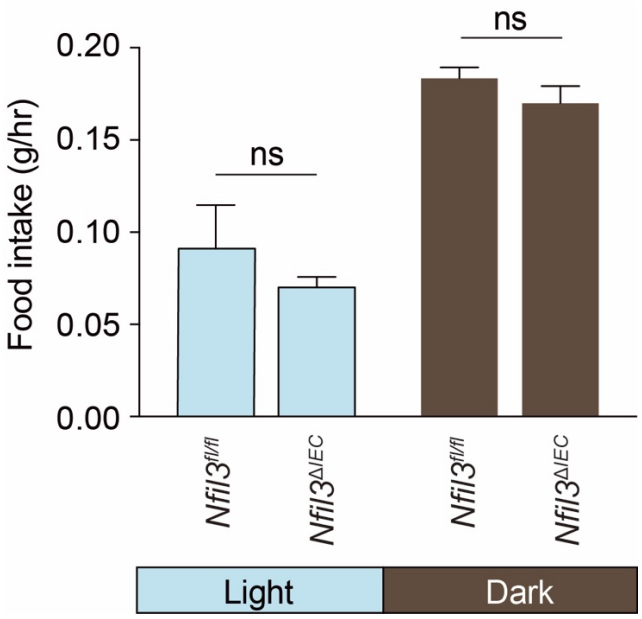

FIGURE 5: Normal food intake in *Nfil3*$^{\Delta IEC}$ mice

Food intake rate (grams per hour) of *Nfil3*$^{fl/fl}$ and *Nfil3*$^{\Delta IEC}$ mice maintained on a chow diet during day and night. N=6 mice per group. Male mice were used. Error bars represent SEM; statistics were performed with Student's t-test. ns, not significant.

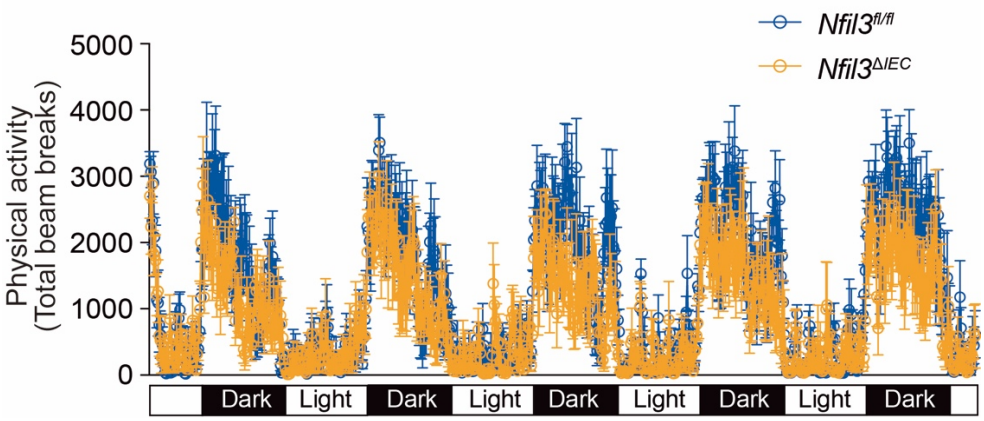

FIGURE 6: Normal movement pattern in *Nfil3*$^{\Delta IEC}$ mice

Recording of total physical activity of *Nfil3*$^{fl/fl}$ and *Nfil3*$^{\Delta IEC}$ mice maintained on a chow diet over consecutive 5 days. N=6 mice per group. Male mice were used. Error bars represent SEM; statistics were performed with Student's t-test.

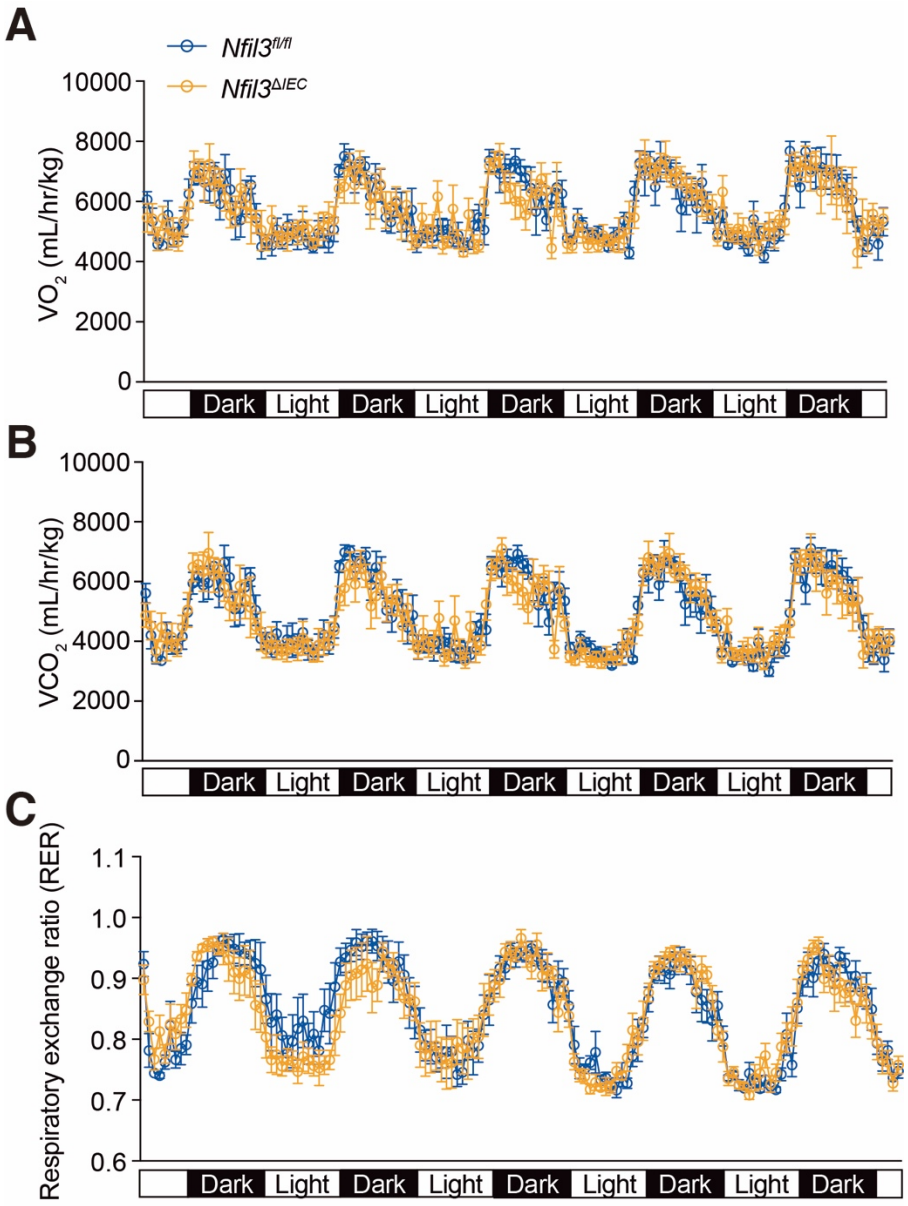

FIGURE 7: Normal energy utilization in *Nfil3*$^{\Delta IEC}$ mice

(A) Oxygen consumption rate of *Nfil3*$^{fl/fl}$ and *Nfil3*$^{\Delta IEC}$ mice recorded over 5 days. N=6 mice per group. **(B)** CO_2 production rate of *Nfil3*$^{fl/fl}$ and *Nfil3*$^{\Delta IEC}$ mice recorded over 5 days. N=6 mice per group. **(C)** Respiratory exchange ratio of *Nfil3*$^{fl/fl}$ and *Nfil3*$^{\Delta IEC}$ mice recorded over 5 days. N=6 mice per group. All mice were fed on chow diet. Male mice were used. Error bars represent SEM; statistics were performed with Student's t-test.

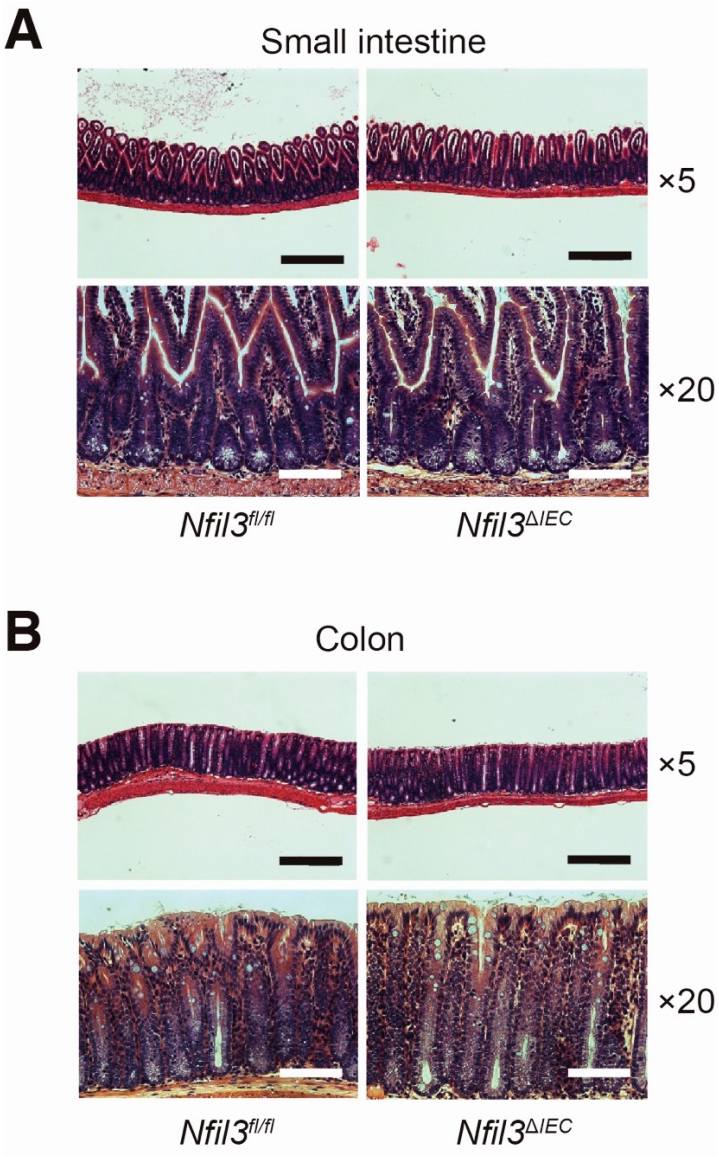

FIGURE 8: Normal histological morphology of the intestine in *Nfil3*$^{\Delta IEC}$ mice

(A) Hematoxylin & eosin (H&E) staining of small intestine from *Nfil3*$^{fl/fl}$ and *Nfil3*$^{\Delta IEC}$ mice. Scale bar (white)=100 µm. **(B)** Hematoxylin & eosin (H&E) staining of colons from *Nfil3*$^{fl/fl}$ and *Nfil3*$^{\Delta IEC}$ mice. Scale bar (black)=400 µm,

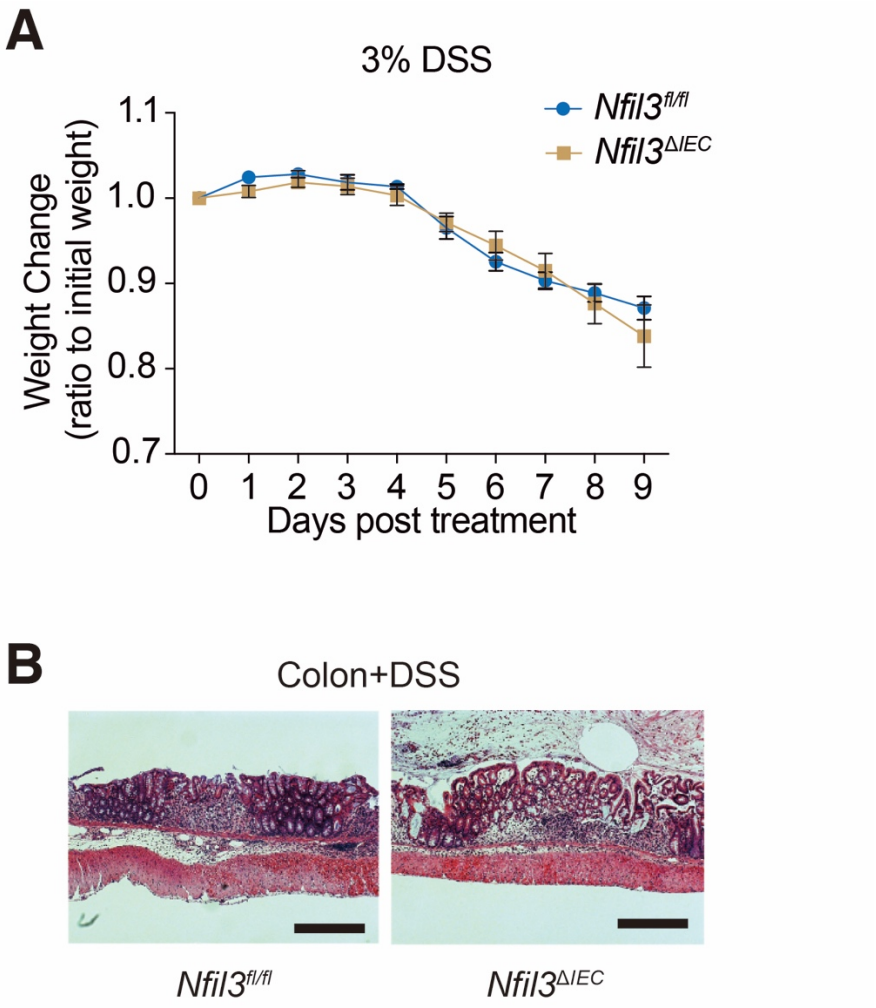

FIGURE 9: *Nfil3*$^{fl/fl}$ and *Nfil3*$^{\Delta IEC}$ mice have a similar response to DSS-induced intestinal injury

(A) Body weight change of *Nfil3*$^{fl/fl}$ and *Nfil3*$^{\Delta IEC}$ mice treated with 3% dextran sulfate sodium (DSS) water. N=10 per group. Male mice were used. Error bars represent SEM; statistics were performed with Student's t-test. **(B)** Hematoxylin & eosin (H&E) staining of colon from DSS treated *Nfil3*$^{fl/fl}$ and *Nfil3*$^{\Delta IEC}$ mice. Scale bar=400 µm.

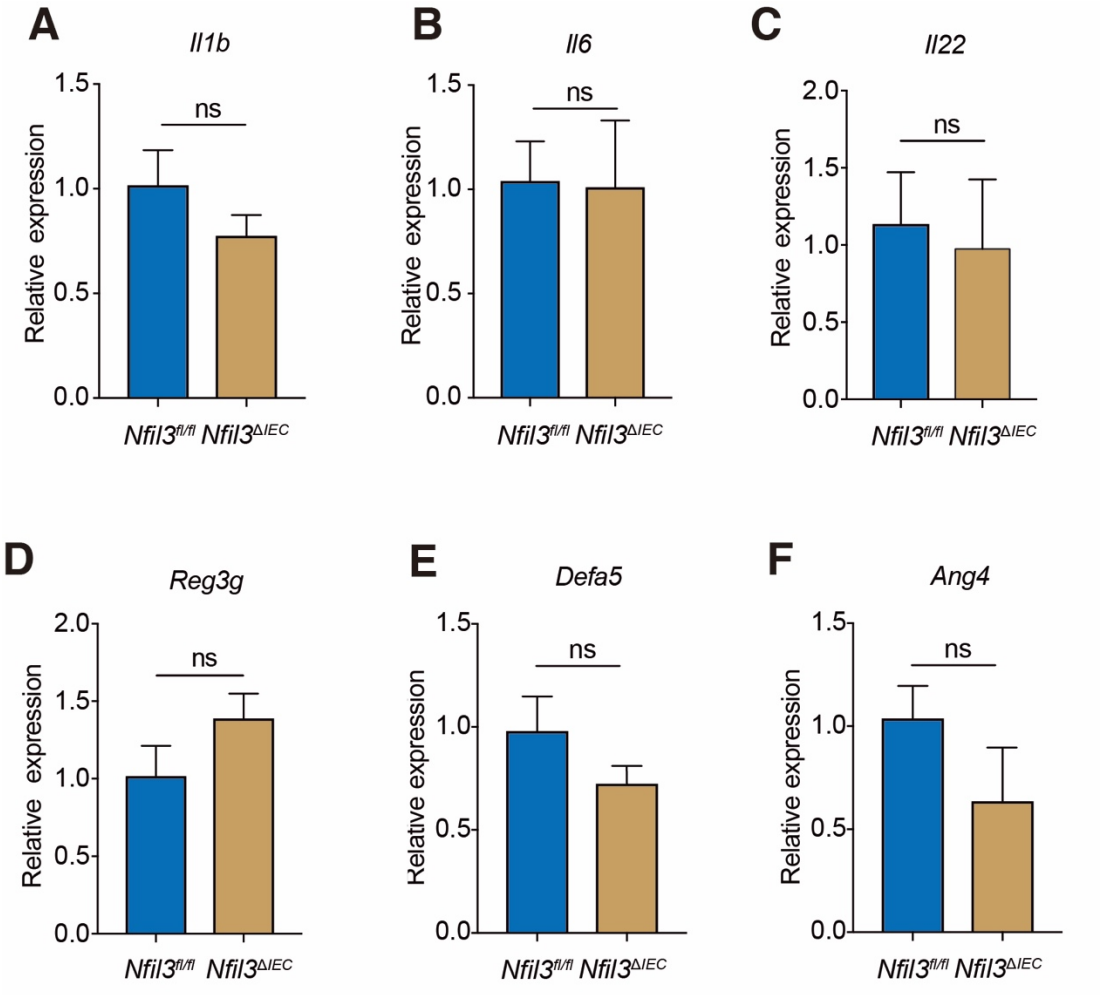

FIGURE 10: Normal expression of key pro-inflammatory cytokines and antimicrobial proteins in *Nfil3*$^{\Delta IEC}$ mouse intestine

(A-F) qRT-PCR analysis of *Il1b* **(A)**, *Il6* **(B)**, *Il22* **(C)**, *Reg3g* **(D),** *Defa5* **(E)** and *Ang4* **(F)** expression in distal ileum from *Nfil3*$^{fl/fl}$ and *Nfil3*$^{\Delta IEC}$ mice. N=3 per each group. Error bars represent SEM; statistics were performed with Student's t-test. ns, not significant.

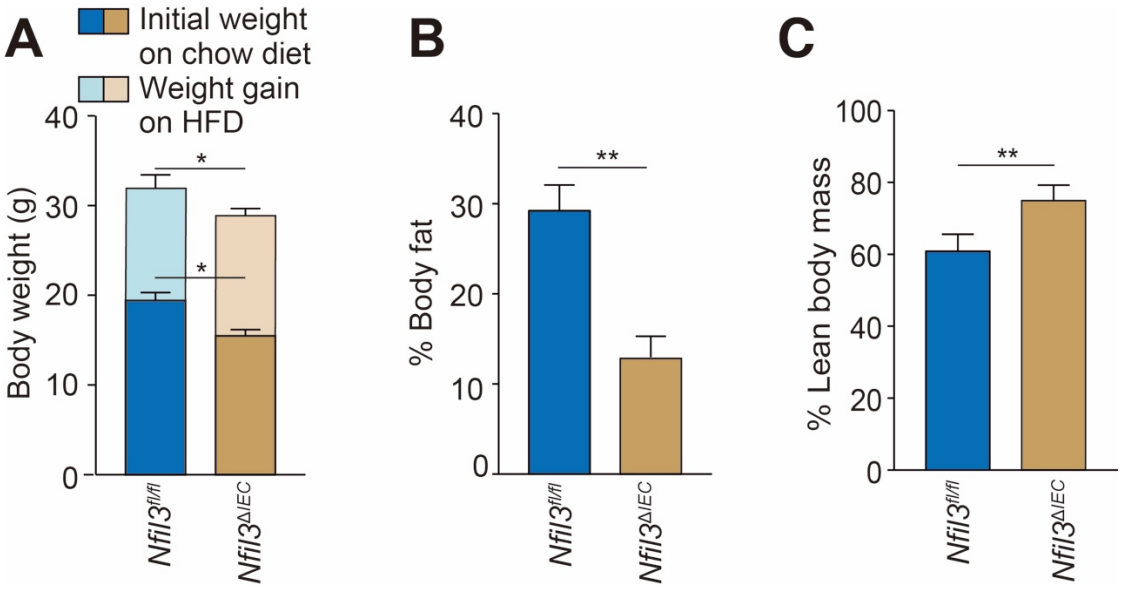

FIGURE 11: Minimal body fat gain in *Nfil3*$^{\Delta IEC}$ mice fed a HFD

(A-C) Age-matched *Nfil3*$^{fl/fl}$ and *Nfil3*$^{\Delta IEC}$ mice were co-housed and placed on a high-fat diet (HFD) for 10 weeks. **(A)** Body weights of *Nfil3*$^{fl/fl}$ and *Nfil3*$^{\Delta IEC}$ mice measured before and after diet switching. **(B)** Body fat percentages of *Nfil3*$^{fl/fl}$ and *Nfil3*$^{\Delta IEC}$ mice after 10 weeks on the HFD. (**C**) Lean body mass percentage of *Nfil3*$^{fl/fl}$ and *Nfil3*$^{\Delta IEC}$ mice after 10 weeks on the HFD. N=4-6 mice for group. Male mice were used. Error bars represent SEM; statistics were performed with Student's t-test. *$p<0.05$; *$p<0.01$.

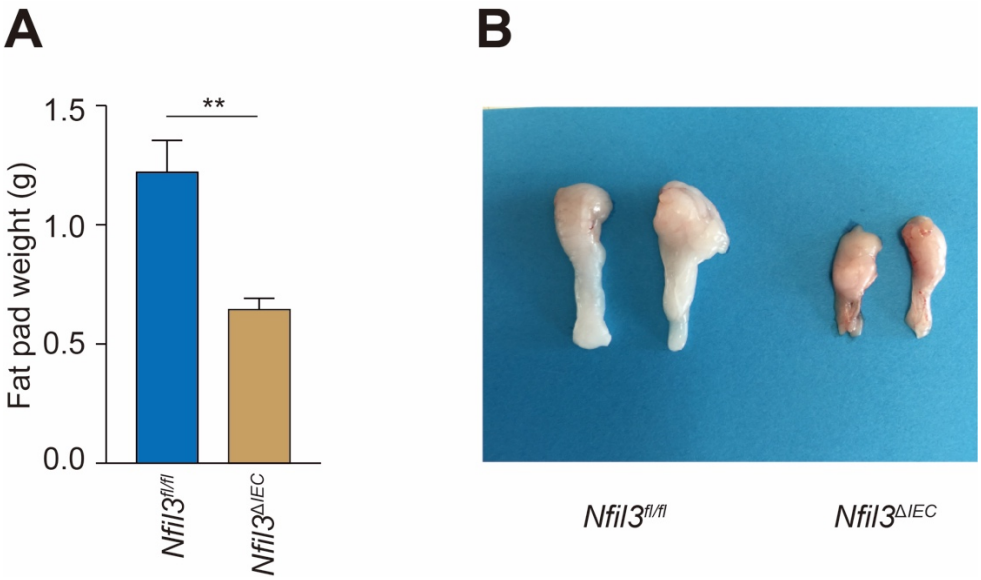

FIGURE 12: Smaller fat pads in *Nfil3*$^{\Delta IEC}$ mice fed a HFD

(A) Epididymal fat pad weight of *Nfil3*$^{fl/fl}$ and *Nfil3*$^{\Delta IEC}$ mice fed on HFD for 10 weeks. N=4-6 mice for each group. Male mice were used. Error bars represent SEM; statistics were performed with Student's t-test. **p<0.01. **(B)** Picture of epididymal fat pads of *Nfil3*$^{fl/fl}$ and *Nfil3*$^{\Delta IEC}$ mice fed on HFD for 10 weeks.

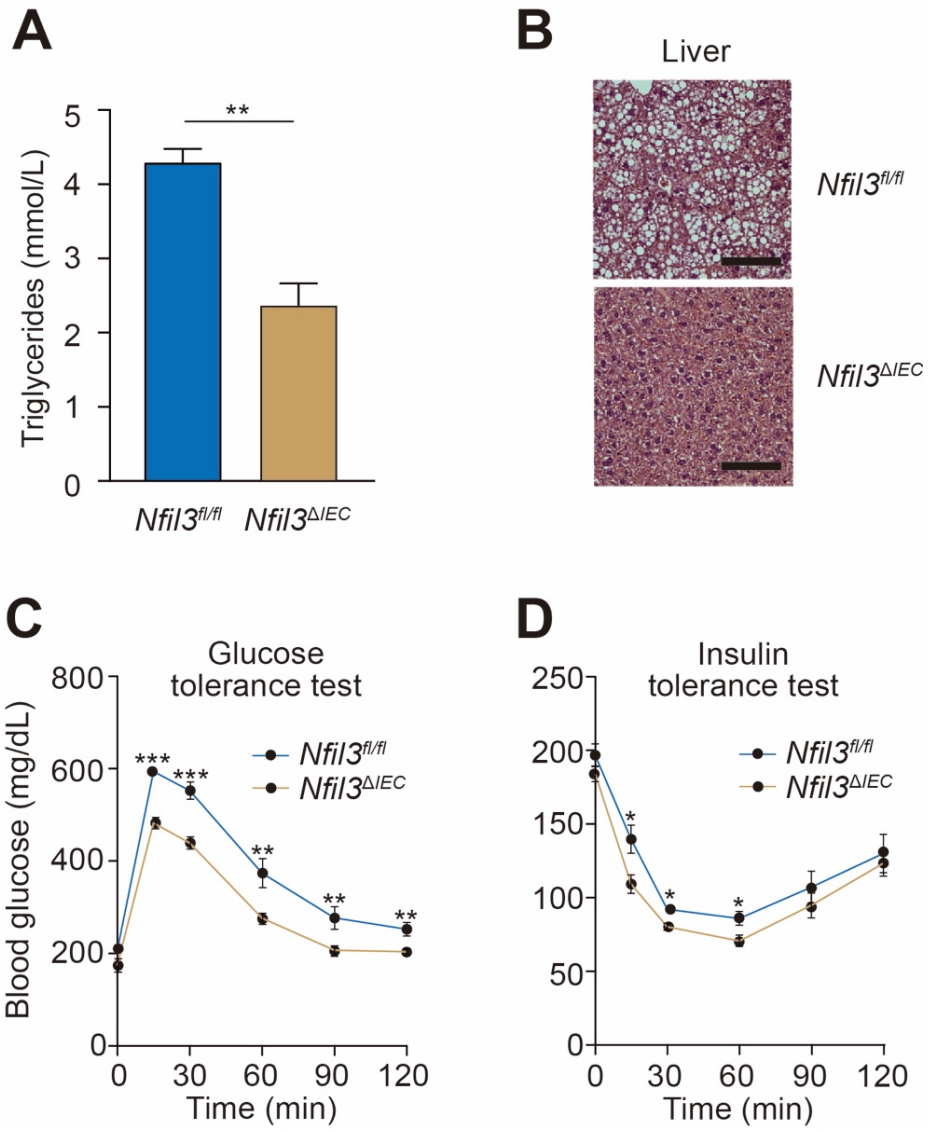

FIGURE 13: *Nfil3*$^{\Delta IEC}$ mice are protected from HFD-induced obesity

(A) Serum triglyceride concentrations in *Nfil3*$^{fl/fl}$ and *Nfil3*$^{\Delta IEC}$ mice fed on HFD for 10 weeks. **(B)** Hematoxylin & eosin (H&E) staining of livers from *Nfil3*$^{fl/fl}$ and *Nfil3*$^{\Delta IEC}$ mice fed on HFD for 10 weeks. Scale bar=100 μm. **(C)** Glucose tolerance test on *Nfil3*$^{fl/fl}$ and *Nfil3*$^{\Delta IEC}$ mice fed on HFD for 10 weeks. **(D)** Insulin tolerance test *Nfil3*$^{fl/fl}$ and *Nfil3*$^{\Delta IEC}$ mice fed on HFD for 10 weeks. N= 4-8 mice per group in A,C,D. Male mice were used. Means±SEM are plotted; statistics were performed with Student's t-test. **p<0.01; ***p<0.001.

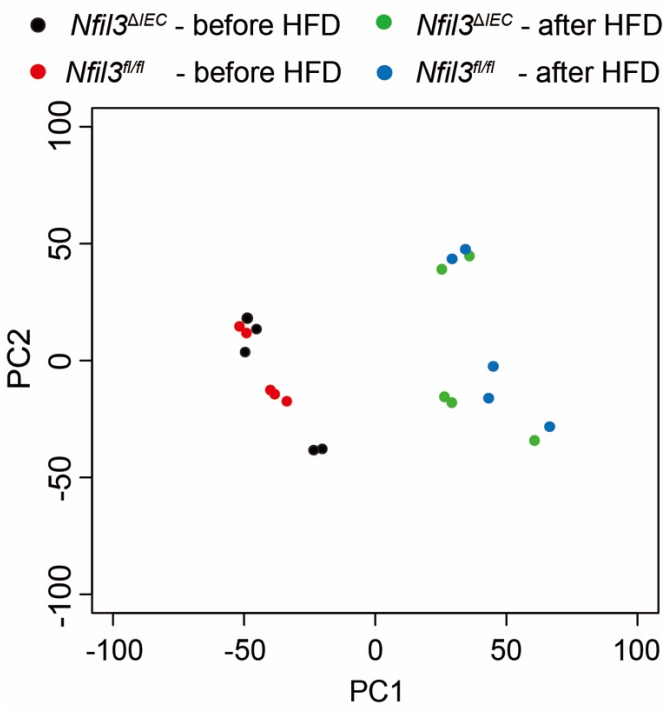

FIGURE 14: *Nfil3*$^{fl/fl}$ and *Nfil3*$^{\Delta IEC}$ mice have similar microbiotas

Principal coordinate analysis of 16S rRNA sequencing of fecal samples from *Nfil3*$^{fl/fl}$ and *Nfil3*$^{\Delta IEC}$ mice. The mice were littermates of heterozygous crosses that remained cohoused. Fecal samples were collected and sequenced before and after switching from a chow diet to HFD. Each dot represents one mouse.

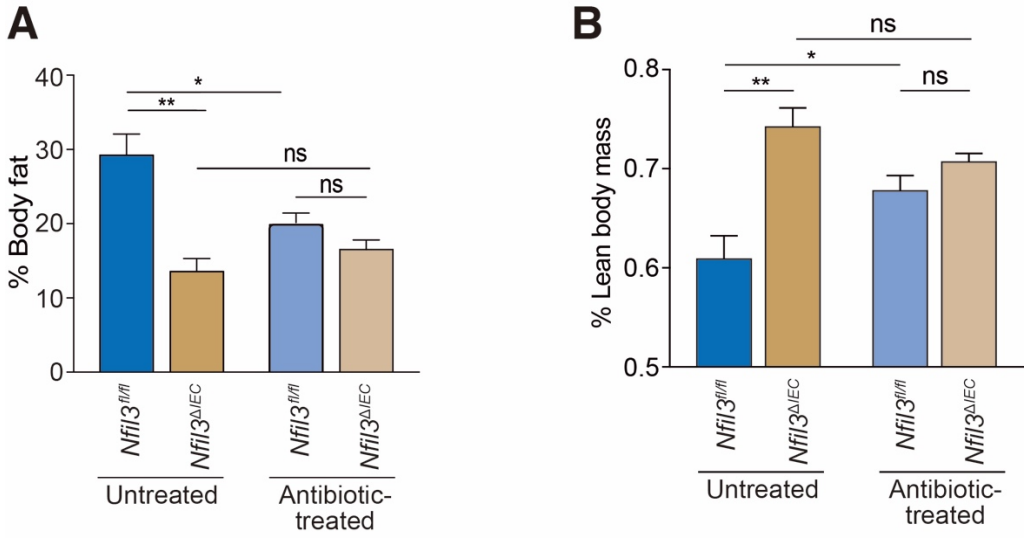

FIGURE 15: The microbiota is required for NFIL3-dependent body fat accumulation

(A) Body fat percentages of *Nfil3*$^{fl/fl}$ and *Nfil3*$^{\Delta IEC}$ mice treated with or without antibiotics after switching to HFD for 10 weeks. **(B)** Lean body mass of *Nfil3*$^{fl/fl}$ and *Nfil3*$^{\Delta IEC}$ mice treated with or without antibiotics after switching to HFD for 10 weeks. N=4-6 mice per group. Male mice were used. Error bars represent SEM; statistics were performed with one-way ANOVA. *$p<0.05$; **$p<0.01$; ns, not significant.

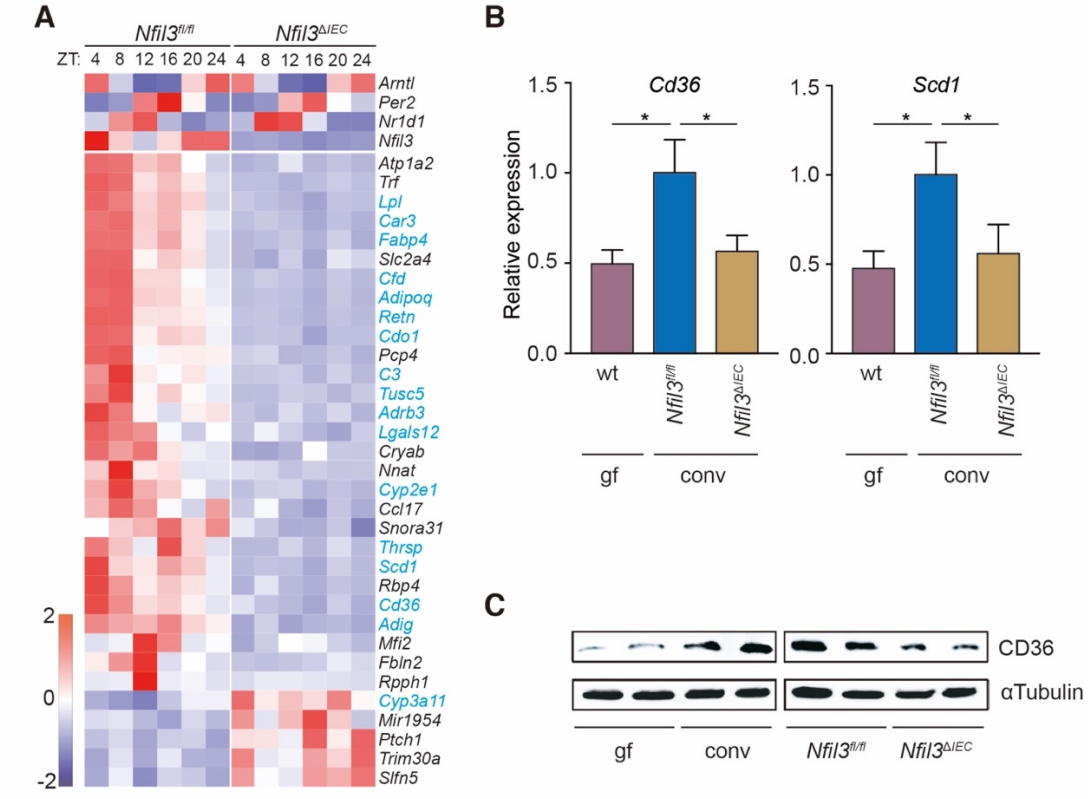

FIGURE 16: Epithelial NFIL3 regulates the circadian expression of key lipid metabolic genes

(A) RNAseq analysis of epithelial cell transcripts in *Nfil3*$^{fl/fl}$ and *Nfil3*$^{\Delta IEC}$ mice across a circadian cycle. The heatmap visualizes expression levels of the 33 genes that have altered expression in *Nfil3*$^{\Delta IEC}$ mice as compared to *Nfil3*$^{fl/fl}$ mice. Genes encoding proteins that function in lipid metabolism are highlighted in blue. The top panels show sustained circadian expression of the core clock genes *Bmal1 (Arnt1)*, *Per2*, and *Nr1d1* (*Rev-erb*α) in *Nfil3*$^{\Delta IEC}$ mice. **(B)** qRT-PCR analysis of epithelial *Cd36* and *Scd1* expression in germ-free wild-type (wt) and conventional *Nfil3*$^{fl/fl}$ and *Nfil3*$^{\Delta IEC}$ mice at ZT4. N=5-8 mice per group. Means±SEM are plotted; statistics were performed with Student's t-test. *p<0.05. **(C)** Western blot of epithelial CD36 in germ-free (gf) and conventional wild-type (conv) mice, and in conventional *Nfil3*$^{fl/fl}$ and *Nfil3*$^{\Delta IEC}$ mice. All mice were fed a HFD**.** Mice were sacrificed at ZT4. α-tubulin is the loading control. ZT, Zeitgeber time.

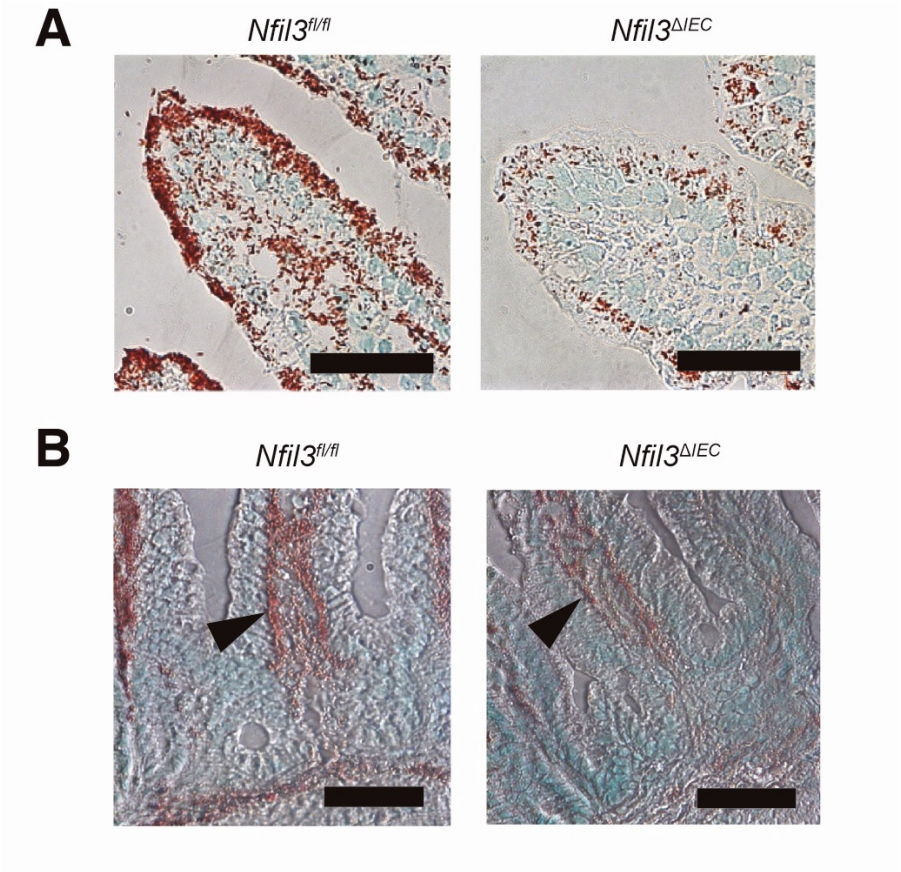

FIGURE 17: Reduced lipid accumulation in intestinal epithelial and subepithelial tissues of *Nfil3*$^{\Delta IEC}$ mice fed a HFD

(A) Oil red O detection of lipids in the small intestinal epithelium of *Nfil3*$^{fl/fl}$ and *Nfil3*$^{\Delta IEC}$ mice fed on HFD. Nuclei were stained with Methyl Green. Scale bar=40 μm. **(B)** Oil Red O staining of subepithelial tissues of *Nfil3*$^{fl/fl}$ and *Nfil3*$^{\Delta IEC}$ mice fed on HFD. There is reduced lipid accumulation in the subepithelial tissue (black arrowhead), suggesting reduced export to lymphatic capillaries, which transport packaged lipids to the bloodstream. Nuclei were stained with methyl green. Scale bar=40 μm.

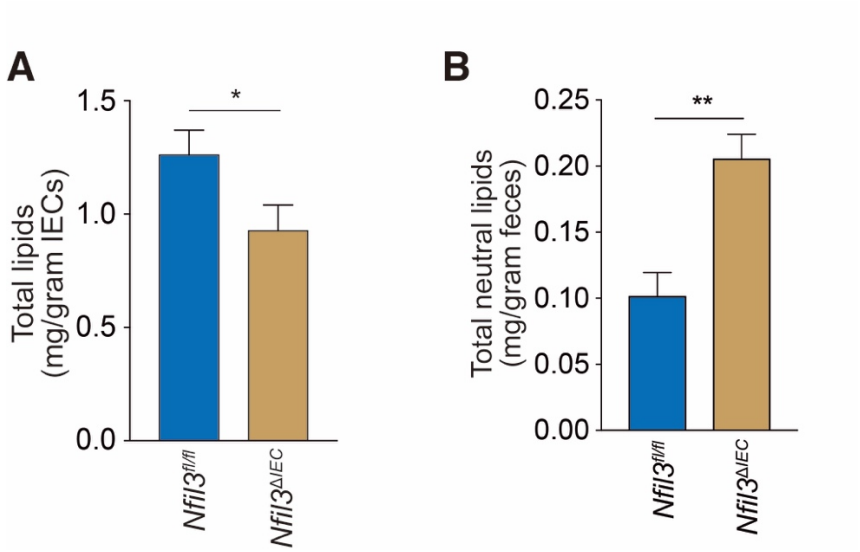

FIGURE 18: Reduced epithelial and fecal lipid concentrations in *Nfil3*$^{\Delta IEC}$ mice fed a HFD

(A) Total lipid concentrations in isolated small intestinal epithelial cells from *Nfil3*$^{fl/fl}$ and *Nfil3*$^{\Delta IEC}$ mice fed a HFD for 10 weeks. **(B)** Total neutral lipid concentrations in feces of *Nfil3*$^{fl/fl}$ and *Nfil3*$^{\Delta IEC}$ mice fed on HFD for 10 weeks. N=5 mice per group. Means±SEM are plotted; statistics were performed with Student's t-test. *p<0.05; **p<0.01.

CHAPTER FOUR

THE MICROBIOTA REGULATES EPITHELIAL NFIL3 EXPRESSION THROUGH A SUBEPITHELIAL IMMUNE RELAY CIRCUIT

Data presented in this chapter has been published in *Science*, volume 357, pages 912-916 (2017).

INTRODUCTION TO INTESTINAL IMMUNE CELLS

The intestinal lumen houses trillions of commensal bacteria. Although many benefits are provided by this microbial colonization, prevention of bacterial invasion into the host is crucial in maintaining the peaceful status of this mutualistic host-microbial relationship. The hose has evolved many strategies to prevent the translocation of the commensals. First, host tissues are separated from intestinal luminal content by a single layer of epithelial cells, which acts as a front-line rampart that limits commensal from direct contact with host tissue (Mukherjee et al., 2008). Second, goblet cells embedded in the epithelium constantly secrete mucin to form a dense mucus layer, which traps bacteria and limits their penetration (Johansson et al., 2008; Shan et al., 2013). Third, epithelial cells produce various antimicrobial proteins, such as lysozyme (Bel et al., 2017), REG3γ (Vaishnava et al., 2011) and defensins (Chen, 2012), which actively kill bacteria that come too close to the epithelial barrier. Fourth, when small numbers of bacteria accidentally invade epithelial cells, a cell-intrinsic autophagy mechanism is activated to eliminate the invading bacteria (Benjamin et al., 2013). In addition to these strategies, the intestine is also equipped with an elegant

and sophisticated immune system which further ensures host health.

The major players in the intestinal immune system are the various immune cells. These cells reside in the intestinal compartment called the lamina propria (LP) which is located immediately below the epithelial layer (Peterson and Artis, 2014). Most intestinal immune cells are scattered throughout the LP, but some can form organized lymphoid structures, such as Peyer's patches, cryptopatches and isolated lymphoid follicles (Tomasello and Bedoui, 2013). Intestinal immune cells can be classified into two groups: adaptive immune cells and innate immune cells. Adaptive immune cells require antigen presenting and react to pathogens in a highly specific manner that depends on antigens that they have encountered (Zhang et al., 2014). Adaptive immune cells usually have immunological memory and can provide long-lasting protection from infection (Schenkel et al., 2014). Two major groups of adaptive immune cells are T cells and B cells, both of which can be further classified into numerous subgroups based on specific functions (Barton and Medzhitov, 2002). Unlike adaptive immune cells, innate immune cells lack antigen specificity and can react to a wide range of pathogens. Therefore, they provide immediate and generic protection to the host (Spits et al., 2013). The innate immune cells encompass many cell types, including dendritic cells, mast cells, macrophages, neutrophils, basophils, eosinophils, γδT cells, and recently-discovered innate lymphoid cells (Akira et al., 2006; Serafini et al., 2014). Due to the scope of this chapter, I would like to highlight two types of innate immune cells.

Dendritic cells

Dendritic cells (DCs) are phagocytic cells with a shape that resembles to neuronal dendrites. The most well-known function of dendritic cells is to process antigen material and present it on the cell surface to adaptive immune cells, such as T cells and B cells (Sato and Fujita, 2007). Thus,

dendritic cells are also known as antigen presenting cells (APC), and act as a link between the innate and adaptive immune system. During antigen presentation, DCs secrete cytokines including IL-12, IL-23 or IL-10, as well as costimulatory molecules, such as OX40-L or ICOS-1, to help activate and polarize immature T cells to develop into various mature functional T helper cells (BLANCO et al., 2008). Dendritic cells are derived from common myeloid progenitor (CMP) cells in the bone marrow. When CMP give rise to pre-DCs, they migrate from the bone marrow to lymphoid and non-lymphoid tissues. Dendritic cells can be found in most organs, including skin, liver, kidney, heart, gastrointestinal tract, and other connective tissues and tend to be associated with vascular structures. However, only a small number of DCs can be found in the blood stream (Liu and Nussenzweig, 2010; Mellman and Steinman, 2001). Dendritic cells can be classified based on cell surface markers and their anatomical location. In mouse, a predominant number of DCs are $CD11c^{+}MHC\ II^{+}$, and subgroups can be further classified based on the expression of CD4, CD8, CD11b, CD103 and CD205 (Liu and Nussenzweig, 2010).

In the intestine, dendritic cells are found throughout the intestinal lamina propria, and also reside in Peyer's patches and mesenteric lymph nodes (MLNs), which lie between the layers of mesentery. At steady state, intestinal dendritic cells initiate antigen sampling in the lamina propria and Peyer's patches, then migrate to MLNs to present antigens to T cells (Coombes and Powrie, 2008). Notably, the $CD103^{+}$ intestinal DCs have been shown to be able to project their dendrites between epithelial cells, which allows those DCs to sample bacterial antigens in the gut lumen. This is probably because CD103 can bind integrin β7 to form the heterodimeric integrin molecule αEβ7, which then binds to E-cadherin on epithelial cells (Cerovic et al., 2013; Farache et al., 2013).

Innate lymphoid cells

Innate lymphoid cells (ILCs) are a family of developmentally related cells that are involved in immunity and in tissue development and remodeling (Spits et al., 2013). ILCs are derived from the common lymphoid progenitor (CLP) in the bone marrow and belong to the lymphoid lineage. Morphologically, ILCs resemble adaptive lymphoid cells, such as T cells and B cells, and do not express myeloid or dendritic cell surface markers. However, ILCs are devoid of recombination activating gene (RAG)-dependent rearranged antigen receptors. Thus the activation of ILCs does not require antigen priming and can immediately respond to a wide range of immune stimulation (Serafini et al., 2014; Spits et al., 2013). Natural killer (NK) cells and lymphoid tissue-inducer (LTi) cells were the first ILCs to be characterized (Artis and Spits, 2015). After that, other groups of ILCs with distinct cellular markers and functions were discovered. To better group those cells, a new classification of ILCs was created (Spits et al., 2013).

The current classification of ILCs is based primarily on the differentiation markers and cytokines they secrete. So far, three groups of ILCs have been named: ILC group 1, 2 and 3. Group 1 ILC (ILC1) comprises ILCs that require the transcription factors T-bet and/or Eomesodermin (EOMES) for their differentiation. They produce cytokine interferon-γ (IFNγ) and thus functionally resemble T helper 1 (T_H1) cells (Constantinides et al., 2014; Klose et al., 2014). Group 2 ILC (ILC2) comprises ILCs that require transcription factor GATA binding protein 3 (GATA-3) and retinoic acid receptor-related orphan receptor α (RORα) for their development. They produce type 2 cytokines, such as IL-5 and IL-13, and functionally resemble T_H2 cells (Bernink et al., 2014; Licona-Limón et al., 2013). Group 3 ILC (ILC3) comprises ILCs that require transcription factor RORγt and produce IL17 and/or IL-22, hence resembling T_H17 cells (Geiger

et al., 2014; van de Pavert et al., 2015; Yu et al., 2014). According to this classification, NK cells therefore belong to ILC1, and LTi cells belong to ILC3.

RESULTS

As described in chapter three, I have uncovered a fundamental role for epithelial NFIL3 in mediating microbiota- induced lipid storage and body fat accumulation in mice. In this chapter, I will extend this finding further and discuss the underlying mechanism by which the microbiota regulates the expression of epithelial NFIL3.

Epithelial *Nfil3* is regulated by the circadian transcriptional suppressor REV-ERBα

The expression of *Nfil3* is controlled by the circadian clock and thus its expression is diurnally rhythmic (Gibbs et al., 2012). To study the circadian expression of *Nfil3* in epithelial cells, I isolated intestinal epithelial cells by laser capture microdissection from 4 time points across a 24-hour day-night cycle, and analyzed the transcript abundance of *Nfil3* at each time point. Similar to prior studies on other cell types, the expression of epithelial *Nfil3* exhibited strong circadian oscillation with peak expression at Zeitgiber time 2 (ZT2) and trough expression at ZT14 (FIGURE 19A). I further found that the amplitude of circadian expression of epithelial *Nfil3* was significantly dampened in epithelial cells from germ-free mice, confirming the prior finding that the microbiota is required for the maximal expression of epithelial *Nfil3* (FIGURE 19A). The circadian transcription of epithelial *Nfil3* and the requirement for the microbiota were also reflected in protein expression levels as analyzed by Western blot of isolated epithelial cells (FIGURE 19B).

In T cells and liver cells, the expression of NFIL3 is regulated by the core circadian clock repressor REV-ERBα. In those cells, REV-ERBα directly binds to a consensus sequence in the

Nfil3 promoter and represses its transcription, resulting in a diurnal *Nfil3* expression pattern (Yu et al., 2013). Similarly, in intestinal epithelial cells, the transcript and protein abundance of *Rev-erbα* also exhibited strong circadian oscillation and with peak expression at ZT8 and trough expression at ZT20 (FIGURE 19C). In germ-free mice, the amplitude of epithelial *Rev-erbα* circadian expression was significantly increased relative to conventional mice (FIGURE 19D), which is opposite to *Nfil3* and suggesting that epithelial *Nfil3* may also be regulated by REV-ERBα.

Indeed, REV-ERBα directly bound to the promoter of epithelial *Nfil3* as shown by chromatin immunoprecipitation (ChIP) assay on isolated intestinal epithelial cells. DNA fragments containing *Nfil3* promoter were highly enriched in the sample precipitated using REV-ERBα specific antibody than in the group precipitated using a non-specific antibody control (FIGURE 20A). In addition, antibiotic depletion of the intestinal microbiota in *Rev-erbα*$^{-/-}$ mice did not lead to suppression of epithelial *Nfil3* expression as seen in conventional wild-type mice (FIGURE 20B), indicating a requirement for REV-ERBα in the microbiota-induced epithelial *Nfil3* expression. Together, these results supported the idea that expression of epithelial *Nfil3* is directly regulated by REV-ERBα.

Microbiota regulation of epithelial *Nfil3* expression requires dendritic cell MyD88 signaling

Various pattern-recognition receptor (PRR) pathways recognize and transduce pathogen-associated molecular patterns (PAMPs) in cells. In intestinal epithelial cells, many key genes regulated by the microbiota are controlled by Toll-like receptors (TLRs) and their common signaling adaptor MyD88. Examples include *Reg3g* (Vaishnava et al., 2011), *Defb4* (Vora et al., 2004) and *Ang4* (Mukherjee et al., 2008). To determine whether MyD88 is required for microbiota regulation of *Rev-erbα* and *Nfil3* expression in epithelial cells, I quantified the transcript

abundances of *Rev-erbα* and *Nfil3* in isolated epithelial cells from co-housed *Myd88*$^{-/-}$ mice and wild-type littermates at ZT4, which is when *Nfil3* expression is near-peak in conventional mice (FIGURE 21A). The expression of *Rev-erbα* increased in *Myd88*$^{-/-}$ mice and was not significantly different from the levels seen in germ-free mice. Consequently, the expression of *Nfil3* was decreased in *Myd88*$^{-/-}$ mice to levels that were similar to those of germ-free mice (FIGURE 21B). This indicated that microbiota regulation of the epithelial *Rev-erbα*-*Nfil3* cascade requires MyD88 signaling.

However, when I quantified the transcript abundances of *Rev-erbα* and *Nfil3* in epithelial cells from epithelial cell-specific *Myd88* knockout mice (*Myd88*$^{\Delta IEC}$ mice), the expression of both *Rev-erbα* and *Nfil3* did not change (FIGURE 21A,B), suggesting epithelial cell-intrinsic MyD88 was dispensable for regulating the epithelial *Rev-erbα*-*Nfil3* cascade. Instead, when I isolated epithelial cells from dendritic cell-specific *Myd88* knockout mice (*Myd88*$^{\Delta DC}$ mice) and quantified the transcript abundances of *Rev-erbα* and *Nfil3*, increased expression of *Rev-erbα* and decreased expression of *Nfil3* were observed (FIGURE 21A,B). This indicated that dendritic cell MyD88 but not epithelial cell MyD88 was required for the microbiota regulation of epithelial *Rev-erbα*-*Nfil3* cascade.

To further test for dendritic cell involvement, I quantified the abundances of *Rev-erbα* and *Nfil3* transcripts in epithelial cells from a mouse model that has dendritic cell specific depletion achieved by *Diphtheria* toxin administration. In those mice, *Diphtheria* toxin receptors (DTR) are selectively expressed on dendritic cells under the control of the *Cd11c* promoter (Patsouris et al., 2008). *Cd11c*$^{+}$ cells, which include most dendritic cells, are selectively killed after oral administration of *Diphtheria* toxin (Patsouris et al., 2008). On *Cd11c*$^{+}$ cell depletion, the

expression of *Rev-erbα* increased and the expression of *Nfil3* decreased to germ-free levels (FIGURE 22A,B), supporting the conclusion that dendritic cells are required for microbiota induction of epithelial *Nfil3*.

A DC-ILC3 relay circuit is required for microbiota regulation of epithelial *Nfil3*

Previous studies have identified a subepithelial cellular signaling relay in the small intestine that captures bacterial signals and passes them to epithelial cells to regulate key epithelial genes, such as *Fut2* (Pickard et al., 2014) and *Saa* (Sano et al., 2015). In this circuit, bacteria activate the TLR-MyD88 pathway in dendritic cells, and bacterial signals are relayed to group 3 innate lymphoid cells (ILC3) through dendritic cell production of cytokine interleukin-23 (IL-23). Activated ILC3 then pass this signal to epithelial cells through the production of IL-22 (Pickard et al., 2014). Given that dendritic cell MyD88 is indispensable for bacteria induction of epithelial *Nfil3*, I hypothesized that the microbiota regulation of epithelial *Nfil3* is dependent on this DC-ILC3 relaying circuit.

To test this hypothesis, I quantified the abundances of *Rev-erbα* and *Nfil3* transcripts in epithelial cells from *Rag2* and common gamma chain double knockout mice (*Rag2*$^{-/-}$*;Il2rg*$^{-/-}$ mice). In *Rag2*$^{-/-}$*;Il2rg*$^{-/-}$ mice, all subsets of ILCs, T cells and B cells are developmentally deficient (Yu et al., 2014). Compared to wild-type littermates, the epithelial expression of *Rev-erbα* was increased and expression of *Nfil3* was decreased in *Rag2*$^{-/-}$*;Il2rg*$^{-/-}$ mice (FIGURE 22A,B). To rule out the possibility that increased expression of epithelial *Rev-erbα* and decreased expression of epithelial *Nfil3* in *Rag2*$^{-/-}$*;Il2rg*$^{-/-}$ mice were due to the deficiency of T and B cells, I used *Rag1*$^{-/-}$ mice, which are T and B cell deficient but with ILCs intact (Goto et al., 2014). In contrast to *Rag2*$^{-/-}$*;Il2rg*$^{-/-}$ mice, the epithelial expression of *Rev-erbα* was decreased and expression of *Nfil3* was increased in *Rag1*$^{-/-}$ mice (FIGURE 22A,B), establishing that T and B cells were not required for

bacterial reduction of epithelial *Rev-erbα* expression. The reason that *Nfil3* expression was higher in *Rag1*$^{-/-}$ mice than in conventional wild-type mice is likely due to the elevated bacterial loads as well as aberrant expansion of ILCs in the small intestines of these mice (Goto et al., 2014). To further test the requirement for ILCs, I also used ID2 deficient mice (*Id2*$^{gfp/gfp}$), which are known to lack all known ILC subsets (Boos et al., 2007; Savage et al., 2008). In *Id2*$^{gfp/gfp}$ mice, epithelial expression of *Rev-erbα* was increased and expression of *Nfil3* was decreased (FIGURE 22A,B), supporting the idea that ILCs are required for microbiota regulation of epithelial *Rev-erbα*.

Previous studies have shown that group 3 ILC is the major ILCs subset that relays bacterial signals to epithelial cells (Pickard et al., 2014). To test whether this is also true in microbiota regulation of epithelial *Nfil3*, I analyzed the abundance of *Rev-erbα* and *Nfil3* transcripts across a 24-hour cyle in epithelial cells from RORγt-deficient mice (*Rorc*$^{gfp/gfp}$ mice), which lack both T_H17 cell (a specific $CD4^+$ T cell lineage) and ILC3. As expected, the circadian expression patterns of both epithelial *Rev-erbα* and *Nfil3* in *Rorc*$^{gfp/gfp}$ mice were similar to germ-free mice (FIGURE 23A,B), supporting the necessity of ILC3 for microbiota induction of epithelial *Nfil3* expression through REV-ERBα.

In the DC-ILC3 relay circuit, bacterial signals are relayed from DC to ILC3 through IL-23 production, then further relayed from ILC3 to epithelial cells through IL-22 (Pickard et al., 2014). To test whether these cytokines are also required for microbiota-regulated *Nfil3* expression, I treated *Myd88*$^{-/-}$ mice with recombinant IL-23 or IL-22. After IL-23 or IL-22 treatment, the epithelial *Rev-erbα* and *Nfil3* expression was rescued to the conventional wild-type level (FIGURE 24A,B), confirming the requirement of both IL-23 and IL-22 in microbiota regulation of epithelial *Nfil3*. This finding further supports the idea that the subepithelial DC-ILC3 circuit relays bacterial signals to epithelial cells to regulate *Nfil3* expression.

Flagellin and lipopolysaccharide (LPS) are two molecules of Gram-negative bacteria that are recognized by TLRs. Both flagellin and LPS can activate the intestinal DC-ILC3 circuit (Kinnebrew et al., 2012; Pickard et al., 2014). Accordingly, treatment of germ-free mice with flagellin or LPS resulted in decreased expression of epithelial *Rev-erbα* and increased expression of epithelial *Nfil3* (FIGURE 25A,B). Further, monoassociation of germ-free mice with Gram-negative, flagellated bacterial species *Salmonella typhimurium* or *Escherichia coli* also suppressed *Rev-erbα* expression and induced *Nfil3* expression (FIGURE 25A,B). In contrast, the expression of epithelial *Rev-erbα* and *Nfil3* was not markedly altered upon monoassociation of germ-free mice with the Gram-positive strain *Enterococcus faecalis* (FIGURE 25A,B). Interestingly, when germ-free mice were monoassociated with the Gram-negative, non-flagellated species *Bacteroides thetaiotaomicron,* the epithelial expression of both *Rev-erbα* and *Nfil3* remained at the germ-free level (FIGURE 25A,B), suggesting that epithelial *Nfil3* expression is selectively activated by Gram-negative, motile bacteria. This is likely because such bacteria produce both flagellin and LPS, and because they can readily penetrate the intestinal epithelial barrier and contact lamina propria DCs to activate TLR-MyD88 signaling.

As discussed in chapter three, epithelial NFIL3 is responsible for regulating the transcription of key epithelial metabolic genes (FIGURE 16A). Given that epithelial *Nfil3* expression is regulated by DC-ILC3 relay circuit, mice lacking elements of the circuit should exhibit reduced expression of those genes in epithelial cells. Indeed, when I quantified the transcript abundances of *Cd36* and *Scd1* in epithelial cells from $Id2^{-/-}$ mice, the expression of both genes was reduced as compared to wild-type littermates (FIGURE 26A,B). This supports the conclusion that NFIL3 is a key regulator of microbiota-dependent body fat accumulation.

STAT3 directly regulates the transcription of epithelial *Rev-erbα*

Bacterial signals are relayed from ILC3 to epithelial cells through the cytokine IL-22. Previous studies have identified the transcription factor STAT3 as the major response element downstream of the IL-22 receptor (IL-22R) (Pickert et al., 2009). On IL-22 activation, IL-22R leads to phosphorylation of STAT3, which then binds to the promoters of its target genes and either activates or inhibits their transcription (Pickert et al., 2009). To determine if STAT3 directly regulates epithelial *Rev-erbα*, I performed ChIP analysis on isolated intestinal epithelial cells. Chromatin precipitated with STAT3-specific antibody was highly enriched in DNA fragments containing the *Rev-erbα* promoter, but not enriched in fragments containing a *Rev-erbα* exon (FIGURE 27A,B), suggesting that STAT3 directly binds to the *Rev-erbα* promoter. Importantly, STAT3 binding to the *Rev-erbα* promoter was markedly reduced in epithelial cells from germ-free (FIGURE 27A,B), which was consistent with the finding that *Rev-erbα* expression was increased in epithelial cells from germ-free mice. These results indicated an inhibitory role for STAT3 in regulating *Rev-erbα* transcription.

The STAT3 inhibition of *Rev-erbα* promoter function was further analyzed by a luciferase reporter assay. When HEK-293T cells were co-transfected with STAT3-encoding vectors and luciferase reporters were fused to the *Rev-erbα* promoter, the luciferase activity was significantly reduced compared to HEK-293T cells that were co-transfected with empty vector and the same luciferase reporters (FIGURE 27C). The luciferase activity was further suppressed when switching wild-type STAT3-encoding vectors to a dominant active form of STAT3-encoding vectors

(FIGURE 27C). This result confirmed that STAT3 directly binds to the *Rev-erb*α promoter and inhibits its transcription.

To further test the role of STAT3 in repressing *Rev-erb*α transcription, I used cultured intestinal organoids. When recombinant IL-22 was added to organoid cultures, STAT3 quickly became phosphorylated (FIGURE 28A), supporting prior findings that IL-22 activates STAT3 in intestinal epithelial cells (Pickert et al., 2009). At the same time, expression of *Rev-erb*α was decreased and expression of *Nfil3* was consequently increased as compared to control groups (FIGURE 28B,C). In contrast, when a STAT3 phosphorylation inhibitor (Stattic) was added to the organoid culture together with recombinant IL-22, the phosphorylation of STAT3 was completely inhibited (FIGURE 28B,C), and the expression of *Rev-erb*α and *Nfil3* remained the similar to the controls (FIGURE 28B,C). These results further indicate that STAT3 is a transcriptional repressor of *Rev-erb*α.

In order to test the requirement for STAT3 in repressing *Rev-erb*α transcription *in vivo*, I generated a mouse model that has *Stat3* specifically deleted in epithelial cells ($Stat3^{\Delta IEC}$ mice). Compared to wild-type littermates, the abundance of epithelial *Rev-erb*α transcripts was increased in $Stat3^{\Delta IEC}$ mice, and the abundance of epithelial *Nfil3* transcripts was reduced, consistent with *in vitro* findings (FIGURE 29A,B). Notably, the expression of *Stat3* and the phosphorylation of STAT3 in intestinal epithelial cells did not exhibit diurnal oscillations (FIGURE 30A,B), suggesting that the rhythmicity of *Rev-erb*α and *Nfil3* expression was not generated by STAT3. This indicated that the circadian rhythms of epithelial *Nfil3* expression is generated by the central circadian clock through REV-ERBα, and the amplitude of these rhythms is fine-tuned by the microbiota through STAT3.

Similar to the *Id2*$^{-/-}$ mice discussed above, reduced expression of epithelial *Nfil3* in *Stat3*$^{\Delta IEC}$ mice should lead to decreased expression of key epithelial metabolic genes. Indeed, transcript abundances of *Cd36* and *Scd1* in epithelial cells from *Stat3*$^{\Delta IEC}$ mice were both decreased as compared to their floxed littermates (FIGURE 31A,B). This confirmed STAT3 as the response element downstream of IL-22R, and further supported the idea that the microbiota regulates lipid metabolism and body composition through epithelial NFIL3.

CONCLUSIONS

In this chapter, I have revealed the underlying mechanism by which the microbiota regulates epithelial NFIL3 expression. First, LPS or flagellin produced by Gram-negative bacteria triggers the activation of dendritic cells residing underneath the epithelium through TLR-MyD88 signaling. Then, activated dendritic cells relay this bacterial signal to group 3 ILCs through production of IL-23. When group 3 ILCs are activated by IL-23, they further relay the signal to epithelial cells through production of IL-22. Once epithelial cells receive IL-22 through IL-22R, epithelial intrinsic STAT3 gets phosphorylated and directly binds to the promoter of *Rev-erb*α to inhibit *Rev-erb*α transcription. Finally, reduced abundance of REV-ERBα in epithelial cells leads to increased expression of epithelial *Nfil3*. With this understanding the mechanisms of microbiota-induced epithelial NFIL3 expression, my studies have established NFIL3 as an essential molecular link among the microbiota, the circadian clock, and host metabolism.

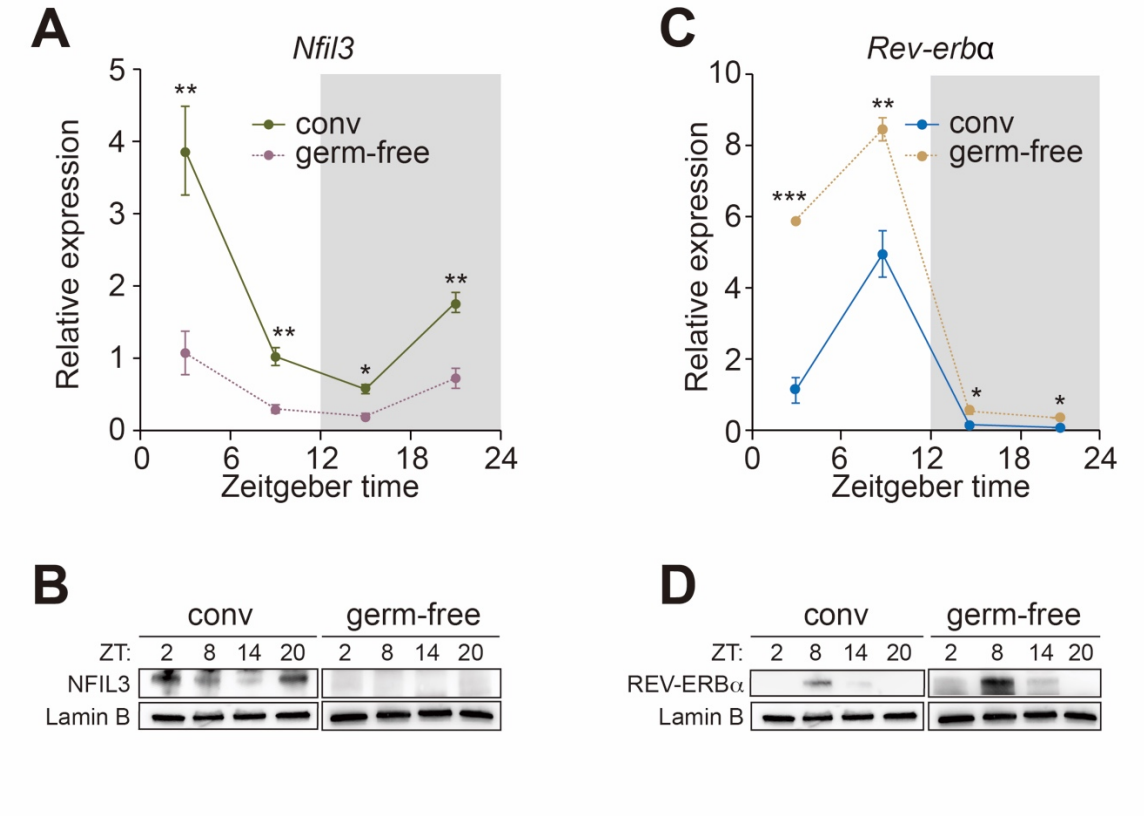

FIGURE 19: Circadian expression of epithelial NFIL3 and REV-ERBα

(A-D) qRT-PCR analysis of *Nfil3* **(A)** and *Rev-erbα* **(C)** transcript abundance in small intestinal epithelial cells from germ-free (dotted line) and conventional mice (solid line) across a 24-hour day-night light cycle. Western blot analysis of NFIL3 **(B)** and REV-ERBα **(D)** was performed on small intestinal epithelial cells isolated from conventional or germ-free mice. Lamin B is the loading control. N=3-8 mice per group. Means±SEM are plotted; statistics were performed with Student's t-test. *p<0.05; **p<0.01; ***p<0.001; conv, conventional; ZT, Zeitgeber time.

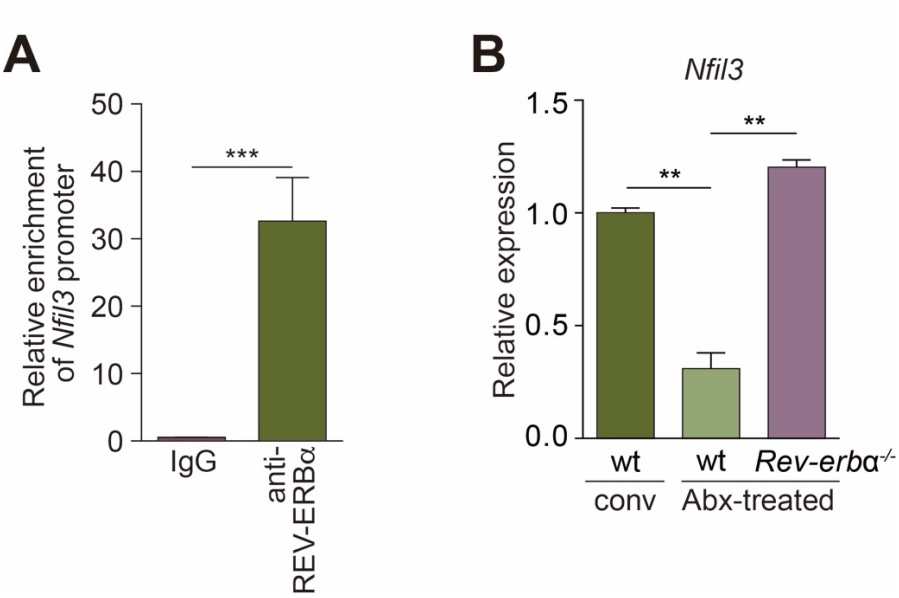

FIGURE 20: REV-ERBα directly regulates epithelial *Nfil3* expression

(A) Chromatin immunoprecipitation assay on intestinal epithelial cells using immunoglobulin G (IgG) or anti-REV-ERBα antibody. Precipitated fragments of the *Nfil3* promoter were detected by qRT-PCR. **(B)** qRT-PCR analysis of epithelial *Nfil3* expression in conventional wild-type, antibiotic (Abx)-treated wild-type or Abx-treated *Rev-erbα*$^{-/-}$ mice. N=3-5 mice per group. Means±SEM are plotted; statistics were performed with Student's t-test or one-way ANOVA. **p<0.01; ***p<0.001.

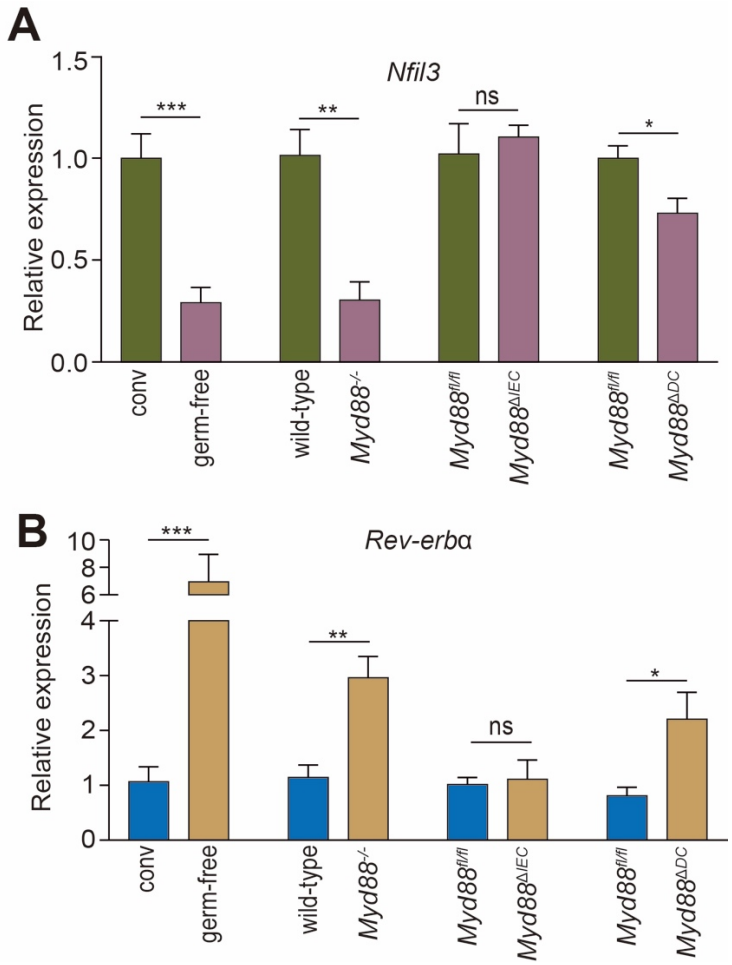

FIGURE 21: Dendritic cell MyD88 is required for microbiota-induced *Nfil3* expression

(A) qRT-PCR analysis of epithelial *Nfil3* expression in germ-free and conventional wild-type mice and conventional $Myd88^{fl/fl}$, $Myd88^{-/-}$, $Myd88^{\Delta IEC}$ (epithelial cell-specific knockout) and $Myd88^{\Delta DC}$ (DC-specific knockout) mice. **(B)** qRT-PCR analysis of epithelial *Rev-erbα* expression in germ-free and conventional wild-type mice and conventional $Myd88^{fl/fl}$, $Myd88^{-/-}$, $Myd88^{\Delta IEC}$ and $Myd88^{\Delta DC}$ mice. Mice were sacrificed at ZT4. N=3-8 mice per group. Means±SEM are plotted; statistics were performed with Student's t-test. *p<0.05; **p<0.01; ***p<0.001; ns, not significant.

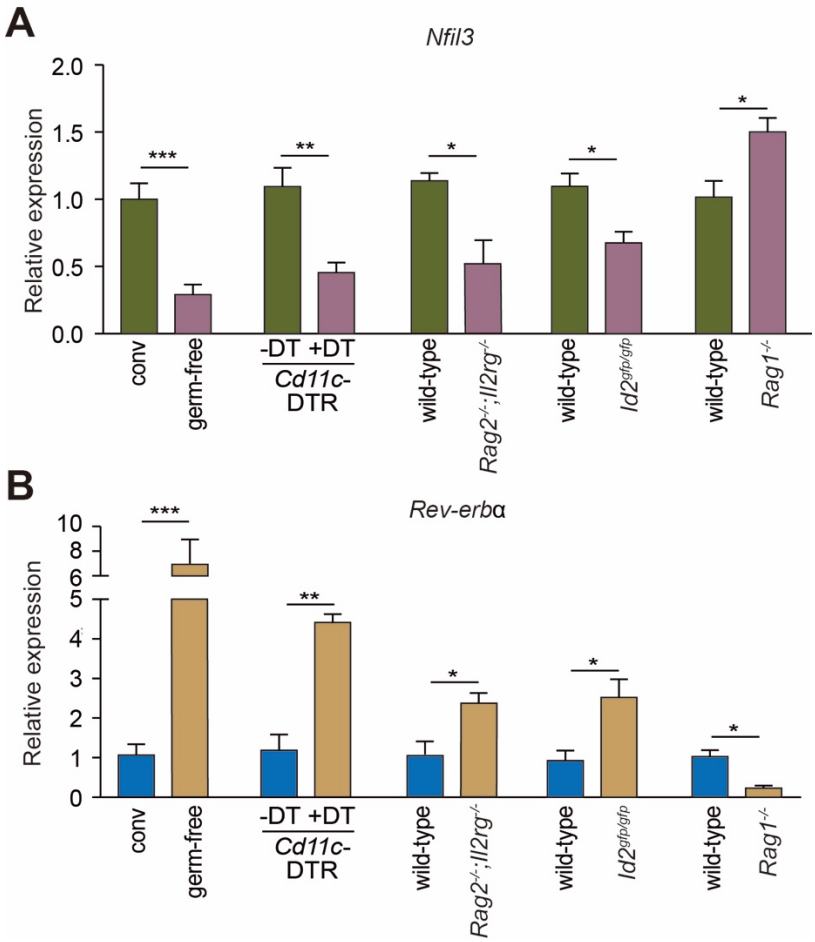

FIGURE 22: DCs and ILCs are required for microbiota-induced *Nfil3* expression

(A) qRT-PCR analysis of epithelial *Nfil3* expression in germ-free and conventional wild-type mice, conventional *Cd11c*-DTR mice that were untreated or treated with *Diphtheria* toxin (DT), *Rag2*$^{-/-}$*;Il2rg*$^{-/-}$, *Id2*$^{gfp/gfp}$ and *Rag1*$^{-/-}$ mice. **(B)** qRT-PCR analysis of epithelial *Rev-erb*α expression in germ-free and conventional wild-type mice, conventional *Cd11c*-DTR mice that were untreated or treated with *Diphtheria* toxin (DT), *Rag2*$^{-/-}$*;Il2rg*$^{-/-}$, *Id2*$^{gfp/gfp}$ and *Rag1*$^{-/-}$ mice. Mice were sacrificed at ZT4. N=3-8 mice per group. Means±SEM are plotted; statistics were performed with Student's t-test. *p<0.05; **p<0.01; ***p<0.001.

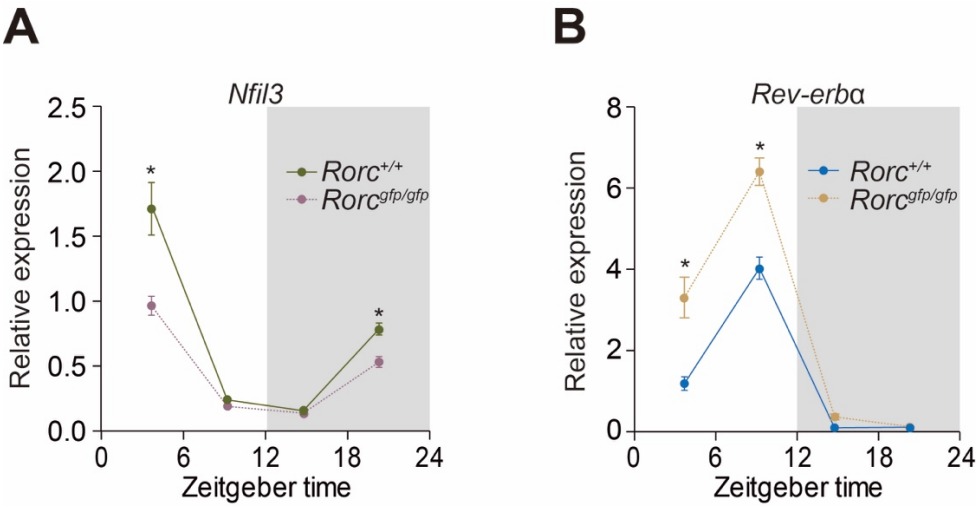

FIGURE 23: ILC3 are required for microbiota-induced *Nfil3* expression

(A) qRT-PCR analysis of epithelial *Nfil3* expression in *Rorc*$^{+/+}$ (solid line) and *Rorc*$^{gfp/gfp}$ (dotted line) mice across a 24-hour circadian cycle. **(B)** qRT-PCR analysis of epithelial *Rev-erbα* expression in *Rorc*$^{+/+}$ (solid line) and *Rorc*$^{gfp/gfp}$ (dotted line) mice across a 24-hour circadian cycle. N=5-8 mice per group. Means±SEM are plotted; statistics were performed with Student's t-test. *p<0.05.

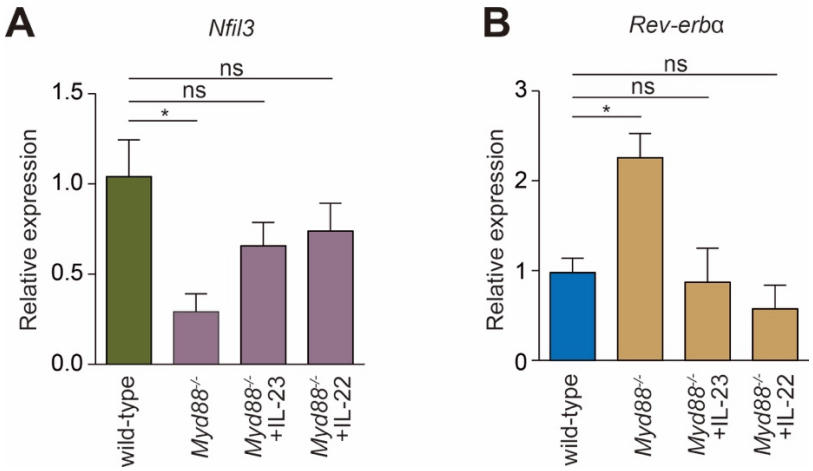

FIGURE 24: IL-22 and IL-23 rescue epithelial *Nfil3* and *Rev-erbα* expression in *Myd88*$^{-/-}$ mice

(A) qRT-PCR analysis of epithelial *Nfil3* expression in *Myd88*$^{-/-}$ mice treated with recombinant IL-23, IL-22 or vehicle. **(B)** qRT-PCR analysis of epithelial *Rev-erbα* expression in *Myd88*$^{-/-}$ mice treated with recombinant IL-23, IL-22 or vehicle. Mice were sacrificed at ZT4. N=3-5 mice per group. Means±SEM are plotted; statistics were performed with one-way ANOVA. *$p<0.05$; ns, not significant.

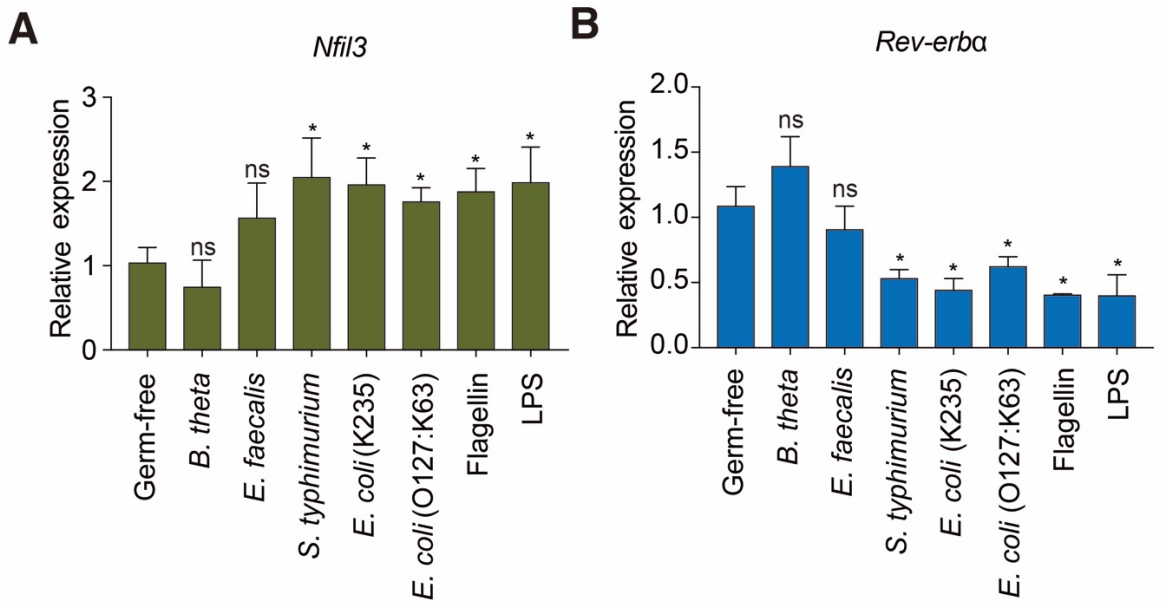

FIGURE 25: Epithelial *Nfil3* expression can be induced by flagellin or LPS

(A,B) qRT-PCR quantification of epithelial *Rdev-erbα* **(A)** and *Nfil3* **(B)** transcripts in germ-free mice, germ-free mice mono-colonized with *Bacteroides thetaiotaomicron* (*B. theta*), *Enterococcus faecalis*, *Salmonella typhimurium*, non-pathogenic *Escherichia coli* strain K235 or the pathogenic *Escherichia coli* strain O127:K63 through oral gavage, and germ-free mice treated with flagellin or LPS through retro orbital vein. Mice were sacrificed at ZT4. N=3-6 per group. Error bars represent SEM; statistics were performed with Student's t-test. *p<0.05; ns, not significant.

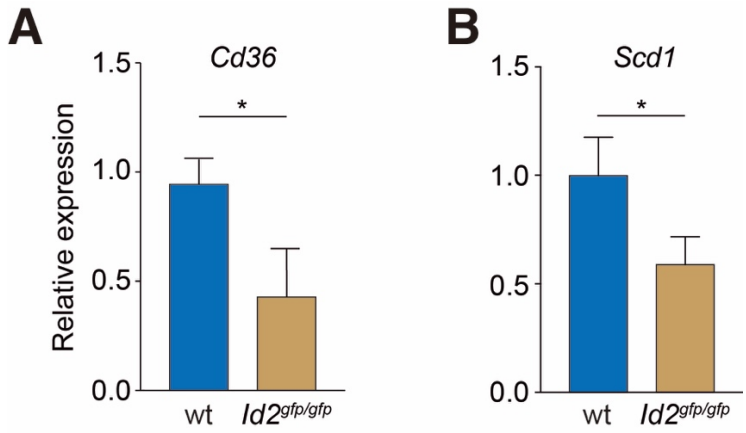

FIGURE 26: Reduced epithelial *Cd36* and *Scd1* expression in *Id2*$^{gfp/gfp}$ mice

(A) qRT-PCR analysis of epithelial *Cd36* expression in conventional wild-type (wt) and ID2-deficient (*Id2*$^{gfp/gfp}$) mice. **(B)** qRT-PCR analysis of epithelial *Scd1* expression in conventional wild-type (wt) and ID2-deficient (*Id2*$^{gfp/gfp}$) mice. Mice were sacrificed at ZT4. N=5-12 mice per group. Means±SEM are plotted; statistics were performed with Student's t-test. *$p<0.05$.

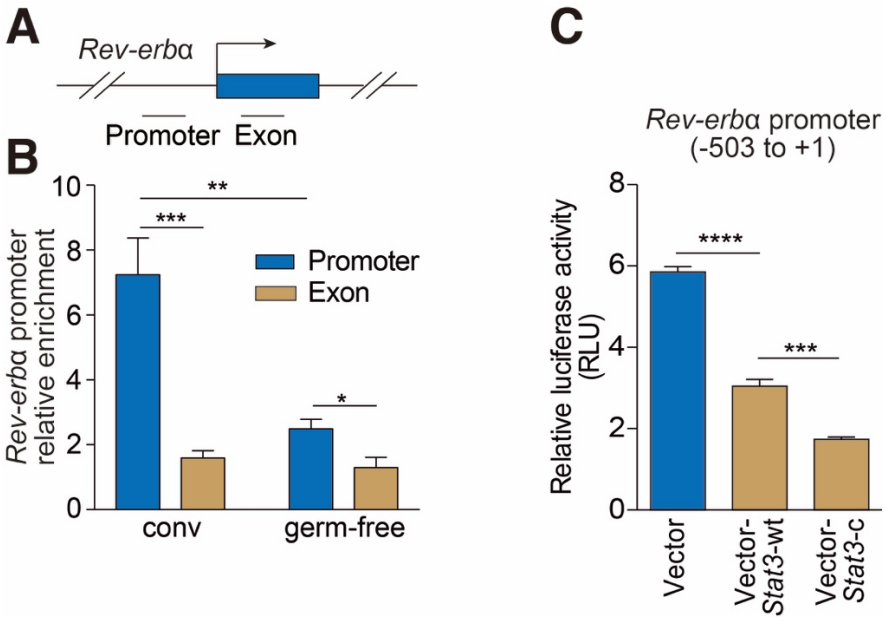

FIGURE 27: STAT3 directly binds to the *Rev-erbα* promoter and inhibits its activity

(A) Schematic of the *Rev-erbα* gene promoter. **(B)** ChIP analysis of intestinal epithelial cells from conventional (conv) or germ-free mice using immunoglobulin G (IgG) or anti-STAT3 antibody. Precipitated fragments of the *Rev-erbα* promoter or control exon were detected by qRT-PCR. **(C)** Luciferase reporter assay. A 504 bp fragment of *Rev-erbα* promoter was fused to a firefly luciferase reporter. HEK-293T cells were transfected with reporters and either empty vector, a wild-type STAT3-encoding vector (*Stat3*-wt), or a dominant active STAT3-encoding vector (*Stat3*-c). N=4 samples per group. Means±SEM are plotted; statistics were performed with Student's t-test or one-way ANOVA. *p<0.05; **p<0.01; ***p<0.001; ****p<0.0001.

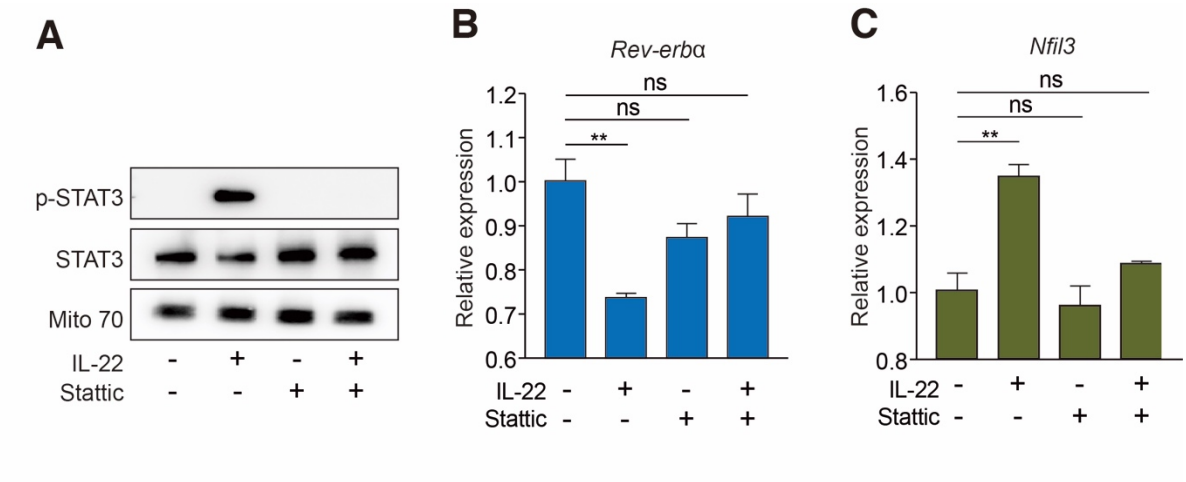

FIGURE 28: STAT3 regulates *Rev-erbα* expression in intestinal organoids

(A) Western-blot of total STAT3, phosphorylated STAT3 (p-STAT3) in small intestinal organoids treated with IL-22 and/or the STAT3 inhibitor Stattic. Mito 70 is the loading control. **(B)** qRT-PCR analysis of *Rev-erbα* expression in small intestinal organoids treated with IL-22 and/or Stattic. **(C)** qRT-PCR analysis of *Nfil3* expression in small intestinal organoids treated with IL-22 and/or Stattic. N=4 samples per group. Means±SEM are plotted; statistics were performed with one-way ANOVA. **p<0.01; ns, not significant.

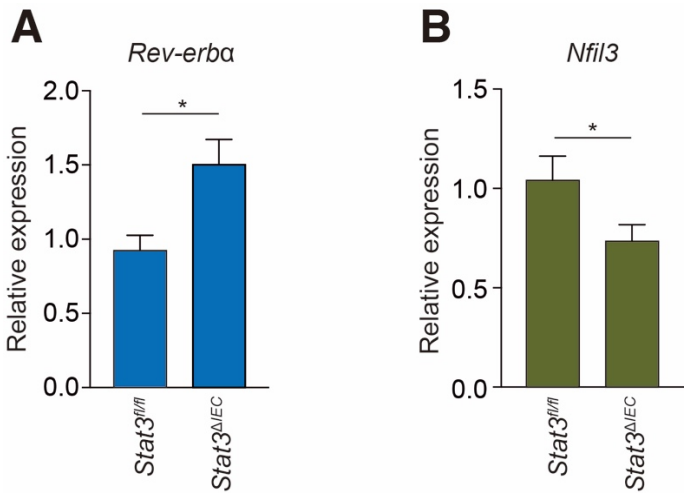

FIGURE 29: STAT3 regulates *Rev-erbα* expression *in vivo*

(A) qRT-PCR analysis of epithelial *Rev-erbα* expression in $Stat3^{fl/fl}$ and $Stat3^{\Delta IEC}$ mice at ZT4. **(B)** qRT-PCR analysis of epithelial *Nfil3* expression in $Stat3^{fl/fl}$ and $Stat3^{\Delta IEC}$ mice at ZT4. N=5-8 samples per group. Means±SEM are plotted; statistics were performed with Student's t-test. *$p<0.05$.

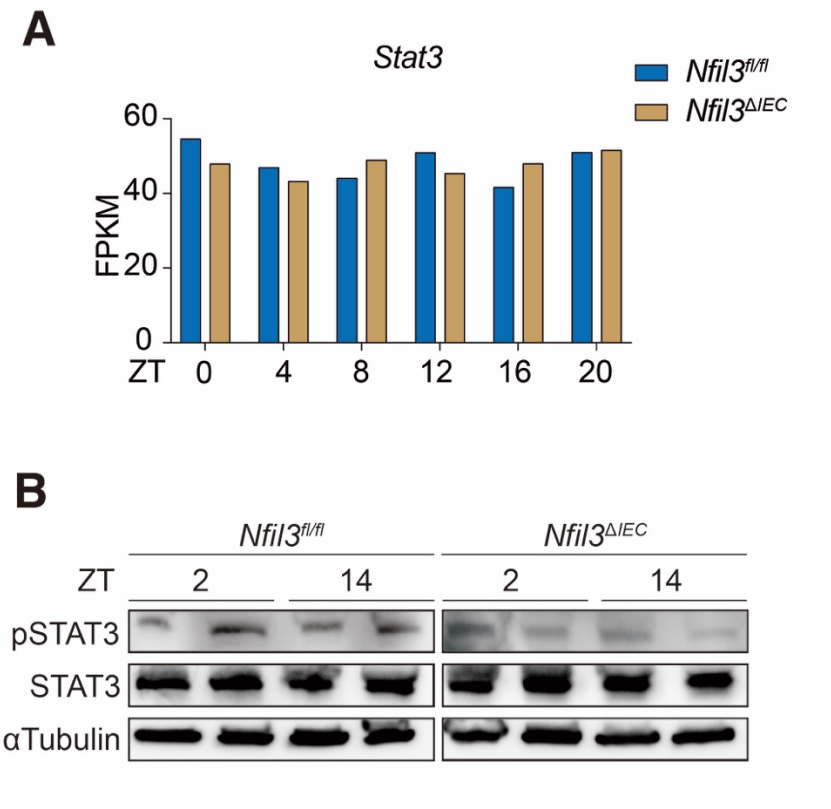

FIGURE 30: The expression and activation of epithelial STAT3 do not exhibit circadian rhythms in *Nfil3*$^{fl/fl}$ and *Nfil3*$^{\Delta IEC}$ mice

(A) RNA-seq analysis of Fragments Per Kilobase of transcript per Million mapped reads (FPKM) of *Stat3* across a circadian cycle in isolated intestinal epithelial cells from *Nfil3*$^{fl/fl}$ and *Nfil3*$^{\Delta IEC}$ mice. **(B)** Western-blot of STAT3 and phosphorylated STAT3 in isolated intestinal epithelial cells from *Nfil3*$^{fl/fl}$ and *Nfil3*$^{\Delta IEC}$ mice at ZT2 and ZT14. αTubulin is the loading control.

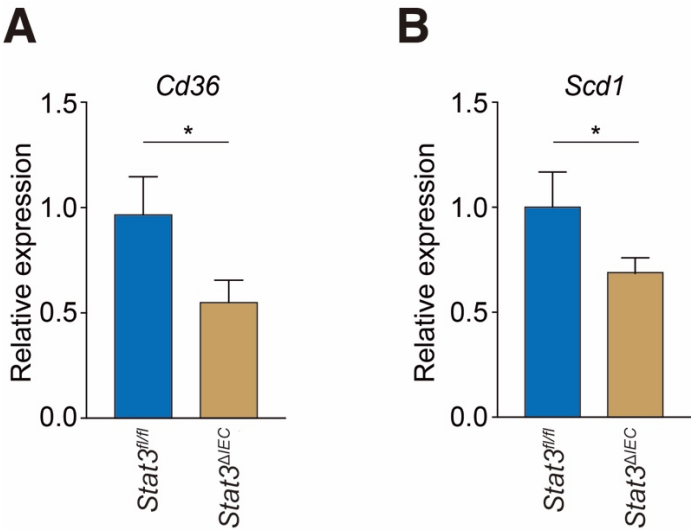

FIGURE 31: Reduced epithelial *Cd36* and *Scd1* expressions in *Stat3*$^{\Delta IEC}$ mice

(A) qRT-PCR analysis of epithelial *Cd36* expression in *Stat3*$^{fl/fl}$ and *Stat3*$^{\Delta IEC}$ mice. **(B)** qRT-PCR analysis of epithelial *Scd1* expression in *Stat3*$^{fl/fl}$ and *Stat3*$^{\Delta IEC}$ mice. Mice were sacrificed at ZT4. N=8 mice per group. Means±SEM are plotted; statistics were performed with Student's t-test. *$p<0.05$.

CHAPTER FIVE

DISCUSSION AND FUTURE DIRECTIONS

DISCUSSION

The microbiota is an environmental factor that markedly impacts mammalian metabolism. Accumulating evidence has established a strong relationship between the microbiota and the occurrence of various of metabolic diseases, such as malnutrition, insulin resistance, and obesity (Blanton et al., 2016; Nicholson et al., 2012; Tilg et al., 2009). The intestinal microbiota is required for proper energy storage and body fat accumulation, and therefore mice raised in a complete sterile environment have lower body weights and body fat, and are protected from high-fat diet-induced obesity (Bäckhed et al., 2004; Rabot et al., 2010a). In addition, the composition of the intestinal microbiota serves as a determinant of host body composition. Obese patients have been shown to carry microbiotas that are distinct from those of healthy people (Cani, 2011). Transplantation of microbiotas from obese patients into germ-free mice results in a spontaneous obese phenotype (Ridaura et al., 2013). Although tight correlations between the microbiota and host metabolism have been well-acknowledged, the detailed mechanisms of how the host interacts with the intestinal microbiota to impact metabolic activities is poorly understood.

The 24-hour day-night cycle is another environmental factor that markedly impacts mammalian metabolism. Metabolic diseases such as diabetes, obesity and cardiovascular disease are frequently observed in people having shift work, frequent international travel or sleep disorders (Bass and Takahashi, 2010; Scheer et al., 2009). Recent studies have revealed close interactions between the host circadian clock and the microbiota. The host circadian clock can be rapidly reset by either microbiota compositional alteration, diet switching or antibiotics. For example, mice

fed a HFD exhibit reprogrammed diurnal transcriptional rhythms in the liver, which are distinct from those of mice fed a normal chow diet (Eckel-Mahan et al., 2013). Further, mice having intestinal bacteria depleted by antibiotics show alterations in the amplitude of expression of many circadian clock genes (Mukherji et al., 2013). On the other hand, the microbiota exhibits its own diurnal rhythms in species abundances. Disruptions of the regular sleep cycle or feeding cycle act directly on the microbiota to reset this compositional oscillation, and in turn alter whole body metabolic activities in the host (Thaiss et al., 2014; Leone et al., 2015b). These emerging findings have demonstrated the essential physiological importance of interactions among the microbiota, the circadian clock and metabolism. However, additional efforts are needed to understand the underlying mechanisms of these interactions.

In this dissertation, I have identified circadian transcription factor NFIL3 as a link among the microbiota, the circadian clock and metabolism. In intestinal epithelial cells, the microbiota induces *Nfil3* expression through a subepithelial DC-ILC3 relay circuit, and in turn influences epithelial lipid metabolism and full body composition through NFIL3-regulated circadian transcriptions of key metabolic genes. (FIGURE 32).

Regulation of body composition by epithelial NFIL3

Using a *Nfil3* epithelial cell specific knockout mouse model, I have discovered that epithelial NFIL3 is essential in regulating body composition in mice. Epithelial NFIL3 regulates the expression of many key metabolic genes, such as *CD36, Scd1, Fabp4* and *Cyp2e1*. These metabolic genes play crucial roles in mediating uptake of dietary fatty acids into epithelial cells (Coburn et al., 2000), transport of fatty acids (Furuhashi and Hotamisligil, 2008), and synthesis of triglycerides and chylomicrons (Abumrad and Davidson, 2012). Mice lacking epithelial NFIL3

have diminished expression of these key metabolic genes and exhibit decreased dietary lipid absorption and reduced body fat accumulation. Feeding these mice with HFD does not induce obesity symptoms.

The expression of key metabolic genes has been shown to oscillate diurnally in order to track with the daily sleep-wake cycle and fasting-feeding cycle. (Liu et al., 2013). Unhealthy behaviors, such as irregular eating habits, high-fat diet consumption, and staying up late can perturb this expressional rhythmicity, and results in an increased occurrence of metabolic diseases (Thaiss et al., 2014; Leone et al., 2015b). By performing RNA-seq transcriptome profiling, I have observed diurnal transcriptional oscillations of key metabolic genes in isolated intestinal epithelial cells from conventional wild-type mice, which accords with prior findings. However, those genes lose their diurnal expression rhythms when epithelial *Nfil3* is knocked out. Given that NFIL3 is a circadian transcription factor, this result suggests that the circadian transcriptional rhythms of these metabolic genes are generated by epithelial NFIL3, and also partially explains why disturbance of the circadian clock is associated with metabolic disease.

In addition, prior studies have revealed a requirement for the microbiota in promoting body fat accumulation, as seen in germ-free mice which have reduced body weight and body fat mass. However, the underlying mechanism is still elusive. In my studies, I have shown that the expression of epithelial NFIL3 can be markedly induced by the microbiota, and that microbiota-induced body fat accumulation requires epithelial NFIL3. Together, my studies have identified epithelial NFIL3 as an essential link between the microbiota and metabolism.

Mechanism of microbiota regulation of epithelial NFIL3 expression

The expression of epithelial NFIL3 is regulated by both the circadian clock and the microbiota. The circadian clock determines the diurnal rhythmicity of NFIL3, while the microbiota regulates the amplitude of this rhythm. Similar to liver cells and T cells (Yu et al., 2013), my studies have revealed that the circadian transcriptional repressor REV-ERBα is the direct regulator of epithelial *Nfil3*. REV-ERBα rhythmically binds to the *Nfil3* promoter to inhibit its transcription, which allows epithelial *Nfil3* to exhibit strong circadian rhythms in its expression. My studies have further revealed that microbiota-induced epithelial NFIL3 expression occurs through repression of REV-ERBα. In conventional mice, the microbiota represses *Rev-erbα* transcription and results in a low abundance of epithelial REV-ERBα, which in turn leads to increased expression of *Nfil3*.

Toll-like receptors (TLRs) are a group of receptors that specifically recognize different components of bacterial proteins and metabolites. Upon contacting their ligands, the TLRs, together with the common adaptor protein MyD88 and other components, form a signaling pathway to activate transcription of a variety of target genes (Abreu, 2010). Intestinal epithelial cells express their own TLRs on the cell surface. Epithelial cell-intrinsic TLR signaling regulates many important epithelial genes, such as *Reg3g* (Vaishnava et al., 2011), *Defb4* (Vora et al., 2004) and *Ang4* (Mukherjee et al., 2008). However, my studies show that the expression of epithelial *Rev-erbα* and *Nfil3* is not regulated by the epithelial cell-intrinsic TLR-MyD88 signaling pathway. Instead, microbiota signals govern expression of these genes through a subepithelial bacterial relay circuit, which involves dendritic cells, group 3 innate lymphoid cells and epithelial cells. In this relay circuit, DCs serve as the bacterial sensor that is activated by bacteria through TLR-MyD88 signaling. Activated DCs then relay the signal to ILC3 through production of IL-23. ILC3 then produce IL-22 to further relay the signal to epithelial cells. Once epithelial cells receive the signal

through IL-22R, epithelial intrinsic STAT3 gets phosphorylated and binds to the *Rev-erbα* promoter to suppress its transcription.

It is interesting to consider why the relay circuit strategy, but not the direct sensing strategy, has been chosen by evolution to regulate epithelial genes such as *Rev-erbα* and *Nfil3*. It seems apparent that the direct sensing strategy is simpler and energy-conserving than the relay circuit strategy, raising the question of why the latter strategy has been selected? One possible reason, in my opinion, is that the relay circuit strategy is more efficient in distributing and synchronizing bacterial signals across cells along the intestine. The intestine is a long tubular organ and is comprised of billions of epithelial cells and a variety of subepithelial immune cells (Donaldson et al., 2015). Efficiently synchronizing biological activities in all of these cells is key for maintaining homeostasis in the intestine. The involvement of immune cells, which are mobile, and cytokines, which are diffusible, maximize the number of epithelial cells that receive bacterial signals. This is especially important when the initial bacterial stimulation is confined to a small portion of the intestine. In contrast, bacterial activation through direct sensing can only activate epithelial cells that have direct contact with bacteria. Thus, though direct sensing is likely more energy efficient, it lacks the ability to synchronize bacterial signaling to all epithelial cells of the gastrointestinal tract. Nevertheless, future studies are required to test this hypothesis.

FUTURE DIRECTIONS

In this dissertation, I have identified epithelial NFIL3 as a link among the microbiota, metabolism and the circadian clock. I have further shown that the microbiota regulation of NFIL3 is dependent on a subepithelial DC-ILC3 relay circuit. However, future studies are required to address following questions.

Which metabolic genes are direct targets of epithelial NFIL3?

Although my studies have identified a number of metabolic genes that are differentially expressed between epithelial cells from NFIL3 epithelial cell specific knockout mice and epithelial cells from floxed littermates, it is still unclear whether these genes are directly regulated by epithelial NFIL3. In order to fully understand the mechanism of how epithelial NFIL3 regulates lipid metabolism, it is important to identify the direct targets of epithelial NFIL3. By analyzing promoter sequences, I have identified some key metabolic genes that have the classical NFIL3 binding site [TTANNTAA (Mitsui, 2001)] in their promoters. These include *Cd36, Fabp4* and *Scd1*. In the future, it will be interesting to apply techniques, such as chromatin immunoprecipitation sequencing (ChIP-seq), ChIP-qPCR and luciferase reporter assay, to definitively identify the direct targets of epithelial NFIL3.

Is epithelial NFIL3 activated by specific group of bacteria?

Epithelial NFIL3 expression is activated by the microbiota. My studies have shown that both flagellin and LPS are capable of inducing the expression of epithelial NFIL3. Interestingly, when I challenged germ-free mice with different species of bacteria, only Gram-negative bacteria, such as *Salmonella typhimurium* and *Escherichia coli,* which produce both flagellin and LPS, were able to trigger NFIL3 expression. One possibility is that these bacteria can more easily penetrate the epithelial barrier and directly contact DCs to activate TLR-MyD88 signaling. However, further effort will be required to test this hypothesis. In addition, MyD88 can also contribute to signaling via IL-1R (Medzhitov et al., 1998). It will be interesting to determine whether epithelial NFIL3 can also be induced by IL1-MyD88 signaling, or if it is exclusive to TLR-MyD88 signaling.

Does microbiota activation of the DC-ILC3 circuit exhibit a circadian rhythm?

My work has provided convincing evidence to show that the circadian transcriptional rhythm of epithelial NFIL3 is generated by the circadian clock through REV-ERBα, and that its amplitude is fine-tuned by the microbiota. However, recent studies have revealed a diurnal fluctuation of gut microbiota composition triggered mainly by feeding behavior (Liang et al., 2015; Thaiss et al., 2014). Therefore, it is possible that microbiota activation of DC-ILC3 circuit also oscillates diurnally in accordance with the fluctuation of microbial compositional change. Although my studies have shown that the activation of epithelial STAT3, which directly regulates *Rev-erb*α, does not exhibit diurnal rhythms in my mice, this does not rule out the possibility that the microbiota can rhythmically activate DCs but somehow lost this rhythmicity when the signal reaches the epithelium. In addition, it also does not rule out the possibility that a specific group of bacteria is required to rhythmically activate DC-ILC3 circuit.

What is the physiological importance of NFIL3 transcriptional rhythm?

The rhythmic expression of NFIL3 is regulated by the circadian clock through REV-ERBα. My studies have revealed the physiological function of epithelial NFIL3 in regulating lipid metabolism. However, the rhythmic transcription of *Nfil3* itself may also play an important role in maintaining intestinal homeostasis. Accumulating evidence has revealed the link between disrupted circadian rhythms and metabolic diseases. Given that my work has identified key epithelial metabolic genes which have strong circadian transcriptional rhythms generated by NFIL3, it will be interesting in the future to uncouple epithelial NFIL3 expression from the circadian clock and study the physiological consequences of this uncoupling.

CONCLUSIONS

In this dissertation, I have identified epithelial NFIL3 as an essential molecular link among the microbiota, the circadian clock, and host metabolism (Wang et al., 2017). Epithelial NFIL3 mediates lipid uptake and processing in intestinal epithelial cells by regulating a circadian transcriptional program of key epithelial metabolic genes. The microbiota markedly induces epithelial NFIL3 expression through a subepithelial DC-ILC3 relay circuit and in turn impacts lipid metabolism and body composition. My studies have unraveled the molecular circuitry through which the microbiota interacts with the clock, and provide new insights into how the intestinal microbiota regulates host metabolism and body composition. My studies also potentially provide insight into why perturbing microbiota-clock interactions can lead to metabolic disease. These findings could also help to explain why circadian clock disruptions in humans, arising from shift work or international travel, are associated with an increased occurrence of metabolic diseases including obesity, diabetes, and cardiovascular disease. Ultimately, my studies could lead to new strategies for treating metabolic disease by targeting NFIL3, STAT3, the microbiota, or the circadian clock.

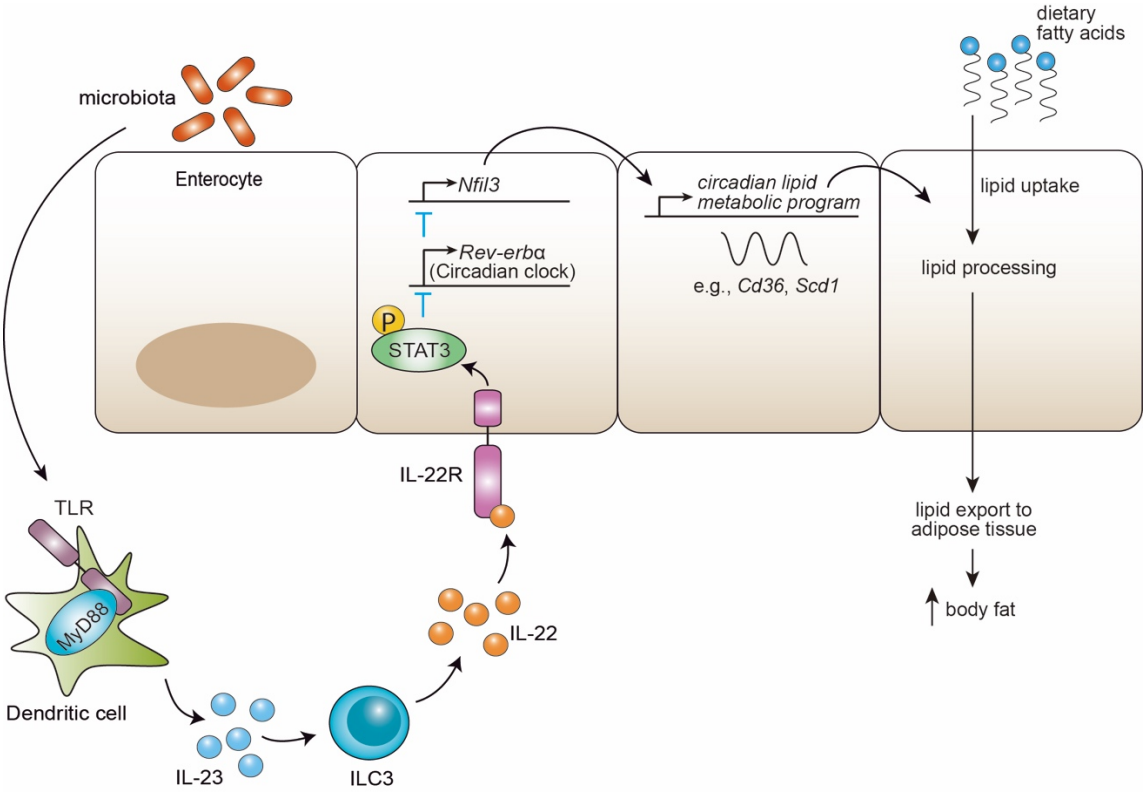

FIGURE 32: Model of microbiota regulation of epithelial NFIL3 expression

Microbiota modulation of NFIL3 expression involves a subepithelial regulatory circuit comprised of dendritic cells, group 3 innate lymphoid cell (ILC3) and activation of the epithelial transcription factor STAT3. Upon bacterial activation of Toll-like receptor (TLR)-MyD88 signaling, dendritic cells secrete the cytokine IL-23 to induce the activation of ILC3, which further triggers the phosphorylation of epithelial STAT3 through production of IL-22. Activated STAT3 inhibits the expression of the circadian clock transcriptional suppressor REV-ERBα. Because REV-ERBα represses *Nfil3*, STAT3 inhibition of REV-ERBα expression results in an increased amplitude of oscillating NFIL3 expression. Thus, diurnal rhythms in NFIL3 expression are generated by the circadian clock through REV-ERBα, while the amplitude of these rhythms is fine-tuned by the micro-biota through STAT3. Epithelial NFIL3 regulates a circadian lipid metabolic program in enterocytes and promotes lipid uptake into intestinal epithelial cells.

ACKNOWLEDGEMENTS

Foremost, I would like to express my sincere gratitude to my mentor, Dr. Lora Hooper for her continuous support and guidance of my Ph.D study and research. It is her patience, motivation, encouragement and immense knowledge by which helped me grown from a "novice scientist" into a real scientist. Everyone should have "turning point" in his/her life, joining the Hooper Lab is the biggest, and also the most important turning point in my life. My gratitude also goes to the rest of my thesis committee members, Dr. Yi Liu, Dr. Carla Green and Dr. Yihong Wan. Their inspirational suggestions, critical questions and patience was essential for the success of my thesis research and career development. I would also like to thank our collaborator, Dr. Masato Kubo for his generosity in providing the *Nfil3*$^{fl/fl}$ mice. I would not have been able to start my thesis research without having those mice.

My sincere thanks also goes to all the current and former Hooper Lab members. To Xiaofei, whom I always considered as my "mini mentor", and my entire thesis research was built on top of his work. To Zheng, his advanced experience and knowledge in performing ChIP experiments and in analyzing deep sequencing data solved the biggest hurdle during my thesis research. To Kelly, for her hard work in maintaining such a big mouse colony, and her expertise in mouse genotyping. To Cassie, for her patient help and instructions in handling germ-free mice. To Shai, his motivation and enthusiasm always inspires me. To Breck, he was a very good teacher when I had questions about microbiology. To Zehan, it is always inspiring when I discuss science with him. To Yun, she acts like a big sister and brings a lot of fun when chatting with her. To John, his joining makes the "circadian team" in the lab more diverse and productive. To Dan, I really enjoy his funny jokes. To Tamia, she always brings fresh ideas and knowledge outside of lab. To Sureka and Mihir, I

greatly enjoy the fun time we have had in the lab as graduate students. To Andrew, Brain and Tess, for their kind assistance in lab and in germ-free room.

My last and deepest gratitude goes to my parents. I would not be able to reach this point without their heartful support and sacrifice. I am the only child in the family, and I deeply understand how badly they wanted me to stay close to home. However, when I told them my decision to pursue a Ph.D overseas, they gave me their full support without hesitation and complaint. For these years, I always remember the words they told me when the day I left home: "follow your heart and do not give up." I cannot forget to thank my uncles Yu and Xiang, they are also biologists and are my role models since I was very little. It is their enthusiasm and motivation on science by which encouraged me to become a scientist.

BIBLIOGRAPHY

Abreu, M.T. (2010). Toll-like receptor signalling in the intestinal epithelium: how bacterial recognition shapes intestinal function. Nat Rev Immunol *10*, 131–144.

Abumrad, N.A., and Davidson, N.O. (2012). Role of the gut in lipid homeostasis. Physiological Reviews *92*, 1061–1085.

Akira, S., Uematsu, S., and Takeuchi, O. (2006). Pathogen Recognition and Innate Immunity. Cell *124*, 783–801.

Artis, D., and Spits, H. (2015). The biology of innate lymphoid cells. Science *517*, 293–301.

Arvidson, N.G., Gudbjörnsson, B., Elfman, L., Rydén, A.C., Tötterman, T.H., and Hällgren, R. (1994). Circadian rhythm of serum interleukin-6 in rheumatoid arthritis. Ann. Rheum. Dis. *53*, 521–524.

Asher, G., Gatfield, D., Stratmann, M., Reinke, H., Dibner, C., Kreppel, F., Mostoslavsky, R., Alt, F.W., and Schibler, U. (2008). SIRT1 Regulates Circadian Clock Gene Expression through PER2 Deacetylation. Cell *134*, 317–328.

Bailey, S.M., Udoh, U.S., and Young, M.E. (2014). Circadian regulation of metabolism. J. Endocrinol. *222*, R75–R96.

Barratt, M.J., Lebrilla, C., Shapiro, H.-Y., and Gordon, J.I. (2017). The Gut Microbiota, Food Science, and Human Nutrition: A Timely Marriage. Cell Host & Microbe *22*, 134–141.

Barton, G.M., and Medzhitov, R. (2002). Control of adaptive immune responses by Toll-like receptors. Current Opinion in Immunology *14*, 380–383.

Bass, J., and Takahashi, J.S. (2010). Circadian Integration of Metabolism and Energetics. Science *330*, 1349–1354.

Bäckhed, F., Ding, H., Wang, T., Hooper, L.V., Koh, G.Y., Nagy, A., Semenkovich, C.F., and Gordon, J.I. (2004). The gut microbiota as an environmental factor that regulates fat storage.

Proceedings of the National Academy of Sciences *101*, 15718–15723.

Bäckhed, F., Manchester, J.K., Semenkovich, C.F., and Gordon, J.I. (2007). Mechanisms underlying the resistance to diet-induced obesity in germ-free mice. Proceedings of the National Academy of Sciences *104*, 979–984.

Bel, S., Pendse, M., Wang, Y., Li, Y., Ruhn, K.A., Hassell, B., Leal, T., Winter, S.E., Xavier, R.J., and Hooper, L.V. (2017). Paneth cells secrete lysozyme via secretory autophagy during bacterial infection of the intestine. Science *357*, eaal4677–1052.

Belenky, P., Bogan, K.L., and Brenner, C. (2007). NAD+ metabolism in health and disease. Trends in Biochemical Sciences *32*, 12–19.

Benjamin, J.L., Sumpter, R., Jr, Levine, B., and Hooper, L.V. (2013). Intestinal Epithelial Autophagy Is Essential for Host Defense against Invasive Bacteria. Cell Host & Microbe *13*, 723–734.

Bernink, J.H., Germar, K., and Spits, H. (2014). The role of ILC2 in pathology of type 2 inflammatory diseases. Current Opinion in Immunology *31*, 115–120.

Besten, den, G., van Eunen, K., Groen, A.K., Venema, K., Reijngoud, D.-J., and Bakker, B.M. (2013). The role of short-chain fatty acids in the interplay between diet, gut microbiota, and host energy metabolism. J. Lipid Res. *54*, 2325–2340.

BLANCO, P., PALUCKA, A., PASCUAL, V., and Banchereau, J. (2008). Dendritic cells and cytokines in human inflammatory and autoimmune diseases. Cytokine & Growth Factor Reviews *19*, 41–52.

Blanton, L.V., Charbonneau, M.R., Salih, T., Barratt, M.J., Venkatesh, S., Ilkaveya, O., Subramanian, S., Manary, M.J., Trehan, I., Jorgensen, J.M., et al. (2016). Gut bacteria that prevent growth impairments transmitted by microbiota from malnourished children. Science *351*, aad3311–aad3311.

Bolli, G.B., and Gerich, J.E. (1984). The “dawn phenomenon--”a common occurrence in both non-insulin-dependent and insulin-dependent diabetes mellitus. N. Engl. J. Med. *310*, 746–750.

Boos, M.D., Yokota, Y., Eberl, G., and Kee, B.L. (2007). Mature natural killer cell and lymphoid tissue-inducing cell development requires Id2-mediated suppression of E protein activity. Journal of Experimental Medicine *204*, 1119–1130.

Bremner, W.F., Sothern, R.B., Kanabrocki, E.L., Ryan, M., McCormick, J.B., Dawson, S., Connors, E.S., Rothschild, R., Third, J.L.H.C., Vahed, S., et al. (2000). Relation between circadian patterns in levels of circulating lipoprotein(a), fibrinogen, platelets, and related lipid variables in men. American Heart Journal *139*, 164–173.

Brown, S.A., Zumbrunn, G., Fleury-Olela, F., Preitner, N., and Schibler, U. (2002). Rhythms of mammalian body temperature can sustain peripheral circadian clocks. Current Biology *12*, 1574–1583.

Cani, P.D., Amar, J., Iglesias, M.A., Poggi, M., Knauf, C., Bastelica, D., Neyrinck, A.M., Fava, F., Tuohy, K.M., Chabo, C., et al. (2007). Metabolic Endotoxemia Initiates Obesity and Insulin Resistance. Diabetes *56*, 1761–1772.

Cani, P.D., Bibiloni, R., Knauf, C., Waget, A., Neyrinck, A.M., Delzenne, N.M., and Burcelin, R. (2008). Changes in Gut Microbiota Control Metabolic Endotoxemia-Induced Inflammation in High-Fat Diet-Induced Obesity and Diabetes in Mice. Diabetes *57*, 1470–1481.

Cani, P.D., Possemiers, S., Van de Wiele, T., Guiot, Y., Everard, A., Rottier, O., Geurts, L., Naslain, D., Neyrinck, A., Lambert, D.M., et al. (2009). Changes in gut microbiota control inflammation in obese mice through a mechanism involving GLP-2-driven improvement of gut permeability. Gut *58*, 1091–1103.

Cani, P.D. (2011). Altered gut microbiota and endocannabinoid system tone in obese and diabetic leptin-resistant mice: impact on apelin regulation in adipose tissue. 1–17.

Cash, H.L., Whitham, C.V., Behrendt, C.L., and Hooper, L.V. (2006). Symbiotic bacteria direct expression of an intestinal bactericidal lectin. Science *313*, 1126–1130.

Caton, M.L., Smith-Raska, M.R., and Reizis, B. (2007). Notch–RBP-J signaling controls the homeostasis of CD8 −dendritic cells in the spleen. Journal of Experimental Medicine *204*, 1653–1664.

Cerovic, V., Houston, S.A., Scott, C.L., Aumeunier, A., Yrlid, U., Mowat, A.M., and Milling, S.W.F. (2013). Intestinal CD103(-) dendritic cells migrate in lymph and prime effector T cells. Mucosal Immunol *6*, 104–113.

Chen, C. (2012). Regulatory role of defensins in inflammatory bowel disease. Oji *02*, 78–84.

Cho, H., Zhao, X., Hatori, M., Yu, R.T., Barish, G.D., Lam, M.T., Chong, L.-W., DiTacchio, L., Atkins, A.R., Glass, C.K., et al. (2016). Regulation of circadian behaviour and metabolism by REV-ERB-α and REV-ERB-β. Science *485*, 123–127.

Clarke, G., Stilling, R.M., Kennedy, P.J., Stanton, C., Cryan, J.F., and Dinan, T.G. (2014). Minireview: Gut Microbiota: The Neglected Endocrine Organ. Molecular Endocrinology *28*, 1221–1238.

Clodong, S., Dühring, U., Kronk, L., Wilde, A., Axmann, I., Herzel, H., and Kollmann, M. (2007). Functioning and robustness of a bacterial circadian clock. Mol Syst Biol *3*, 913–919.

Coburn, C.T., Knapp, F.F., Febbraio, M., Beets, A.L., Silverstein, R.L., and Abumrad, N.A. (2000). Defective Uptake and Utilization of Long Chain Fatty Acids in Muscle and Adipose Tissues of CD36 Knockout Mice. The Journal of Biological Chemistry *275*, 32523–32529.

Constantinides, M.G., McDonald, B.D., Verhoef, P.A., and Bendelac, A. (2014). A committed precursor to innate lymphoid cells. Science 1–14.

Coombes, J.L., and Powrie, F. (2008). Dendritic cells in intestinal immune regulation. Nat Rev Immunol *8*, 435–446.

Cowell, I.G., Skinner, A., and Hurst, H.C. (1992). Transcriptional repression by a novel member of the bZIP family of transcription factors. Molecular and Cellular Biology *12*, 3070–3077.

Cowell, I.G. (2002). E4BP4/NFIL3, a PAR-related bZIP factor with many roles. Bioessays *24*, 1023–1029.

Curtis, A.M., Bellet, M.M., Sassone-Corsi, P., and O'Neill, L.A.J. (2014). Circadian Clock Proteins and Immunity. Immunity *40*, 178–186.

Damiola, F., Le Minh, N., Preitner, N., Kornmann, B., Fleury-Olela, F., and Schibler, U. (2000). Restricted feeding uncouples circadian oscillators in peripheral tissues from the central pacemaker in the suprachiasmatic nucleus. Genes & Development *14*, 2950–2961.

David, L.A., Maurice, C.F., Carmody, R.N., Gootenberg, D.B., Button, J.E., Wolfe, B.E., Ling, A.V., Devlin, A.S., Varma, Y., Fischbach, M.A., et al. (2015). Diet rapidly and reproducibly alters the human gut microbiome. Science *505*, 559–563.

Do, M.T.H., and Yau, K.-W. (2010). Intrinsically photosensitive retinal ganglion cells. Physiological Reviews *90*, 1547–1581.

Dodd, A.N., Salathia, N., Hall, A., Kévei, E., Tóth, R., Nagy, F., Hibberd, J.M., Millar, A.J., and Webb, A.A.R. (2005). Plant circadian clocks increase photosynthesis, growth, survival, and competitive advantage. Science *309*, 630–633.

Donaldson, G.P., Lee, S.M., and Mazmanian, S.K. (2015). Gut biogeography of the bacterial microbiota. Nature Publishing Group *14*, 20–32.

Douris, N., Kojima, S., Pan, X., Lerch-Gaggl, A.F., Duong, S.Q., Hussain, M.M., and Green, C.B. (2011). Nocturnin Regulates Circadian Trafficking of Dietary Lipid in Intestinal Enterocytes. Current Biology *21*, 1347–1355.

Duerkop, B.A., Vaishnava, S., and Hooper, L.V. (2009). Immune Responses to the Microbiota at the Intestinal Mucosal Surface. Immunity *31*, 368–376.

Duez, H., van der Veen, J.N., Duhem, C., Pourcet, B., Touvier, T., Fontaine, C., Derudas, B., Baugé, E., Havinga, R., Bloks, V.W., et al. (2008). Regulation of Bile Acid Synthesis by the Nuclear Receptor Rev-erbα. Gastroenterology *135*, 689–698.e5.

Dunn, A.L., Marcus, B.H., Kampert, J.B., Garcia, M.E., Kohl, H.W., and Blair, S.N. (1999). Comparison of lifestyle and structured interventions to increase physical activity and cardiorespiratory fitness: a randomized trial. Jama *281*, 327–334.

Eckel-Mahan, K.L., Patel, V.R., de Mateo, S., Orozco-Solis, R., Ceglia, N.J., Sahar, S., Dilag-Penilla, S.A., Dyar, K.A., Baldi, P., and Sassone-Corsi, P. (2013). Reprogramming of the

Circadian Clock by Nutritional Challenge. Cell *155*, 1464–1478.

Evans, D.F., Pye, G., Bramley, R., Clark, A.G., Dyson, T.J., and Hardcastle, J.D. (1988). Measurement of gastrointestinal pH profiles in normal ambulant human subjects. Gut *29*, 1035–1041.

Faith, J.J., Guruge, J.L., Charbonneau, M., Subramanian, S., Seedorf, H., Goodman, A.L., Clemente, J.C., Knight, R., Heath, A.C., Leibel, R.L., et al. (2013). The long-term stability of the human gut microbiota. Science *341*, 1237439–1237439.

Farache, J., Koren, I., Milo, I., Gurevich, I., Kim, K.-W., Zigmond, E., Furtado, G.C., Lira, S.A., and Shakhar, G. (2013). Luminal Bacteria Recruit CD103+ Dendritic Cells into the Intestinal Epithelium to Sample Bacterial Antigens for Presentation. Immunity *38*, 581–595.

Fei, N., and Zhao, L. (2012). An opportunistic pathogen isolated from the gut of an obese human causes obesity in germfree mice. The ISME Journal *7*, 880–884.

Fischer, A.H., Jacobson, K.A., Rose, J., and Zeller, R. (2008). Hematoxylin and Eosin Staining of Tissue and Cell Sections. Cold Spring Harbor Protocols *2008*, pdb.prot4986–pdb.prot4986.

Furuhashi, M., and Hotamisligil, G.S. (2008). Fatty acid-binding proteins: role in metabolic diseases and potential as drug targets. Nat Rev Drug Discov *7*, 489–503.

Gallego, M., and Virshup, D.M. (2007). Post-translational modifications regulate the ticking of the circadian clock. Nat Rev Mol Cell Biol *8*, 139–148.

Gao, Z., Yin, J., Zhang, J., Ward, R.E., Martin, R.J., Lefevre, M., Cefalu, W.T., and Ye, J. (2009). Butyrate improves insulin sensitivity and increases energy expenditure in mice. Diabetes *58*, 1509–1517.

Gaudio, E., Taddei, G., Vetuschi, A., Sferra, R., and Frieri, G. (1999). Dextran Sulfate Sodium (DSS)Colitis in Rats. Digestive Diseases and Sciences *44*, 1458–1475.

Geiger, T.L., Abt, M.C., Gasteiger, G., Firth, M.A., O'Connor, M.H., Geary, C.D., O'Sullivan, T.E., van den Brink, M.R., Pamer, E.G., Hanash, A.M., et al. (2014). Nfil3 is crucial for

development of innate lymphoid cells and host protection against intestinal pathogens. J. Exp. Med. *80*, 62.

Gibbs, J.E., Blaikley, J., Beesley, S., Matthews, L., Simpson, K.D., Boyce, S.H., Farrow, S.N., Else, K.J., Singh, D., Ray, D.W., et al. (2012). The nuclear receptor REV-ERB mediates circadian regulation of innate immunity through selective regulation of inflammatory cytokines. Proceedings of the National Academy of Sciences *109*, 582–587.

Goodrich, J.K., Waters, J.L., Poole, A.C., Sutter, J.L., Koren, O., Blekhman, R., Beaumont, M., Van Treuren, W., Knight, R., Bell, J.T., et al. (2014). Human Genetics Shape the Gut Microbiome. Cell *159*, 789–799.

Goto, Y., Obata, T., Kunisawa, J., Sato, S., Ivanov, I.I., Lamichhane, A., Takeyama, N., Kamioka, M., Sakamoto, M., Matsuki, T., et al. (2014). Innate lymphoid cells regulate intestinal epithelial cell glycosylation. Science *345*, 1254009–1254009.

Greiner, T., and Bäckhed, F. (2011). Effects of the gut microbiota on obesity and glucose homeostasis. Trends in Endocrinology & Metabolism *22*, 117–123.

Griffin, N.W., Ahern, P.P., Cheng, J., Heath, A.C., Ilkayeva, O., Newgard, C.B., Fontana, L., and Gordon, J.I. (2016). Prior Dietary Practices and Connections to a Human Gut Microbial Metacommunity Alter Responses to Diet Interventions. Cell Host & Microbe 1–33.

Haemmerle, G., Lass, A., Zimmermann, R., Gorkiewicz, G., Meyer, C., Rozman, J., Heldmaier, G., Maier, R., Theussl, C., Eder, S., et al. (2006). Defective lipolysis and altered energy metabolism in mice lacking adipose triglyceride lipase. Science *312*, 734–737.

Haslam, D.W., and James, W.P.T. (2005). Obesity. The Lancet *366*, 1197–1209.

Hoogerwerf, W.A., Hellmich, H.L., Cornélissen, G., Halberg, F., Shahinian, V.B., Bostwick, J., Savidge, T.C., and Cassone, V.M. (2007). Clock Gene Expression in the Murine Gastrointestinal Tract: Endogenous Rhythmicity and Effects of a Feeding Regimen. Gastroenterology *133*, 1250–1260.

Hooper, L.V., and Gordon, J.I. (2001). Commensal host-bacterial relationships in the gut. Science *292*, 1115–1118.

Hylemon, P.B., Zhou, H., Pandak, W.M., Ren, S., Gil, G., and Dent, P. (2009). Bile acids as regulatory molecules. The Journal of Lipid Research *50*, 1509–1520.

Ishikawa, K., and Shimazu, T. (1980). Circadian rhythm of liver glycogen metabolism in rats: effects of hypothalamic lesions. Am. J. Physiol. *238*, E21–E25.

Johansson, M.E.V., Phillipson, M., Petersson, J., Velcich, A., Holm, L., and Hansson, G.C. (2008). The inner of the two Muc2 mucin-dependent mucus layers in colon is devoid of bacteria. Pnas *105*, 15064–15069.

Junghans, D., Chauvet, S., Buhler, E., Dudley, K., Sykes, T., and Henderson, C.E. (2004). The CES-2-related transcription factor E4BP4 is an intrinsic regulator of motoneuron growth and survival. Development *131*, 4425–4434.

Kalsbeek, A., Foppen, E., Schalij, I., Van Heijningen, C., van der Vliet, J., Fliers, E., and Buijs, R.M. (2008). Circadian Control of the Daily Plasma Glucose Rhythm: An Interplay of GABA and Glutamate. PLoS ONE *3*, e3194–11.

Kashiwada, M., Levy, D.M., McKeag, L., Murray, K., Schroder, A.J., Canfield, S.M., Traver, G., and Rothman, P.B. (2010). IL-4-induced transcription factor NFIL3/E4BP4 controls IgE class switching. Pnas *107*, 821–826.

Kashiwada, M., Pham, N.L.L., Pewe, L.L., Harty, J.T., and Rothman, P.B. (2011). NFIL3/E4BP4 is a key transcription factor for CD8 + dendritic cell development. Blood *117*, 6193–6197.

Keniry, M., Pires, M.M., Mense, S., Lefebvre, C., Gan, B., Justiano, K., Lau, Y.-K.I., Hopkins, B., Hodakoski, C., Koujak, S., et al. (2013). Survival factor NFIL3 restricts FOXO-induced gene expression in cancer. Genes & Development *27*, 916–927.

Kida, K., Nishio, T., Yokozawa, T., Nagai, K., Matsuda, H., and Nakagawa, H. (1980). The circadian change of gluconeogenesis in the liver in vivo in fed rats. J. Biochem. *88*, 1009–1013.

King, D.P., Zhao, Y., Sangoram, A.M., Wilsbacher, L.D., Tanaka, M., Antoch, M.P., Steeves, T.D., Vitaterna, M.H., Kornhauser, J.M., Lowrey, P.L., et al. (1997). Positional cloning of the mouse circadian clock gene. Cell *89*, 641–653.

Kinnebrew, M.A., Buffie, C.G., Diehl, G.E., Zenewicz, L.A., Leiner, I., Hohl, T.M., Flavell, R.A., Littman, D.R., and Pamer, E.G. (2012). Interleukin 23 Production by Intestinal CD103+CD11b+ Dendritic Cells in Response to Bacterial Flagellin Enhances Mucosal Innate Immune Defense. Immunity *36*, 276–287.

Klose, C.S.N., Flach, M., Möhle, L., Rogell, L., Hoyler, T., Ebert, K., Fabiunke, C., Pfeifer, D., Sexl, V., Fonseca-Pereira, D., et al. (2014). Differentiation of Type 1 ILCs froma Common Progenitor to All Helper-like Innate Lymphoid Cell Lineages. Cell *157*, 340–356.

Kobayashi, T., Matsuoka, K., Sheikh, S.Z., Elloumi, H.Z., Kamada, N., Hisamatsu, T., Hansen, J.J., Doty, K.R., Pope, S.D., Smale, S.T., et al. (2011). NFIL3 Is a Regulator of IL-12 p40 in Macrophages and Mucosal Immunity. The Journal of Immunology *186*, 4649–4655.

Koike, N., Yoo, S.-H., Huang, H.-C., Kumar, V., Lee, C., Kim, T.-K., and Takahashi, J.S. (2012). Transcriptional architecture and chromatin landscape of the core circadian clock in mammals. Science *338*, 349–354.

Kume, K., Zylka, M.J., Sriram, S., Shearman, L.P., Weaver, D.R., Jin, X., Maywood, E.S., Hastings, M.H., and Reppert, S.M. (1999). mCRY1 and mCRY2 are essential components of the negative limb of the circadian clock feedback loop. Cell *98*, 193–205.

La Fleur, S.E., Kalsbeek, A., Wortel, J., and Buijs, R.M. (1999). A suprachiasmatic nucleus generated rhythm in basal glucose concentrations. J. Neuroendocrinol. *11*, 643–652.

Lamia, K.A., Storch, K.-F., and Weitz, C.J. (2008). Physiological significance of a peripheral tissue circadian clock. Pnas *105*, 15172–15177.

Lang, R., Patel, D., Morris, J.J., Rutschman, R.L., and Murray, P.J. (2002). Shaping gene expression in activated and resting primary macrophages by IL-10. The Journal of Immunology *169*, 2253–2263.

Leclercq, I.A., Farrell, G.C., Field, J., Bell, D.R., Gonzalez, F.J., and Robertson, G.R. (2000). CYP2E1 and CYP4A as microsomal catalysts of lipid peroxides in murine nonalcoholic steatohepatitis. J. Clin. Invest. *105*, 1067–1075.

Lee, C., Etchegaray, J.P., Cagampang, F.R., Loudon, A.S., and Reppert, S.M. (2001). Posttranslational mechanisms regulate the mammalian circadian clock. Cell *107*, 855–867.

Lee, J.-H., Wood, T.K., and Lee, J. (2015). Roles of Indole as an Interspecies and Interkingdom Signaling Molecule. Trends in Microbiology *23*, 707–718.

Leone, V., Gibbons, S.M., Martinez, K., Hutchison, A.L., Huang, E.Y., Cham, C.M., Pierre, J.F., Heneghan, A.F., Nadimpalli, A., Hubert, N., et al. (2015a). Effects of Diurnal Variation of Gut Microbes and High-Fat Feeding on Host Circadian Clock Function and Metabolism. Cell Host & Microbe *17*, 681–689.

Leone, V., Gibbons, S.M., Martinez, K., Hutchison, A.L., Huang, E.Y., Cham, C.M., Pierre, J.F., Heneghan, A.F., Nadimpalli, A., Hubert, N., et al. (2015b). Effects of Diurnal Variation of Gut Microbes and High-Fat Feeding on Host Circadian Clock Function and Metabolism. Cell Host & Microbe *17*, 681–689.

Liang, X., Bushman, F.D., and FitzGerald, G.A. (2015). Rhythmicity of the intestinal microbiota is regulated by gender and the host circadian clock. Pnas *112*, 10479–10484.

Licona-Limón, P., Kim, L.K., Palm, N.W., and Flavell, R.A. (2013). TH2, allergy and group 2 innate lymphoid cells. Nat Immunol *14*, 536–542.

Liu, K., and Nussenzweig, M.C. (2010). Origin and development of dendritic cells. Immunol. Rev. *234*, 45–54.

Liu, S., Brown, J.D., Stanya, K.J., Homan, E., Leidl, M., Inouye, K., Bhargava, P., Gangl, M.R., Dai, L., Ben Hatano, et al. (2013). A diurnal serum lipid integrates hepatic lipogenesis and peripheral fatty acid use. Science *502*, 550–554.

Lowrey, P.L., and Takahashi, J.S. (2004). MAMMALIAN CIRCADIAN BIOLOGY: Elucidating Genome-Wide Levels of Temporal Organization. Annu. Rev. Genom. Hum. Genet. *5*, 407–441.

Madison, B.B., Dunbar, L., Qiao, X.T., Braunstein, K., Braunstein, E., and Gumucio, D.L. (2002). Cis elements of the villin gene control expression in restricted domains of the vertical (crypt) and horizontal (duodenum, cecum) axes of the intestine. The Journal of Biological Chemistry *277*, 33275–33283.

Mahowald, M.A., Rey, F.E., Seedorf, H., Turnbaugh, P.J., Fulton, R.S., Wollam, A., Shah, N., Wang, C., Magrini, V., Wilson, R.K., et al. (2009). Characterizing a model human gut microbiota composed of members of its two dominant bacterial phyla. Pnas *106*, 5859–5864.

Male, V., Nisoli, I., Gascoyne, D.M., and Brady, H.J.M. (2012). E4BP4: an unexpected player in the immune response. Trends in Immunology *33*, 98–102.

Marcheva, B., Ramsey, K.M., Buhr, E.D., Kobayashi, Y., Su, H., Ko, C.H., Ivanova, G., Omura, C., Mo, S., Vitaterna, M.H., et al. (2010). Disruption of the clock components CLOCK and BMAL1 leads to hypoinsulinaemia and diabetes. Science *466*, 627–631.

Medzhitov, R., Preston-Hurlburt, P., Kopp, E., Stadlen, A., Chen, C., Ghosh, S., and Janeway, C.A. (1998). MyD88 is an adaptor protein in the hToll/IL-1 receptor family signaling pathways. Molecular Cell *2*, 253–258.

Mellman, I., and Steinman, R.M. (2001). Dendritic cells: specialized and regulated antigen processing machines. Cell *106*, 255–258.

Mitsui, S. (2001). Antagonistic role of E4BP4 and PAR proteins in the circadian oscillatory mechanism. Genes & Development *15*, 995–1006.

Mohawk, J.A., Green, C.B., and Takahashi, J.S. (2012). Central and Peripheral Circadian Clocks in Mammals. Annu. Rev. Neurosci. *35*, 445–462.

Motomura, Y., Kitamura, H., Hijikata, A., Matsunaga, Y., Matsumoto, K., Inoue, H., Atarashi, K., Hori, S., Watarai, H., Zhu, J., et al. (2011). The transcription factor E4BP4 regulates the production of IL-10 and IL-13 in CD4+ T cells. Nat Immunol *12*, 450–459.

Mukherjee, M. (2003). Human digestive and metabolic lipases—a brief review. Journal of Molecular Catalysis B: Enzymatic *22*, 369–376.

Mukherjee, S., Vaishnava, S., and Hooper, L.V. (2008). Multi-layered regulation of intestinal antimicrobial defense. Cell. Mol. Life Sci. *65*, 3019–3027.

Mukherji, A., Kobiita, A., Ye, T., and Chambon, P. (2013). Homeostasis in Intestinal Epithelium Is Orchestrated by the Circadian Clock and Microbiota Cues Transduced by TLRs. Cell *153*, 812–827.

Murakami, M., Tognini, P., Liu, Y., Eckel-Mahan, K.L., Baldi, P., and Sassone-Corsi, P. (2016). Gut microbiota directs PPARγ-driven reprogramming of the liver circadian clock by nutritional challenge. EMBO Rep. e201642463–12.

Murphy, E.F., Cotter, P.D., Healy, S., Marques, T.M., O'Sullivan, O., Fouhy, F., Clarke, S.F., O'Toole, P.W., Quigley, E.M., Stanton, C., et al. (2010). Composition and energy harvesting capacity of the gut microbiota: relationship to diet, obesity and time in mouse models. Gut *59*, 1635–1642.

Nader, N., Chrousos, G.P., and Kino, T. (2010). Interactions of the circadian CLOCK system and the HPA axis. Trends in Endocrinology & Metabolism *21*, 277–286.

Nakahata, Y., Sahar, S., Astarita, G., Kaluzova, M., and Sassone-Corsi, P. (2009). Circadian control of the NAD+ salvage pathway by CLOCK-SIRT1. Science *324*, 654–657.

Ng, M., Fleming, T., Robinson, M., Thomson, B., and Graetz, N. (2014). Global, regional, and national prevalence of overweight and obesity in children and adults during 1980–2013: a systematic analysis for the Global Burden of Disease …. The Lancet.

Nicholson, J.K., Holmes, E., Kinross, J., Burcelin, R., Gibson, G., Jia, W., and Pettersson, S. (2012). Host-Gut Microbiota Metabolic Interactions. Science *336*, 1262–1267.

Noshiro, M., Usui, E., Kawamoto, T., Kubo, H., Fujimoto, K., Furukawa, M., Honma, S., Makishima, M., Honma, K.-I., and Kato, Y. (2016). Multiple Mechanisms Regulate Circadian Expression of the Gene for Cholesterol 7α-Hydroxylase (Cyp7a), a Key Enzyme in Hepatic Bile Acid Biosynthesis. J Biol Rhythms *22*, 299–311.

Ntambi, J.M., Miyazaki, M., Stoehr, J.P., Lan, H., Kendziorski, C.M., Yandell, B.S., Song, Y., Cohen, P., Friedman, J.M., and Attie, A.D. (2002). Loss of stearoyl-CoA desaturase-1 function protects mice against adiposity. Proceedings of the National Academy of Sciences *99*, 11482–11486.

Pan, X., and Hussain, M.M. (2009). Clock is important for food and circadian regulation of macronutrient absorption in mice. J. Lipid Res. *50*, 1800–1813.

Panda, S., Hogenesch, J.B., and Kay, S.A. (2002). Circadian rhythms from flies to human. Science *417*, 329–335.

Parséus, A., Sommer, N., Sommer, F., Caesar, R., Molinaro, A., Ståhlman, M., Greiner, T.U., Perkins, R., and Bäckhed, F. (2016). Microbiota-induced obesity requires farnesoid X receptor. Gut gutjnl–2015–310283–10.

Partch, C.L., Shields, K.F., Thompson, C.L., Selby, C.P., and Sancar, A. (2006). Posttranslational regulation of the mammalian circadian clock by cryptochrome and protein phosphatase 5. Proceedings of the National Academy of Sciences *103*, 10467–10472.

Patsouris, D., Li, P.-P., Thapar, D., Chapman, J., Olefsky, J.M., and Neels, J.G. (2008). Ablation of CD11c-Positive Cells Normalizes Insulin Sensitivity in Obese Insulin Resistant Animals. Cell Metabolism *8*, 301–309.

Peterson, L.W., and Artis, D. (2014). Intestinal epithelial cells: regulators of barrier function and immune homeostasis. Nat Rev Immunol *14*, 141–153.

Pickard, J.M., Maurice, C.F., Kinnebrew, M.A., Abt, M.C., Schenten, D., Golovkina, T.V., Bogatyrev, S.R., Ismagilov, R.F., Pamer, E.G., Turnbaugh, P.J., et al. (2014). Rapid fucosylation of intestinal epithelium sustains host-commensal symbiosis in sickness. Science *514*, 638–641.

Pickert, G., Neufert, C., Leppkes, M., Zheng, Y., Wittkopf, N., Warntjen, M., Lehr, H.A., Hirth, S., Weigmann, B., Wirtz, S., et al. (2009). STAT3 links IL-22 signaling in intestinal epithelial cells to mucosal wound healing. Journal of Experimental Medicine *206*, 1465–1472.

Prasad, K.N. (1980). Butyric acid: a small fatty acid with diverse biological functions. Life Sci. *27*, 1351–1358.

Rabot, S., Membrez, M., Bruneau, A., Gerard, P., Harach, T., Moser, M., Raymond, F., Mansourian, R., and Chou, C.J. (2010a). Germ-free C57BL/6J mice are resistant to high-fat-diet-induced insulin resistance and have altered cholesterol metabolism. The FASEB Journal *24*, 4948–4959.

Rabot, S., Membrez, M., Bruneau, A., Gérard, P., Harach, T., Moser, M., Raymond, F., Mansourian, R., and Chou, C.J. (2010b). Germ-free C57BL/6J mice are resistant to high-fat-diet-induced insulin resistance and have altered cholesterol metabolism. Faseb J. *24*, 4948–4959.

Ramsey, K.M., Yoshino, J., Brace, C.S., Abrassart, D., Kobayashi, Y., Marcheva, B., Hong, H.-K., Chong, J.L., Buhr, E.D., Lee, C., et al. (2009). Circadian clock feedback cycle through NAMPT-mediated NAD+ biosynthesis. Science *324*, 651–654.

Ridaura, V.K., Faith, J.J., Rey, F.E., Cheng, J., Duncan, A.E., Kau, A.L., Griffin, N.W., Lombard, V., Henrissat, B., Bain, J.R., et al. (2013). Gut microbiota from twins discordant for obesity modulate metabolism in mice. Science *341*, 1241214.

Rivera-Chávez, F., Zhang, L.F., Faber, F., Lopez, C.A., Byndloss, M.X., Olsan, E.E., Xu, G., Velazquez, E.M., Lebrilla, C.B., Winter, S.E., et al. (2016). Depletion of Butyrate-Producing Clostridia from the Gut Microbiota Drives an Aerobic Luminal Expansion of Salmonella. Cell Host & Microbe *19*, 443–454.

Rudic, R.D., McNamara, P., Curtis, A.-M., Boston, R.C., Panda, S., Hogenesch, J.B., and FitzGerald, G.A. (2004). BMAL1 and CLOCK, two essential components of the circadian clock, are involved in glucose homeostasis. Plos Biol *2*, e377.

Sadacca, L.A., Lamia, K.A., deLemos, A.S., Blum, B., and Weitz, C.J. (2010). An intrinsic circadian clock of the pancreas is required for normal insulin release and glucose homeostasis in mice. Diabetologia *54*, 120–124.

Saini, C., Petrenko, V., Pulimeno, P., Giovannoni, L., Berney, T., Hebrok, M., Howald, C., Dermitzakis, E.T., and Dibner, C. (2016). A functional circadian clock is required for proper

insulin secretion by human pancreatic islet cells. Diabetes Obes Metab *18*, 355–365.

Sancar, A., Lindsey-Boltz, L.A., Gaddameedhi, S., Selby, C.P., Ye, R., Chiou, Y.-Y., Kemp, M.G., Hu, J., Lee, J.H., and Ozturk, N. (2015). Circadian Clock, Cancer, and Chemotherapy. Biochemistry *54*, 110–123.

Sano, T., Huang, W., Hall, J.A., Yang, Y., Chen, A., Gavzy, S.J., Lee, J.-Y., Ziel, J.W., Miraldi, E.R., Domingos, A.I., et al. (2015). An IL-23R/IL-22 Circuit Regulates Epithelial Serum Amyloid A to Promote Local Effector Th17 Responses. Cell 1–14.

Sato, K., and Fujita, S. (2007). Dendritic cells: nature and classification. Allergol Int *56*, 183–191.

Savage, A.K., Constantinides, M.G., Han, J., Picard, D., Martin, E., Li, B., Lantz, O., and Bendelac, A. (2008). The Transcription Factor PLZF Directs the Effector Program of the NKT Cell Lineage. Immunity *29*, 391–403.

Scheer, F.A.J.L., Hilton, M.F., Mantzoros, C.S., and Shea, S.A. (2009). Adverse metabolic and cardiovascular consequences of circadian misalignment. Pnas *106*, 4453–4458.

Schenkel, J.M., Fraser, K.A., Beura, L.K., Pauken, K.E., Vezys, V., and Masopust, D. (2014). T cell memory. Resident memory CD8 T cells trigger protective innate and adaptive immune responses. Science *346*, 98–101.

Schmittgen, T.D., and Livak, K.J. (2008). Analyzing real-time PCR data by the comparative CT method. Nat Protoc *3*, 1101–1108.

Sehgal, A. (1995). Molecular genetic analysis of circadian rhythms in vertebrates and invertebrates. Curr. Opin. Neurobiol. *5*, 824–831.

Seillet, C., Rankin, L.C., Groom, J.R., Mielke, L.A., Tellier, J., Chopin, M., Huntington, N.D., Belz, G.T., and Carotta, S. (2014). Nfil3 is required for the development of all innate lymphoid cell subsets. Journal of Experimental Medicine *311*, 1924.

Serafini, N., Xu, W., and Di Santo, J.P. (2014). Innate lymphoid cells: of precursors and products…. Curr. Biol. *24*, R573–R576.

Shan, M., Gentile, M., Yeiser, J.R., Walland, A.C., Bornstein, V.U., Chen, K., He, B., Cassis, L., Bigas, A., Cols, M., et al. (2013). Mucus Enhances Gut Homeostasis and Oral Tolerance by Delivering Immunoregulatory Signals. Science *342*, 447–453.

Shirogane, T., Jin, J., Ang, X.L., and Harper, J.W. (2005). SCFbeta-TRCP controls clock-dependent transcription via casein kinase 1-dependent degradation of the mammalian period-1 (Per1) protein. The Journal of Biological Chemistry *280*, 26863–26872.

Shostak, A., Meyer-Kovac, J., and Oster, H. (2013). Circadian regulation of lipid mobilization in white adipose tissues. Diabetes *62*, 2195–2203.

Silvestris, F., Cafforio, P., De Matteo, M., Calvani, N., Frassanito, M.A., and Dammacco, F. (2008). Negative Regulation of the Osteoblast Function in Multiple Myeloma through the Repressor Gene E4BP4 Activated by Malignant Plasma Cells. Clinical Cancer Research *14*, 6081–6091.

Son, G.H., Chung, S., Choe, H.K., Kim, H.-D., Baik, S.-M., Lee, H., Lee, H.-W., Choi, S., Sun, W., Kim, H., et al. (2008). Adrenal peripheral clock controls the autonomous circadian rhythm of glucocorticoid by causing rhythmic steroid production. Pnas *105*, 20970–20975.

Spits, H., Artis, D., Colonna, M., Diefenbach, A., Di Santo, J.P., Eberl, G., Koyasu, S., Locksley, R.M., McKenzie, A.N.J., Mebius, R.E., et al. (2013). Innate lymphoid cells — a proposal for uniform nomenclature. Nat Rev Immunol *13*, 145–149.

Stappenbeck, T.S., Hooper, L.V., and Manchester, J.K. (2002). Laser capture microdissection of mouse intestine (…).

Stokkan, K.A., Yamazaki, S., Tei, H., Sakaki, Y., and Menaker, M. (2001). Entrainment of the circadian clock in the liver by feeding. Science *291*, 490–493.

Su, X., Yan, H., Huang, Y., Yun, H., Zeng, B., Wang, E., Liu, Y., Zhang, Y., Liu, F., Che, Y., et al. (2015). Expression of FABP4, adipsin and adiponectin in Paneth cells is modulated by gut Lactobacillus. Nature Publishing Group *5*, 1–10.

Taicher, G.Z., Tinsley, F.C., Reiderman, A., and Heiman, M.L. (2003). Quantitative magnetic resonance (QMR) method for bone and whole-body-composition analysis. Analytical and Bioanalytical Chemistry *377*, 990–1002.

Takahashi, J.S. (2016). Transcriptional architecture of the mammalian circadian clock. Nature Reviews Genetics 1–16.

Takahashi, J.S., Hong, H.-K., Ko, C.H., and McDearmon, E.L. (2008a). The genetics of mammalian circadian order and disorder: implications for physiology and disease. Nature Reviews Genetics *9*, 764–775.

Takahashi, J.S., Hong, H.-K., Ko, C.H., and McDearmon, E.L. (2008b). The genetics of mammalian circadian order and disorder: implications for physiology and disease. Nature Reviews Genetics *9*, 764–775.

Tasan, R.O., Lin, S., Hetzenauer, A., Singewald, N., Herzog, H., and Sperk, G. (2009). Increased novelty-induced motor activity and reduced depression-like behavior in neuropeptide Y (NPY)–Y4 receptor knockout mice. Nsc *158*, 1717–1730.

Thaiss, C.A., Zeevi, D., Levy, M., and Zilberman-Schapira, G. (2014). Transkingdom Control of Microbiota Diurnal Oscillations Promotes Metabolic Homeostasis. Cell.

Thaiss, C.A., Levy, M., Korem, T., Dohnalová, L., Shapiro, H., Jaitin, D.A., David, E., Winter, D.R., Gury-BenAri, M., Tatirovsky, E., et al. (2016). Microbiota Diurnal Rhythmicity Programs Host Transcriptome Oscillations. 1–29.

Tilg, H., Moschen, A.R., and Kaser, A. (2009). Obesity and the Microbiota. Ygast *136*, 1476–1483.

Tomasello, E., and Bedoui, S. (2013). Intestinal innate immune cells in gut homeostasis and immunosurveillance. Immunology and Cell Biology *91*, 201–203.

Turek, F.W., Joshu, C., Kohsaka, A., Lin, E., Ivanova, G., McDearmon, E., Laposky, A., Losee-Olson, S., Easton, A., Jensen, D.R., et al. (2005). Obesity and metabolic syndrome in circadian Clock mutant mice. Science *308*, 1043–1045.

Turnbaugh, P.J., Ridaura, V.K., Faith, J.J., Rey, F.E., Knight, R., and Gordon, J.I. (2009a). The Effect of Diet on the Human Gut Microbiome: A Metagenomic Analysis in Humanized Gnotobiotic Mice. Science Translational Medicine *1*, 6ra14–6ra14.

Turnbaugh, P.J., Hamady, M., Yatsunenko, T., Cantarel, B.L., Duncan, A., Ley, R.E., Sogin, M.L., Jones, W.J., Roe, B.A., Affourtit, J.P., et al. (2009b). A core gut microbiome in obese and lean twins. Science *457*, 480–484.

Turnbaugh, P.J., Ley, R.E., Mahowald, M.A., Magrini, V., Mardis, E.R., and Gordon, J.I. (2006). An obesity-associated gut microbiome with increased capacity for energy harvest. Science *444*, 1027–1131.

Vaishnava, S., Yamamoto, M., Severson, K.M., Ruhn, K.A., Yu, X., Koren, O., Ley, R., Wakeland, E.K., and Hooper, L.V. (2011). The Antibacterial Lectin RegIII Promotes the Spatial Segregation of Microbiota and Host in the Intestine. Science *334*, 255–258.

van de Pavert, S.A., Ferreira, M., Domingues, R.G., Ribeiro, H., Molenaar, R., Moreira-Santos, L., Almeida, F.F., Ibiza, S., Barbosa, I., Goverse, G., et al. (2015). Maternal retinoids control type 3 innate lymphoid cells and set the offspring immunity. Science *508*, 123–127.

Vora, P., Youdim, A., Thomas, L.S., Fukata, M., Tesfay, S.Y., Lukasek, K., Michelsen, K.S., Wada, A., Hirayama, T., Arditi, M., et al. (2004). Beta-defensin-2 expression is regulated by TLR signaling in intestinal epithelial cells. The Journal of Immunology *173*, 5398–5405.

Vujovic, N., Davidson, A.J., and Menaker, M. (2008). Sympathetic input modulates, but does not determine, phase of peripheral circadian oscillators. Am. J. Physiol. Regul. Integr. Comp. Physiol. *295*, R355–R360.

Wang, X., Ota, N., Manzanillo, P., Kates, L., Zavala-Solorio, J., Eidenschenk, C., Zhang, J., Lesch, J., Lee, W.P., Ross, J., et al. (2014). Interleukin-22 alleviates metabolic disorders and restores mucosal immunity in diabetes. Science *514*, 237–241.

Wang, Y., Kuang, Z., Yu, X., Ruhn, K.A., Kubo, M., and Hooper, L.V. (2017). The intestinal microbiota regulates body composition through NFIL3 and the circadian clock. Science *357*, 912–916.

Weisberg, S.P., McCann, D., Desai, M., Rosenbaum, M., Leibel, R.L., and Ferrante, A.W., Jr. (2003). Obesity is associated with macrophage accumulation in adipose tissue. J. Clin. Invest. *112*, 1796–1808.

Welsh, D.K., Takahashi, J.S., and Kay, S.A. (2010). Suprachiasmatic Nucleus: Cell Autonomy and Network Properties. Annu. Rev. Physiol. *72*, 551–577.

Yeung, J., O'Sullivan, E., Hubank, M., and Brady, H.J.M. (2004). E4BP4 expression is regulated by the t(17;19)-associated oncoprotein E2A-HLF in pro-B cells. Br J Haematol *125*, 560–567.

Yin, L., Wang, J., Klein, P.S., and Lazar, M.A. (2006). Nuclear receptor Rev-erbalpha is a critical lithium-sensitive component of the circadian clock. Science *311*, 1002–1005.

Yu, X., Rollins, D., Ruhn, K.A., Stubblefield, J.J., Green, C.B., Kashiwada, M., Rothman, P.B., Takahashi, J.S., and Hooper, L.V. (2013). TH17 Cell Differentiation Is Regulated by the Circadian Clock. Science *342*, 727–730.

Yu, X., Wang, Y., Deng, M., Li, Y., Ruhn, K.A., Zhang, C.C., and Hooper, L.V. (2014). The basic leucine zipper transcription factor NFIL3 directs the development of a common innate lymphoid cell precursor. Elife *3*.

Zeisel, S.H., and Blusztajn, J.K. (1994). Choline and human nutrition. Annu. Rev. Nutr. *14*, 269–296.

Zeng, H. (2014). Mechanisms linking dietary fiber, gut microbiota and colon cancer prevention. Wjgo *6*, 41–12.

Zhang, H., Sparks, J.B., Karyala, S.V., Settlage, R., and Luo, X.M. (2014). Host adaptive immunity alters gut microbiota. *9*, 770–781.

Zhang, W., Zhang, J., Kornuc, M., Kwan, K., Frank, R., and Nimer, S.D. (1995). Molecular cloning and characterization of NF-IL3A, a transcriptional activator of the human interleukin-3 promoter. Molecular and Cellular Biology *15*, 6055–6063.

Zhao, L. (2013). The gut microbiota and obesity: from correlation to causality. Nat Rev Micro *11*, 639–647.

Zong, H., Armoni, M., Harel, C., Karnieli, E., and Pessin, J.E. (2012). Cytochrome P-450 CYP2E1 knockout mice are protected against high-fat diet-induced obesity and insulin resistance. AJP: Endocrinology and Metabolism *302*, E532–E539.